SURFACE WAVE INTERACTION WITH OBLIQUE INTERNAL WAVES

by

MIRMOSADEGH JAMALI

B.A.Sc. Sharif University of Technology, 1987
M.A.Sc. Sharif University of Technology, 1990

A THESIS SUBMITTED IN PARTIAL FULFILMENT OF
THE REQUIREMENTS FOR THE DEGREE OF

DOCTOR OF PHILOSOPHY

in

THE FACULTY OF GRADUATE STUDIES

(Department of Civil Engineering)

We accept this thesis as conforming
to the required standard

THE UNIVERSITY OF BRITISH COLUMBIA

December 1998

In presenting this thesis in partial fulfilment of the requirements for an advanced degree at the University of British Columbia, I agree that the Library shall make it freely available for reference and study. I further agree that permission for extensive copying of this thesis for scholarly purposes may be granted by the head of my department or by his or her representatives. It is understood that copying or publication of this thesis for financial gain shall not be allowed without my written permission.

Department of Civil Engineering

The University of British Columbia
Vancouver, Canada

Date Feb. 5, 99

DE-6 (2/88)

Abstract

The results of a theoretical and experimental study of a resonant interaction between a surface wave and two internal waves are presented. It is shown that the motion of a surface wave in a horizontally infinite two-layer fluid can lead to generation of two oblique internal waves. The internal waves are short compared to the surface wave and have nearly opposite propagation directions. The frequencies of the internal waves are approximately half of the frequency of the surface wave.

Two analytical models are developed. The first model is based on a three-dimensional formulation of weakly non-linear interaction of the waves in a two-layer medium. The problem is initially formulated assuming that both layers are inviscid, but after obtaining the evolution equations of the internal waves, the damping due to a viscous lower layer is incorporated in the analysis. A standard technique is employed to obtain the evolution equations of the internal waves. The second model has a two-dimensional viscous formulation and serves to explore the effects of the viscosity of the lower layer on both forcing and damping in the interaction. The model places no limitation on the viscosity of the lower layer.

Using the three-dimensional model, the effects of different parameters of the system on the interaction are investigated by changing each parameter separately and observing the effects on the evolution of the internal waves. Of particular importance is the effect of the direction angle of the internal wave pair on the interaction. It is shown that the more oblique the internal waves are to the surface wave, the higher their growth rates are. In a medium without side constraints the internal waves are nearly perpendicular to the surface wave at the maximum growth rate.

Besides producing further damping, higher viscosity may also enhance the generation of the internal waves by increasing the surface-wave induced shear at the interface. The two-dimensional viscous model is used to investigate this effect of viscosity along with the corresponding dissipation effect on the interaction. The results indicate that although the forcing increases with viscosity, the damping effect of viscosity is more significant. At large viscosity, the internal waves are heavily damped and hence can not grow. As the viscosity approaches zero, the results of the viscous model become asymptotic to those of the three-dimensional model for two-dimensional interactions.

A series of experiments were carried out in a wave flume to test the theoretical results. Salt water was used as the lower layer and fresh water as the upper layer. The experiments led to generation of a three-dimensional internal wave pattern at the interface. It is shown that the pattern is created by the reflection of the oblique internal waves from the flume sidewalls. Wavelengths, frequencies, and amplitudes of the internal waves were measured for comparison with the theoretical values. The experiments confirm the theoretical results in general.

In contrast with the past theoretical studies, it is shown that viscosity is not essential to the excitation and growth of the internal waves. Also, it is shown that contrary to Hill's (1997) theoretical results, there are no specific bounds for growth of the internal waves on the density ratio of the two layers, the frequency of the surface wave, and the direction angle of the internal waves. In particular, it is demonstrated that the instability of the internal waves is not a selective process, and it may occur over wide ranges of the parameters.

Table of Contents

List of Tables

List of Figures

List of Major Symbols

a_i	half of the amplitude of wave i at the free surface
A_i	non-dimensional amplitude of wave i
α	mean forcing coefficient of the internal waves, equal to $\sqrt{\alpha_1 \alpha_2}$
α_i	forcing coefficient of internal wave i
B	flume width
b_i	half of the amplitude of wave i at the interface
β	mean damping coefficient of the internal waves, equal to $(\beta_1 + \beta_2)/2$
β_i	damping coefficient of wave i
d	depth of the lower layer
δ	$\Delta\rho / \rho$
$\Delta\rho$	$\rho - \rho'$
E_i	energy density of wave i
ε	non-dimensional wave amplitude
η	interface displacement
$\phi(x, y, z)$	potential in the lower layer in the 3D inviscid model (Chapter 2)
$\phi(x, z)$	potential in the upper layer in the 2D viscous model (Chapter 4)
$\phi'(x, y, z)$	potential in the upper layer in the 3D inviscid model (Chapter 2)
g	gravity constant
γ	growth parameter of the internal waves
$\gamma_{capillary}$	capillary constant of water surface and air
H	total depth of the layers
H_s	surface wave height
h	depth of the upper layer

h_p	half of the thickness of the interface
$Im[\quad]$	imaginary part
k_{exp}	wave number of the 3D standing internal wave from the experiment, equal to $2\pi / l_{\exp}$
k_i	$\left\|\vec{k}_i\right\|$
$\vec{k}_i$	vector wave number of wave i
ξ	free surface displacement
l_{exp}	wave length of the 3D standing internal wave from the experiment
M_i	momentum content of wave i
n	number of peaks and troughs of the standing internal wave across the flume
ν	kinematic viscosity of the lower layer
ϑ_i	$k_i\, x - \omega_i\, t$
ω_i	frequency of wave i
p	pressure in the lower layer
p'	pressure in the upper layer
$\bar{\theta}$	direction angle of the internal wave pair
θ_i	direction angle of internal wave i with respect to the surface wave
$Re[\quad]$	real part
r	density ratio ρ' / ρ
ρ	density of the lower layer
ρ'	density of the upper layer
σ_{11}, σ_{22}	normal stresses in the lower layer
$\psi(x,z)$	stream function in the lower layer in the 2D viscous model (Chapter 2)
t	time
T_0	period of the surface wave

τ	shear stress in the lower layer
u	velocity in the lower layer in x-direction
w	velocity in the lower layer in z-direction
u'	velocity in the upper layer in x-direction
w'	velocity in the upper layer in z-direction
$\vec{x}$	(x, y)
x	horizontal coordinate in the surface wave direction
y	horizontal coordinate normal to x
z	vertical coordinate

وَهُوَ ٱلَّذِى مَرَجَ ٱلْبَحْرَيْنِ هَٰذَا عَذْبٌ فُرَاتٌ وَهَٰذَا مِلْحٌ أُجَاجٌ
وَجَعَلَ بَيْنَهُمَا بَرْزَخًا وَحِجْرًا مَّحْجُورًا ﴿٥٣﴾ الفرقان

It was He who made two bodies of water meet: one fresh and palatable, and the other salty and bitter; and yet has He set an intermediary between them, an insurmountable barrier.

The Holy Quran, 25:53

CHAPTER 1

INTRODUCTION

1.1 MOTIVATION

The layers of fluid mud found at the bottom of many lakes, estuaries, and coastal waters, and the unconsolidated sludge at the bottom of mine-tailings ponds can often be treated as viscous fluids. Re-suspension of material from these layers can be of significant practical importance. In coastal waters it can lead to the need for substantial dredging or sediment replenishment (U.S. Army Coastal Engineering Research Center, 1984; Mehta et al., 1994). In mine-tailings ponds it can cause blockages in processing plants when the pond water is recycled, and adverse environmental impacts if the pond water flows into natural water courses (Lawrence et al., 1991; Luettich et al., 1990). Re-suspension can be the result of surface wave action triggering instabilities at the interface between the fluid mud (or mine-tailings) and the overlying water.

To investigate the interfacial instabilities, the model of surface wave motion in a two-layer fluid can be adopted. This simplified problem was first studied by Wen (1995) in the context

of surface wave motion over a highly viscous sub-layer. Wen's (1995) study was motivated by her qualitative observations of interfacial wave generation by a surface wave over a fine-sediment bed in a laboratory flume. She found that a resonant interaction between the surface wave and two opposite-travelling internal waves leads to the instability of the interface. Energy transfer from the surface wave causes the internal waves to grow leading to mixing between the two layers. Before discussing this particular instability mechanism in greater detail, it is instructive to review studies of resonant wave interaction in general.

1.2 WAVE INTERACTION

Nonlinear wave interactions are considered to be an important aspect of the dynamics of the oceans (Philips, 1977; Komen et al., 1994) and the atmosphere (Yi and Xiao, 1996). Of particular interest are resonant interactions, which are important in the redistribution of energy among wave modes with different spatial and temporal scales. To study the characteristics of this energy transfer, the theory of resonant wave interaction has been used extensively (Philips, 1981; McComas and Muller, 1981; Hammack and Henderson, 1993; Komen et al., 1994). In principle, the theory addresses the problem of wave generation by weakly non-linear interaction of a group of waves. Each wave in the group can be treated as linear, but when the waves satisfy certain resonance conditions, energy is interchanged preferentially between them (Turner, 1973).

Resonant wave interaction can be described as a non-linear process in which energy is transferred between different natural modes of an oscillatory system by resonance. Consider a non-linear system that is oscillating by one or more of its natural modes. As the system is non-linear, the motion is not simply a summation of the linear modes, but consists of the linear harmonics plus their non-linear coupling. Under resonance conditions the non-linear

coupling between the modes may lead to excitation of another natural mode or modes. The behavior of this excited mode(s) depends on the properties of the original modes and the system. An interesting situation occurs when the created mode(s) grows rapidly in time, being of primary importance in studies of hydrodynamic stability.

It is well known that the development of water waves is non-linear in character, and resonant interactions are of particular importance in this regard (Komen et al., 1994). Two examples of such interactions are the generation of an internal wave by two surface waves (Ball, 1964) and the interaction of an internal wave with two higher-mode internal waves on a thin density interface (Davis and Acrivos, 1967). In the study of oceanic internal gravity waves a considerable amount of work has been based on the concept of resonant wave interaction (Hasselmann, 1966; McComas and Bretherton, 1977; McComas and Muller, 1981, Muller et al., 1986). Resonant interactions are a source of internal wave energy and a mechanism for surface wave modification. Furthermore, they contribute to the redistribution of energy among different modes in the spectrum of internal waves in a continuously stratified fluid (Philips 1981). For similar applications of the theory to atmospheric gravity waves, reference can be made to the works of Yeh and Liu (1981), Fritts et al. (1993), and Yi and Xiao (1996).

The phenomenon of resonant wave interaction was first studied by Philips (1960) and subsequently by Longuett-Higgins (1962). Textbooks by Drazin and Reid (1981), Craik (1985), and Komen et al. (1994) as well as articles by Philips (1981) and Hammack and Henderson (1993) give excellent reviews of the subject. Philips (1960) showed that energy can be exchanged among three deep-water surface waves 1, 2, and 3 provided their frequencies and wave numbers meet the following kinematic conditions.

$$\begin{aligned} 2\vec{k}_1 - \vec{k}_2 &= \vec{k}_3 \\ 2\omega_1 - \omega_2 &= \omega_3 \end{aligned} \tag{1.1}$$

where $\vec{k}_i$ and ω_i are the vector wave number and frequency of the i-th wave respectively. Equation 1.1 is called the kinematic conditions of resonance. In wave interaction problems, the resonance conditions are expressed in terms of certain relations between the wave numbers and the frequencies of the waves involved. Note that the form of equation 1.1 is specific to deep-water waves, and the resonance conditions may differ from one class of waves to another.

Philips (1960) showed that under the resonance conditions (1.1), the amplitude of the third wave, if initially infinitesimal, grows in time due to the transfer of energy from finite-amplitude waves 1 and 2. It should be noted that resonant wave interaction, in general, does not necessarily lead to instability (Hasselmann 1967).

Although the analysis by Philips (1960) showed the possibility of energy transfer between deep-water surface waves, it did not address their long-term behavior. Benny (1962) extended Philips's (1960) analysis by adopting the technique used by Bogoliubov and Mitropolski (1959) in non-linear oscillations. This technique is described later in chapters 2 and 4. Benny (1962) was able to derive a complete set of equations for the time evolution of the wave amplitudes.

After Philips's (1960) work on deep-water waves, the idea of resonant wave interaction was soon extended to other classes of water waves: McGoldrick (1965, 1970, and 1972) studied interaction between capillary-gravity waves in a series of papers. McGoldrick studied the problem when the following conditions of resonance hold between three capillary-gravity waves 1, 2, and 3.

$$\begin{aligned} \vec{k}_1 &= \vec{k}_2 + \vec{k}_3 \\ \omega_1 &= \omega_2 + \omega_3 \end{aligned} \tag{1.2}$$

where $\omega = (gk + \gamma_{capillary} k^3)^{1/2}$, and $\gamma_{capillary}$ is the capillary constant for the interface of air and water. McGoldrick derived the following evolution equations for the wave amplitudes.

$$\begin{aligned} \frac{da_1}{dt} &= i\alpha\omega_1 a_2 a_3 \\ \frac{da_2}{dt} &= i\alpha\omega_2 a_1 \bar{a}_3 \\ \frac{da_3}{dt} &= i\alpha\omega_3 a_1 \bar{a}_2 \end{aligned} \tag{1.3}$$

where α is a constant, and a_i is the amplitude of the i-th wave. The over-bar denotes the complex conjugate.

Simmons (1969) used a variational method and obtained equations 1.3 more quickly. His work was inspired by Whitham's (1965, 1967) averaged Lagrangian method. Simmons (1969) formulated his method quite generally and showed how to find the evolution equations as well as conservation relations for a general wave interaction problem. A variational formulation systematizes and shortens the detailed calculations. This lessens the likelihood of making elementary errors in the long calculations of the interaction coefficients of the evolution equations. Variational formulation also leads more readily to conservation laws such as energy and momentum relations.

Ball (1964) was the first to investigate the resonant interaction in stratified fluids. He studied the resonant interaction between two surface waves and one internal wave in a two-layer fluid and showed that the two surface waves can excite the internal wave to a large amplitude. Denoting the two surface waves as waves 1 and 2 and the internal wave as wave 3, the resonance conditions are the same as given by equation 1.2. As a result, the internal wave has much larger period and wavelength than the surface ones. Ball's (1964) analysis was limited to shallow-water waves. Brekhovskikh et al. (1972) removed this limitation and considered the problem for the whole range of shallow-water to deep-water waves.

Experimental works on the interaction of two surface waves and one internal wave were conducted by Lewis et al. (1974) and Koop and Redekopp (1981). In the former, a layer of fresh water overlay a denser freon-kerosene mixture. Since the density difference between the two layers was small, the surface waves in the triad had close frequencies and wavelength, and the internal wave was a long wave. Hence, according to the resonance conditions the internal wave phase velocity is expected to be close to the group velocity of the surface waves. In the experiments, one surface wave and one internal wave train were generated mechanically as primary waves with the same direction of propagation. The observations confirmed that the strongest modulations of the primary surface wave occurred when the group velocity of the surface waves was close to the phase velocity of the internal wave, in agreement with the theory. The study of Koop and Redekopp (1981) concerned similar interaction of long and short waves on the two interfaces of a three-layer configuration.

Using a different approach from the conventional wave interaction theory, Gargett and Hughes (1972) studied the same interaction theoretically. They modeled the process as one in which the short surface waves interact with a slowly-varying, propagating current supposed and produced by the long internal wave. It then became possible to remove the restriction on the internal wave amplitude and to use the conservation laws for wave trains in slowly-varying media. They found that the variations in the direction and magnitude of the current induced by the internal wave cause local concentrations and reductions in the surface wave amplitudes. Their theoretical analysis was complemented by the field observations of the phenomenon made in the Strait of Georgia, British Columbia.

Resonant wave interaction among internal waves was first studied by Davis and Acrivos (1967). They showed that the lowest-mode internal wave in an infinite two-layer fluid with a

diffuse interface is unstable. The wave forms a resonant triad with two second-mode internal waves that modulate the original wave by extracting energy from it.

In summary, since the original work by Philips (1960), resonant wave interaction has been studied in different classes of wave motion in fluids. In the present study, the focus is on the interaction mechanism responsible for instability of the interface in a two-layer fluid subject to surface wave action.

1.3 INTERNAL WAVE GENERATION BY A SURFACE WAVE

1.3.1 Two-dimensional Interaction

The resonant interaction of two internal waves with a surface wave in a two-layer fluid has been studied in two dimensions by Wen (1995), Hill and Foda (1996), and Jamali (1997a and b). Consistent with the experimental observations of Wen (1995) and Hill and Foda (1996), all the theoretical analyses indicated that the internal waves combine to form a short standing internal wave whose frequency is approximately half of that of the surface wave. The results of the studies mainly differ as to the role of viscosity of the lower layer in the interaction. In all studies the upper layer was assumed to be inviscid, except in Hill and Foda (1996) where the layer was assumed to be weakly viscous although that did not affect the dynamics. The following summarizes these studies.

The configuration of the problem is shown in figure 1.1. Wen (1995) analyzed the problem for both an inviscid and a viscous lower layer. She found that viscosity has a destabilizing effect on the interface and is essential to the growth of the internal waves in real fluids. This issue will be addressed in more detail in chapter 4 of the present study. Wen

(1995) also found that in the inviscid limit the interaction does not result in growth of the internal waves, except for strong stratification of the fluid system ($\rho / \rho' > 1.67$).

Wen's (1995) theoretical work was prompted by her observations of the interaction in a laboratory wave flume where a surface wave was allowed to travel over a fluidized silt bed. In the experiments, fine silt with mean grain size $d_{50} = 50\ \mu m$ constituted the sediment bed. Wen (1995) reported two opposite-traveling internal waves formed at the interface of the clear water and the fluidized silt bed. The internal waves had nearly the same frequencies and wavelengths, and hence formed almost a standing internal wave. The internal waves were also short compared to the surface wave and had a frequency close to the half of the surface wave frequency. Although the recent experiments by Hill (1997) and those of the present study indicate that the interaction has a three-dimensional nature, Wen (1995) did not mention any three-dimensionality. Later in the present study it will be shown that the two-dimensional interaction is possible when there is a considerable density difference between the layers such as that in Wen's (1995) experiments where the density difference between the fresh water and the fluidized sediment was appreciable.

Wen's (1995) work was followed by Hill and Foda (1996), who by taking a similar approach arrived at nearly the same theoretical result regarding the significance of viscosity in the interaction. The basic formulation of the problem in Hill and Foda's (1996) work was very similar to Wen's (1995). Hill and Foda (1996) treated the problem in two dimensions for both an inviscid and a viscous lower layer. Their analysis indicated that there is no growth of the internal waves in the inviscid limit, but when the fluid is viscous, the internal waves may grow in time. In Hill and Foda's (1996) viscous analysis both layers were assumed to be weakly viscous. However, viscosity of the upper layer was considered much smaller than that in the lower layer. As a result, the upper layer was effectively inviscid in their perturbation analysis.

The major difference between Wen's (1995) analysis and Hill and Foda's (1996) is in the approximations used to solve the problem. In Hill and Foda's (1996) perturbation analysis both wave amplitudes and non-dimensionalized weak viscosity of the lower layer were defined as small parameters. However, in Wen's (1995) analysis only wave amplitudes were considered as small parameters, and there was no limitation on the viscosity of the lower layer.

As part of their study, Hill and Foda (1996) also made some qualitative observations on the generation of the internal waves at the interface of fresh water and fluidized sediment as a result of surface wave motion over a bed of fine silt with the same grain size as in Wen's experiment. In the analyses of Wen (1995) and Hill and Foda (1996) the predicted kinematic properties of the waves were in qualitative agreement with experimental observations. Note that determination of the kinematic properties of the interacting waves does not require a perturbation analysis. They can be obtained from the simultaneous solution of the resonance conditions and the dispersion relations of the waves (Wen 1995).

According to the theoretical results of Wen (1995) and Hill and Foda (1996), viscosity has a destabilizing effect on the interface, and one would expect that in a two-layer medium with a highly viscous lower layer, the internal waves would be excited by a surface wave. However, a series of preliminary experiments conducted by the present author in a wave flume with fresh water as the upper layer and corn syrup as the lower layer did not result in appearance of the internal waves even though the experiment was repeated with various surface wave frequencies, depth ratios, and wave heights. These observations led to the hypothesis that excitation of the internal waves is not dependent on the viscosity of the lower layer; in other words, viscosity does not facilitate generation of the internal waves.

The hypothesis was examined through an inviscid analysis of the interaction in two dimensions by Jamali (1997a and b). Contrary to the previous results, the analysis indicated

that the internal waves may grow easily in an inviscid two-layer fluid. To verify his theoretical result, the present author performed some experiments with fresh and salt water as the upper and lower layer respectively. Note that compared to the corn syrup, salt water can be considered as an inviscid fluid. Consistent with the theoretical speculations, the experiments resulted in the appearance of the sub-harmonic internal waves, but with a three-dimensional pattern. These observations motivated the author to develop a three-dimensional model of the phenomenon in a weakly viscous medium such as that in the salt-water experimentation. The study led to new findings, which will be presented in chapters 2 and 3.

1.3.2 Three-dimensional Interaction

Independent of the present study, Hill (1997) investigated the three-dimensional interaction theoretically and experimentally. Hill (1997) carried out a series of experiments in a small wave flume containing a light mineral oil overlying fresh water. The density of the mineral oil was 0.85 g/cm^3. A similar 3D standing wave pattern formed at the interface as in the present author's experiments mentioned earlier. The wavelength across the flume was twice the flume width, and the internal wave frequency was almost half of the surface wave frequency. The time-series of the interface displacement was recorded in each experiment to obtain the frequencies as well as the evolution properties of the interfacial waves.

Hill (1997) also developed a three-dimensional analytical model of the interaction of a surface wave with two oblique internal waves in an inviscid two-layer medium. The frequencies and the growth rates of the internal waves were calculated theoretically and were compared with the measured ones. The comparison indicated a good agreement between the computed frequencies and the measured ones, but the agreement was not as good for the growth rates. It is worth mentioning that although mineral oil has an appreciable viscosity,

Hill (1997) used the results of his inviscid analysis to compare with the measured growth rates.

Hill (1997) addressed the effects of viscosity on the interaction theoretically. The results indicated that viscosity has a dissipative effect on the internal waves, and the internal waves grow when the amplitude of the surface wave is greater than a critical value. This is the same result obtained by Jamali (1997a) in the analysis of the two-dimensional interaction in a viscous medium.

Some results of Hill (1997) are relevant to the present study and need particular attention. According to his analysis of the three-dimensional interaction, Hill (1997) found that there are narrow bands of frequency, density ratio, and direction angle of the internal waves only within which growth of the internal waves is possible. These results led him to conclude:

> "The net effect of these various bounds was that instability of the internal waves, i.e., internal wave growth, was found to be a very selective process, occurring under very specific conditions."

Hill's (1997) results will be addressed later in light of the experimental and theoretical findings of the present study. Hill's (1997) analysis also suggested that there is no growth of the internal waves in the two-dimensional case, in contrast with the theoretical results of Jamali (1997 a and b).

Table 1.1 provides a summary of the studies on the resonant interaction between a surface wave and two internal waves in a two-layer fluid.

1.4 PRESENT STUDY

The present study investigates the resonant interaction between a surface wave and two internal waves both theoretically and experimentally. This includes studying the effects of

the important parameters of the system on the interaction. Of particular interest is the influence of viscosity on the interaction as in the experiments viscosity was found to have a significant damping effect on the interaction process. Also, some issues raised by Wen (1995), Hill and Foda (1996), and Hill (1997) are addressed in detail. With respect to Hill's (1997) study, the present work is different in terms of the methods and the results of the analysis, and the breadth of the experimental investigation.

In chapter 2 a three-dimensional analysis of the generation of oblique internal waves by a surface wave in a weakly viscous two-layer fluid is presented. The analysis follows the conventional procedure in three-wave interaction analysis (e.g., see Drazin and Reid, 1981; Craik, 1985). Initially, the problem is formulated assuming that both layers are inviscid, but later this assumption is relaxed to include the damping effect of the weak viscosity of the lower layer on the internal wave growth. The effects of the important parameters on the interaction are explored in detail.

In chapter 3, the results of the laboratory experiments designed to investigate the three-dimensional interaction are presented. An attempt is made to explain the experimental observations using the theoretical results of chapter 2. The experimental results are also used to address some theoretical issues raised by Hill (1997) on the limitations of the interaction phenomenon.

In chapter 4 the interaction is studied using a viscous model of the interaction where no restrictions are placed on the viscosity. As the viscous formulation adds considerable complexity to the problem, the analysis is limited to two dimensions. Although this may be a deviation from the reality, the analysis still provides useful information about the interaction in a highly viscous medium.

Finally, a summary of the earlier chapters along with the conclusions and recommendations for future studies is presented in chapter 5.

Study	Theory		Experiments
	Analysis*	Main Results	
Wen (1995)	2D	Viscosity is essential to excitation	• Fresh water over fluidized silt • Observation of sub-harmonic internal waves
Hill and Foda (1996)	2D	Viscosity is essential to excitation	• Fresh water over fluidized silt • Observation of sub-harmonic internal waves
Jamali (1997a and b)	2D	• Inviscid excitation is possible • Viscosity inhibits excitation	———
Hill (1997)	3D	• Inviscid excitation is possible only in 3D • Interaction is a very selective process	• Mineral oil over fresh water • 3D internal waves observed • Frequencies well predicted by theory • Growth rates not well predicted

- In all analytical models the upper layer was assumed inviscid, except in Hill and Foda (1996) where it was weakly viscous.

Table 1.1 A summary of the studies of the resonant interaction of a surface wave with two internal waves in a two-layer system.

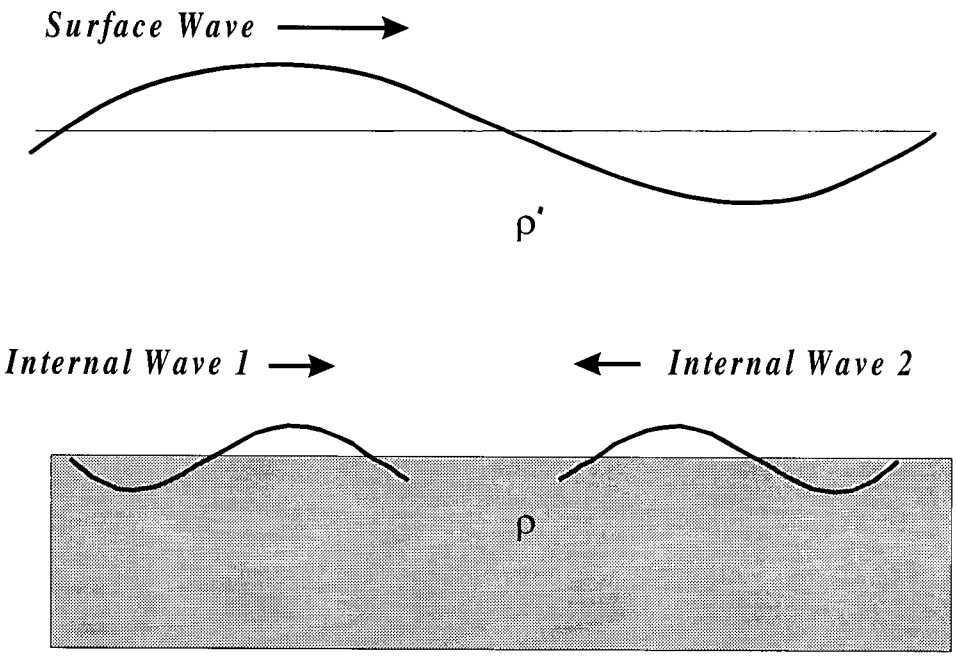

Figure 1.1 Configuration of the problem

CHAPTER 2

THREE-DIMENSIONAL INTERACTION ANALYSIS

2.1 INTRODUCTION

In this chapter, a three-dimensional analysis of the generation of oblique internal waves by a progressive surface wave is presented. The fluid system consists of an inviscid upper layer and a weakly viscous lower layer. A standard weakly nonlinear wave interaction analysis is performed. The evolution equations of the internal waves are derived, and their properties are discussed.

The numerical results for a test case are presented. It is shown that under certain conditions a surface wave can trigger two opposite-traveling internal waves in a two-layer system. The effects of the important parameters of the system on the interaction are studied by changing each parameter in turn and observing the effects on the kinematics and dynamics

of the internal waves. Also, the previous theoretical results are addressed in light of the present study.

2.1.1 Resonant Triad

The present study considers a triad consisting of a surface wave (denoted as wave 0) and two internal waves (denoted as waves 1 and 2) shown in figure 2.1. The three waves satisfy the resonance conditions

$$\begin{aligned} \vec{k}_0 &= \vec{k}_1 + \vec{k}_2 \\ \omega_0 &= \omega_1 + \omega_2 \end{aligned} \tag{2.1}$$

where for each wave i the wave number $\vec{k}_i$ and the frequency ω_i are related by a dispersion relation. For a two-layer inviscid fluid the dispersion relation is given by

$$\frac{\frac{\rho'}{\rho}(\omega^4 - g^2k^2)\tanh(kh)}{(gk\tanh(kh) - \omega^2)} + gk - \omega^2 \coth(kd) = 0 \tag{2.2}$$

(e.g., see Lamb, 1932) where the parameters are defined in figure 2.1. The resonance conditions (2.1) and the individual dispersion relations of the waves form a system of algebraic equations from which the wave numbers and frequencies of the interacting waves can be determined. The existence of the solution to this system of equations is demonstrated graphically in figure 2.2. The triad shown is just one of the possible solutions. In general, there exists infinite number of the internal wave pairs that can be in resonance with a given surface wave. Given that the two internal waves in a pair have nearly opposite directions, a pair is distinguished from the others by its angle from the surface wave (e.g., see Hill, 1997). In nature, the pair having the maximum growth rate is most likely to be observed. For a given surface wave, the locus of the wave numbers of the internal waves is shown

schematically in figure 2.3. Because the roles of the two internal waves can be interchanged in equation 2.1, the two internal waves have the same locus.

2.2 FORMULATION

In this section, a standard three-wave interaction analysis (e.g., refer to Davis and Acrivos, 1967 and Craik, 1984) is performed. Consider the two-layer fluid system shown in figure 2.1. The system is assumed to be infinite horizontally and three-dimensional. The coordinate system xyz is located on the interface. The depth of the upper layer is denoted by h, the depth of the lower layer by d, and the total depth by H. The densities of the upper and lower layers are ρ' and ρ respectively. The lower layer is assumed to have a small kinematic viscosity ν while the upper layer is regarded as inviscid. The surface wave is denoted as wave 0 and the two opposite-traveling internal waves as waves 1 and 2. Without loss of generality, wave 0 is assumed to travel in the positive x direction and the two internal waves in the $x-y$ plane. The internal wave 1 has an arbitrary directional angle θ_1 with respect to the surface wave. Note that from the resonance conditions the direction angle of the internal wave 2 is obtained as a function of θ_1.

Like Davis and Acrivos (1967), the viscosity of the lower layer is neglected initially, and its inclusion in the formulation is deferred until after obtaining the evolution equations of the internal waves. In chapter 4 the interaction will be formulated taking into account the viscosity from the beginning, and it will be shown that the two formulations yield the same results when $\nu \to 0$.

With the assumption of incompressible fluid layers and irrotational flows in the layers, the fluid motion can be described by velocity potentials $\phi'(x,y,z)$ and $\phi(x,y,z)$ in the upper and

lower layer respectively. The potentials satisfy Laplace's equation in the upper and lower fluid domains.

$$\nabla^2\phi' = 0, \qquad 0 < z < h \tag{2.3}$$

$$\nabla^2\phi = 0, \qquad -d < z < 0 \tag{2.4}$$

The above equations are subject to the boundary conditions at the free surface, the interface of the layers, and the solid bed. On the free surface, the boundary conditions are:

$$\xi_t + \phi'_x\xi_x + \phi'_y\xi_y = \phi'_z, \qquad z = h + \xi(x, y, t) \tag{2.5}$$

$$\rho'[\phi'_t + \frac{1}{2}(\phi'^2_x + \phi'^2_y + \phi'^2_z) + gz] = C'(t), \quad z = h + \xi(x, y, t) \tag{2.6}$$

where $\xi(x,y,t) =$ the displacement of the free surface. The first equation represents a kinematic boundary condition while the second equation corresponds to a dynamic one. On the two-layer interface, the kinematic boundary conditions are:

$$\eta_t + \phi'_x\eta_x + \phi'_y\eta_y = \phi'_z, \qquad z = \eta(x,y,t) \tag{2.7}$$

$$\eta_t + \phi_x\eta_x + \phi_y\eta_y = \phi_z, \qquad z = \eta(x,y,t) \tag{2.8}$$

where $\eta(x,y,t) =$ the displacement of the interface, and the dynamic boundary condition is:

$$\rho'[\phi'_t + \frac{1}{2}(\phi'^2_x + \phi'^2_y + \phi'^2_z) + gz - C'(t)] = \rho[\phi_t + \frac{1}{2}(\phi^2_x + \phi^2_y + \phi^2_z) + gz - C(t)], \qquad z = \eta(x,y,t) \tag{2.9}$$

On the bed, the problem is subject to a kinematic boundary condition requiring the normal velocity be zero, i.e.,

$$\phi_z = 0, \qquad z = -d \tag{2.10}$$

For the purpose of the interaction analysis, it is assumed that the amplitudes of the waves are sufficiently small that a weakly nonlinear interaction analysis can be performed. This implies that terms of order ε^3 and higher, where ε is non-dimensional wave amplitude, may be neglected. Accordingly, the following expansions are considered for ξ, η, ϕ' and ϕ.

$$\xi(x,y,t) = a_0\, Exp[i(\vec{k}_0.\vec{x} - \omega_0 t)] + a_1\, Exp[i(\vec{k}_1.\vec{x} - \omega_1 t)] + a_2\, Exp[i(\vec{k}_2.\vec{x} - \omega_2 t)] + \sum_{i=0}^{2}\sum_{j=i}^{2} \xi_{ij}(x,y,t) + complex\ conjugate$$

$$\eta(x,y,t) = b_0\, Exp[i(\vec{k}_0.\vec{x} - \omega_0 t)] + b_1\, Exp[i(\vec{k}_1.\vec{x} - \omega_1 t)] + b_2\, Exp[i(\vec{k}_2.\vec{x} - \omega_2 t)] + \sum_{i=0}^{2}\sum_{j=i}^{2} \eta_{ij}(x,y,t) + complex\ conjugate$$

$$\phi'(x,y,z,t) = \phi'_0(x,y,z,t) + \phi'_1(x,y,z,t) + \phi'_2(x,y,z,t) + \sum_{i=0}^{2}\sum_{j=i}^{2} \phi'_{ij}(x,y,z,t) + complex\ conjugate$$

$$\phi(x,y,z,t) = \phi_0(x,y,z,t) + \phi_1(x,y,z,t) + \phi_2(x,y,z,t) + \sum_{i=0}^{2}\sum_{j=i}^{2} \phi_{ij}(x,y,z,t) + complex\ conjugate \qquad (2.11)$$

where $\vec{x} = (x,y)$; a_i and b_i are half of the amplitudes of wave i at the free surface and the interface respectively; and $\vec{k}_i$ and ω_i are the vector wave number and frequency of wave i respectively. The amplitudes are assumed to be complex numbers in general. The three interacting waves constitute the wave field at first order. The single-indexed terms such as ϕ_i are of $O(\varepsilon)$ while the double-indexed terms such as ϕ_{ij} are of $O(\varepsilon^2)$. Expansions (2.11) follow the standard procedure for three-wave interaction (e.g., see Craik, 1985). The expansions used by Wen (1995), Hill and Foda (1996), and Hill (1997) are essentially the same as the above.

As the three waves are in resonance, certain kinematic conditions hold between their frequencies and wavelengths. The kinematic conditions of resonance are (e.g., see Wen (1995) for the two-dimensional case) given by (2.1). These equations ensure a continuous and effective energy transfer between the waves.

In a weakly non-linear interaction, as far as the short-time behavior of the waves is concerned, the component waves can be regarded as independent and be treated by the linear theory. However, energy is exchanged between the waves as a result of resonance, and the amplitudes of the interacting waves undergo changes with time, but the rate of energy exchange is small, and so are the time variations of the amplitudes. The amplitudes have, in fact, a time scale much greater than the individual wave periods. The time variations of the amplitudes are functions of the amplitudes of the waves; the higher the amplitudes, the faster the amplitude variations. To solve the above perturbation problem, a commonly used technique proposed by Benny (1962) for solution of weakly non-linear interaction problems is employed. The technique makes use of the behavior of the waves in long time and is quite efficient in predicting their dynamics. Benny (1962) assumed that the wave amplitudes are slow functions of time, and the time-derivative of each wave amplitude is a function of the product of the amplitudes of the other waves and hence a second-order quantity. These imply that in the present problem the amplitudes a_0, b_1 and b_2 can be taken as slow functions of time as follows.

$$\frac{da_0}{dt} = O(b_1 b_2), \qquad \frac{db_1}{dt} = O(a_0 \bar{b}_2), \qquad \frac{db_2}{dt} = O(a_0 \bar{b}_1) \tag{2.12}$$

where symbol overbar denotes complex conjugate. The above assumption makes the time derivatives of a_0, b_1, and b_2 appear in the equations at second order. For a lucid discussion of this technique, the interested reader is referred to Drazin and Reid (1981) and Craik

(1985). Appendix B outlines the calculations at second order along with a discussion of the need for existence of the over-bars in (2.12).

Substituting (2.11) in the governing equations and collecting first order terms results in the linear wave theory for waves 0, 1 and 2. The solution to the linear problem is given in Appendix A.

At second order, the nonlinear interaction terms appear in the forcing functions of the resulting inhomogeneous systems of partial differential equations. The forcing terms also include the time derivatives of the wave amplitudes. Due to the resonance conditions, the forcing functions are of the form that produces secular solutions at $O(a_0\bar{b}_1)$, $O(a_0\bar{b}_2)$, $O(b_1 b_2)$, and their complex-conjugate counterparts. A secular solution grows wildly in time and becomes unbounded as time becomes arbitrarily large. From a physical point of view secular solutions are not acceptable here since the energy is bounded. Mathematically, secular solutions destroy uniformity of the underlying asymptotic expansions. To avoid secularity, it becomes then necessary to impose a certain solvability condition on the forcing functions. The desired solvability condition is the requirement that the forcing functions and the homogeneous solution of the adjoint system be orthogonal (Drazin and Reid, 1981, p 385). Applying the solvability condition to the forcing functions result in three equations from which da_0 / dt, db_1 / dt, and db_2 / dt can be explicitly found in the following forms.

$$\frac{da_0}{dt} = \alpha_0 b_1 b_2, \qquad \frac{db_1}{dt} = \alpha_1 a_0 \bar{b}_2, \qquad \frac{db_2}{dt} = \alpha_2 a_0 \bar{b}_1 \tag{2.13}$$

where α_0, α_1 and α_2 are constant. The direct derivation of the interaction coefficients α_1 and α_2 is presented in Appendix B. It will be shown later that (2.13) can be approximated by neglecting the first equation, and hence the need for computing α_0 is eliminated. The

analysis indicates that α_1 and α_2 are purely imaginary. Although Mathematica® was extensively used to simplify these coefficients, they are still long, see Appendix B.

Mathematica® is a mathematical software that is capable of performing numerical and symbolic calculations. It possesses its own programming language, and a mathematical procedure can be defined as a series of commands. In this study, the problem at each order was broken into a number of smaller pieces, and the software was guided through the mathematical procedure to perform the symbolic calculations and to simplify the results.

At this point it is useful to point out a difference between the current analysis and those of Wen (1995), Hill and Foda (1996), and Hill (1997). These authors all took the required solvability condition to be the orthogonality of the forcing functions and the homogeneous solution of the system of equations. This is valid only when the original systems are self-adjoint. However, here the systems of equations at second order are not self-adjoint, see Appendix B, and the correct solvability condition is the orthogonality of the forcing functions and the homogeneous solution of the adjoint system (Drazin and Reid, 1981, p 385).

It is worth mentioning that the evolution coefficients α_0, α_1 and α_2 in (2.13) are not independent. In general, in a medium sustaining a three-wave interaction, if the normalized waves amplitudes A_0, A_1, and A_2 are defined such that the energy density of each wave is given by

$$E_i = CA_i\overline{A}_i\,, \qquad i = 0,\ 1,\ 2 \tag{2.14}$$

where C is a constant, the interaction equations take the specific forms

$$\frac{dA_0}{dt} = i\sigma\omega_0 A_1 A_2\,, \qquad \frac{dA_1}{dt} = i\sigma\omega_1 A_0\overline{A}_2\,, \qquad \frac{dA_2}{dt} = i\sigma\omega_2 A_0\overline{A}_1 \tag{2.15}$$

where the real constant σ is the same in all the three equations (Simmons, 1969).

It is instructive to examine the evolution equations (2.13) in light of the above symmetry properties. In the two-layer medium the wave energy density is given by

$$E = 2\rho' g|a|^2 + 2(\rho - \rho')g|b|^2 \tag{2.16}$$

where as defined before a and b are half of the amplitudes of the wave motion at the free surface and the interface respectively. To simplify the analysis, the density difference $\Delta\rho = \rho - \rho'$ is assumed to be small. Therefore, the energy densities of the two internal waves, E_1 and E_2, are given by

$$E_i = 2\Delta\rho\, g|b_i|^2, \qquad i=1, 2 \tag{2.17}$$

and the energy density of the surface wave by

$$E_0 = 2\rho g|a_0|^2 \tag{2.18}$$

correct to the leading order in $\Delta\rho$. The normalized internal wave amplitudes can then be defined as

$$A_i = \sqrt{\delta}\, b_i, \quad i=1, 2 \tag{2.19}$$

where $\delta = \Delta\rho / \rho$ is a small parameter. The normalized surface wave amplitude can be taken the same as a_0. Note that the ratio of the energy contents of the waves is given by the ratio of the squares of their normalized amplitudes. Having defined the normalized amplitudes, the evolution equations are given by (2.15). If these equations are recast in terms of the actual amplitudes a_0, b_1, and b_2, the interaction coefficients α_0, α_1, and α_2 in equation 2.13 are obtained in terms of the constant σ, $\Delta\rho$, and the frequencies. It follows that the following relations hold among α_0, α_1, and α_2.

$$\frac{\alpha_1}{\omega_1} = \frac{\alpha_2}{\omega_2} = \frac{\alpha_0}{\omega_0\delta} \tag{2.20}$$

The above is correct at least to the leading order in δ. It is interesting to note that according to (2.20) α_0 is much smaller than α_1 and α_2, and hence the growth rate of the surface wave

is negligible compared to the internal waves. This fact is used to simplify equations 2.13 as follows shortly.

Next, the stability theory of Hasselmann (1967) on three-wave resonant interactions is applied to the present problem. The theory states that in a resonant triad when the two normalized amplitudes A_1 and A_2 are much smaller than A_0, and the resonance conditions are given by (2.1), the waves 1 and 2 grow exponentially at the expense of the third wave. This implies that in the present problem the surface wave acts as a 'pump wave' (Craik, 1985) and is unstable to the two internal waves, which grow exponentially at its expense. Note that even when the internal wave amplitudes are physically large, the normalized amplitudes A_1 and A_2 are still small compared to $A_0 = a_0$. Hence, Hasselmann's theory is applicable even when the internal waves have acquired appreciable amplitudes.

The solutions to the set of the non-linear evolution equations 2.13 are known in terms of Jacobi elliptic functions, for example, see Craik (1985). However, to have a better understanding of the problem and avoid complexity, it is useful to approximate equations 2.13. Given that the surface wave has much more energy than the internal waves (compare equations 2.17 and 2.18), the change in the surface wave amplitude due to growth or decay of the internal waves is negligible as predicted by (2.20). Therefore, the first equation in (2.13) can be neglected, and a_0 is assumed to be constant in the other two equations. The result is a system of two linear equations in two unknowns b_1 and b_2, which can be easily reduced to a second-order linear differential equation in terms of b_1 or b_2. Note this approximation is valid even when the internal waves have grown considerably and are quite large in amplitude. Before including viscous effects and solving the resulting equations, it is illuminating to address the conservation laws in the present problem.

2.2.1 Conservation Laws

In a resonant interaction momentum and energy are continuously exchanged between the modes, but the total energy $\sum E$ and total momentum $\sum \vec{M}$ are conserved. The wave energies in terms of the normalized amplitudes were given in (2.14). Consequently, the total energy will be

$$\sum_{i=0}^{2} E_i = C(A_0\overline{A}_0 + A_1\overline{A}_1 + A_2\overline{A}_2) \tag{2.21}$$

Taking the time derivative of $\sum E$ yields

$$\frac{d}{dt}\left(\sum_{i=0}^{2} E_i\right) = C(\frac{dA_0}{dt}\overline{A}_0 + \frac{d\overline{A}_0}{dt}A_0 + \frac{dA_1}{dt}\overline{A}_1 + \frac{d\overline{A}_1}{dt}A_1 + \frac{dA_2}{dt}\overline{A}_2 + \frac{d\overline{A}_2}{dt}A_2) \tag{2.22}$$

Substituting for the time derivatives of the amplitudes from (2.15) gives

$$\frac{d}{dt}\left(\sum_{i=0}^{2} E_i\right) = i\sigma C\left((\omega_0 - \omega_1 - \omega_2)\overline{A}_0 A_1 A_2 - (\omega_0 - \omega_1 - \omega_2)A_0\overline{A}_1\overline{A}_2\right) \tag{2.23}$$

From the resonance conditions (2.1), $\omega_0 - \omega_1 - \omega_2 = 0$. Therefore, the right hand side of (2.23) vanishes indicating that the total energy is conserved.

The conservation of momentum can be shown in a similar fashion. The mean momentum of the i-th wave component is given by

$$\vec{M}_i = E_i\vec{k}_i / \omega_i = CA_i\overline{A}_i\vec{k}_i / \omega_i \tag{2.24}$$

(for example, see Philips, 1977). Taking the time-derivative of the total momentum $\sum \vec{M}_i$ yields

$$\frac{d}{dt}\left(\sum_{i=0}^{2} \vec{M}_i\right) = C\left(\frac{\vec{k}_0}{\omega_0}\left(\frac{dA_0}{dt}\overline{A}_0 + \frac{d\overline{A}_0}{dt}A_0\right) + \frac{\vec{k}_1}{\omega_1}\left(\frac{dA_1}{dt}\overline{A}_1 + \frac{d\overline{A}_1}{dt}A_1\right) + \frac{\vec{k}_2}{\omega_2}\left(\frac{dA_2}{dt}\overline{A}_2 + \frac{d\overline{A}_2}{dt}A_2\right)\right) \tag{2.25}$$

Substituting for the time derivatives of the amplitudes from (2.15) yields

$$\frac{d}{dt}\left(\sum_{i=0}^{2}\vec{M}_i\right)=i\sigma C\left((\vec{k}_0-\vec{k}_1-\vec{k}_2)\overline{A}_0A_1A_2-(\vec{k}_0-\vec{k}_1-\vec{k}_2)A_0\overline{A}_1\overline{A}_2\right) \tag{2.26}$$

According to the resonance conditions (2.1), $\vec{k}_0-\vec{k}_1-\vec{k}_2=0$, and hence the right hand side of (2.26) is identically zero. This proves the conservation of the total mean momentum.

Before leaving this section, it is interesting to explore the evolution properties of the waves derivable from the action partition equations. Action density of a wave is defined as E/ω. Using (2.14) the time derivative of the action density of the surface wave is given by

$$\frac{d}{dt}(E_0/\omega_0)=C\left(\frac{1}{\omega_o}\frac{dA_0}{dt}\overline{A}_0+\frac{1}{\omega_o}\frac{d\overline{A}_0}{dt}A_0\right) \tag{2.27}$$

Using (2.15) and after some reordering, the right hand side can be written as

$$-\frac{C}{\omega_1}\left(\frac{dA_1}{dt}\overline{A}_1+\frac{d\overline{A}_1}{dt}A_1\right)=-\frac{d}{dt}(E_1/\omega_1) \tag{2.28}$$

so that

$$\frac{E_0}{\omega_0}+\frac{E_1}{\omega_1}=const. \tag{2.29}$$

Similarly,

$$\frac{E_1}{\omega_1}-\frac{E_2}{\omega_2}=const. \tag{2.30}$$

A third equation can be obtained from the combination of (2.29) and (2.30):

$$\frac{E_0}{\omega_0}+\frac{E_2}{\omega_2}=const. \tag{2.31}$$

Equation 2.30 indicates that the growths of the two internal waves as well as their decays are simultaneous, and equations 2.29 and 2.31 imply that the energy for growth of the internal waves is maintained by the surface wave.

2.2.2 Viscous Modification

Now the effect of the lower layer viscosity is incorporated into the analysis. In general, adding viscosity affects the interaction mechanism in two ways. First, compared to an inviscid lower layer, the horizontal velocity field due to the surface wave in a viscous lower layer has a sharper gradient at the interface. Secondly, viscosity acts as a dissipater of the wave energies. In the first instance, a higher viscosity adds to the interfacial shear, which is well known to be a cause of instability of many stratified-fluid flows, for example, Kelvin-Helmholtz instability in a two-layer flow (Turner 1973, chapter 4). Therefore, in this respect viscosity has a forcing role in the excitation of the internal waves, while in the second instance it acts as a damper of the internal waves. Combination of these two opposite roles determines the net effect of viscosity on the interaction.

Here it is assumed that the viscosity is weak and serves only as a damper of the internal waves. Justification of this assumption will be made in chapter 4, where a complete viscous interaction analysis is made. To include the viscous damping of the internal waves in the analysis, the evolution equations of the internal waves in (2.13) are modified to (e.g., refer to Davis and Acrivos, 1967)

$$\frac{db_1}{dt} = \alpha_1 a_0 \bar{b}_2 - \beta_1 b_1, \qquad \frac{db_2}{dt} = \alpha_2 a_0 \bar{b}_1 - \beta_2 b_2 \tag{2.32}$$

where β_i is the damping coefficient of the i-th internal wave. The constant β_i is the inverse of the decay time constant of the internal wave i and is a positive real number. The values of β_i's, $i = 1, 2$, can be obtained from the following dispersion relation through a linear viscous analysis of the wave motion in the system shown in figure 2.1 (MacPherson, 1980).

$$\frac{\rho'(\omega^4 - g^2k^2)S_h}{C_h(g\,k\,\frac{S_h}{C_h} - \omega^2)} + \rho g\,k + \rho(2k^2\nu - i\omega)^2\left\{\frac{(2k^2 - i\omega/\nu)[\,\lambda C_k C_\lambda - kS_kS_\lambda\,] - 2k^2\lambda}{(2k^2 - i\omega/\nu)[\,\lambda S_k C_\lambda - k\,C_kS_\lambda\,]}\right\}$$

$$-4\rho k^3\nu^2\lambda\left\{\frac{(2k^2 - i\omega/\nu) - 2k[\,kC_kC_\lambda - \lambda S_kS_\lambda\,]}{2k[\,\lambda S_kC_\lambda - kC_kS_\lambda\,]}\right\} = 0 \qquad (2.33)$$

where $\lambda = \sqrt{k^2 - \frac{i\omega}{\nu}}$ and $i = \sqrt{-1}$, (2.34)

and $S_h = Sinh(kh)$, $S_k = Sinh(kd)$, $S_\lambda = Sinh(\lambda d)$,

$C_h = Cosh(kh)$, $C_k = Cosh(kd)$, $C_\lambda = Cosh(\lambda d)$ (2.35)

By substituting the wave number of each internal wave into the dispersion equation, the frequency corresponding to the motion of the wave in the viscous system is obtained. The computed frequency is a complex number whose real part is almost equal to the computed frequency from the inviscid dispersion relation and its imaginary part is the desired $-\beta$.

When an internal wave is deep in both layers, it can be shown that the damping coefficient from (2.33) reduces to

$$\beta = \nu k^2 \qquad (2.36)$$

Given that the two interacting internal waves are nearly identical in wavelength, the above equation implies that the internal waves have approximately the same damping rate.

It is useful to obtain approximate solutions for $b_1(t)$ and $b_2(t)$ in (2.32). Combining the two equations in (2.32) gives a second-order, constant coefficient differential equation in $b_1(t)$ or $b_2(t)$ with the solution

$$b_1(t) = C_1 e^{\frac{-(\beta_1+\beta_2)+\sqrt{\Delta_1}}{2}t} + C_2 e^{\frac{-(\beta_1+\beta_2)-\sqrt{\Delta_1}}{2}t} \tag{2.37-a}$$

$$b_2(t) = C_3 e^{\frac{-(\beta_1+\beta_2)+\sqrt{\Delta_2}}{2}t} + C_4 e^{\frac{-(\beta_1+\beta_2)-\sqrt{\Delta_2}}{2}t} \tag{2.37-b}$$

where

$$\Delta_1 = (\beta_1 + \beta_2)^2 - 4(\beta_1\beta_2 - \overline{\alpha}_1\alpha_2|a_0|^2) \tag{2.38-a}$$

$$\Delta_2 = (\beta_1 + \beta_2)^2 - 4(\beta_1\beta_2 - \overline{\alpha}_2\alpha_1|a_0|^2) \tag{2.38-b}$$

In (2.37), C_i's, i=1,...,4, are constants. The analysis indicates that α_1 and α_2 as well as β_1 and β_2 are approximately equal as the two internal waves are nearly identical in wavelength and frequency. Considering this and the fact that the second terms in $b_1(t)$ and $b_2(t)$ decay fast with time, the solution can be approximated by

$$b_1(t) = C_1 e^{\gamma t}, \tag{2.39-a}$$

$$b_2(t) = C_3 e^{\gamma t} \tag{2.39-b}$$

where

$$\gamma = \alpha|a_0| - \beta, \tag{2.40}$$

where

$$\alpha = \sqrt{\overline{\alpha}_1\alpha_2} \qquad \text{and} \qquad \beta = \frac{(\beta_1 + \beta_2)}{2}. \tag{2.41}$$

Both α and β are positive real numbers. The quantities $\alpha|a_0|$, β, and γ have dimension of time^{-1} and are the forcing, the damping, and the growth parameters respectively. The experimental results, which will be presented in chapter 3, confirm the exponential evolution of the internal waves in time.

For a given surface wave, the frequencies and wave numbers of the interacting waves can be obtained from the simultaneous solution of (2.1) and the dispersion relations of the waves given by (2.2). The solution to the frequencies and the wave numbers indicates that there are an infinite number of internal wave pairs that can form a resonant triad with a given surface wave. An example pair is shown in figure 2.4. The angles θ_1 and θ_2 are the direction angles of the internal waves 1 and 2 with respect to the surface wave respectively. In the next section it will be shown that the internal waves are short compared to the surface wave. They have almost equal wavelengths but opposite propagation directions. Their frequencies are also close and approximately equal to the half of the frequency of the surface wave. Experimental verification of these properties of the internal waves will be given in chapter 3. The analysis also indicates that the wavelength of an internal wave remains almost constant as θ_1 changes, and hence the main difference between the pairs lies in the propagation direction. These along with the other features of the interaction are explored next through a numerical example.

2.3 NUMERICAL RESULTS AND DISCUSSION

In this section, a test case is considered and the interaction is studied when the depth ratio, the density ratio, the viscosity, the surface wave frequency, the orientation of the internal waves vary. First the system parameters are non-dimensionalized, and then the results are presented.

The important independent parameters in the problem are H, d, ρ', ρ, ν, g, $|a_0|$, k_0, and θ_1. The direction angle of internal wave 2, denoted by θ_2, is a dependent variable in the analysis. Note that either of k_0 and ω_0 can be taken as an independent variable given that

they are related through the dispersion relation (2.2). The independent parameters can be reduced to the following six non-dimensional variables.

$$\pi_1 = \frac{\rho}{\rho'},\ \pi_2 = \frac{|a_0|}{H},\ \pi_3 = \frac{d}{H},\ \pi_4 = \frac{\nu}{\sqrt{gH^3}},\ \pi_5 = k_0 H,\ \pi_6 = \theta_1 \qquad (2.42)$$

The above set has been selected in such a way that a change of any of ρ, $|a_0|$, d, ν, k_0, and θ_1 results in change in just one non-dimensional variable. Note that as k_0 is an increasing function of ω_0 according to the dispersion relation, the non-dimensional parameter $k_0 H$ can be regarded as a measure of the surface wave frequency as well. In the following sections the variation in the surface wave frequency is represented by the corresponding variation in $k_0 H$.

The important dependent parameter describing the evolution of the internal waves during the interaction is the non-dimensional parameter γ / ω_0, which is a measure of the growth of the internal waves during a surface wave period. In fact, $e^{2\pi(\gamma/\omega_0)} - 1$ gives the growth rate (or decay rate when it is negative) of the amplitudes of the internal waves during a surface wave period. Using equation 2.40, the expression for γ / ω_0 can be written as

$$\gamma / \omega_0 = (\alpha H / \omega_0)(|a_0| / H) - \beta / \omega_0 \qquad (2.43)$$

where β / ω_0, $\alpha H / \omega_0$, and $|a_0| / H$ are all positive non-dimensional numbers. The quantity β / ω_0 is a measure of viscous dissipation of the internal waves during a surface wave period and like $\alpha H / \omega_0$ is a dependent parameter. It is recalled that β / ω_0 is calculated from the viscous dispersion relation 2.33, which has been obtained from a linear viscous analysis of wave motion in a two-layer fluid. The term $(\alpha H / \omega_0)|a_0| / H$ is the forcing term and can be separated into two parts: $|a_0| / H$ and $\alpha H / \omega_0$. The quantity $|a_0| / H$ is the non-dimensional surface wave amplitude. The quantity $\alpha H / \omega_0$ is a measure of the efficiency of the energy transfer during the resonant interaction. It is recalled that α is obtained from an inviscid interaction analysis.

In the following, a model problem is used to explore the effects of the different parameters on the interaction. This is achieved by changing each non-dimensional variable in turn and studying the effects on the surface wave forcing as well as the viscous dissipation and the growth rate of the internal waves. For each case the graphs of $\alpha H / \omega_0$, β / ω_0, and γ / ω_0 outline the effects. Mathematica® was used to obtain the numerical values of α, β, and γ as well as the kinematic properties of the waves in the model problem.

Consider a test case where $d = 4.0\ cm$, $H = 16.0\ cm$, $\rho' = 1.00\ gr/cm^3$, $\rho = 1.04\ gr/cm^3$, $\omega_0 = 2\pi / 0.8\ rad/sec$, $\nu = 3\times10^{-6} m^2/sec$ and $\theta_1 = 75^\circ$. The corresponding non-dimensional numbers are

$$\{ \pi_1 = 1.04,\ \pi_2 = a_0(cm)/16,\ \pi_3 = 0.25,\ \pi_4 = 15\times10^{-6},\ \pi_5 = 1.21,\ \pi_6 = 75^\circ \}$$

By numerical solving of the set of algebraic equations consisting of the dispersion relations of the waves and the resonance conditions, the kinematic properties of the waves are obtained as follows.

$(k_0)_x = 7.54\ rad/m$, $(k_0)_y = 0$, $|\vec{k}_o| = 7.54\ rad/m$

$(k_1)_x = 21.00\ rad/m$, $(k_1)_y = 78.35\ rad/m$, $|\vec{k}_1| = 81.11\ rad/m$, $\omega_1 = 3.95\ rad/s$,

$(k_2)_x = -13.45\ rad/m$, $(k_2)_y = -78.35\ rad/m$, $|\vec{k}_2| = 79.5\ rad/m$, $\omega_2 = 3.91\ rad/s$

The above numerical values indicate that the internal waves are nearly identical in frequency and wavelength and propagate almost in opposite directions. Also, the frequencies of the internal waves are close to $\omega_0 / 2$, as stated before. These suggest that the internal waves form nearly a sub-harmonic standing wave at the interface. The wave patterns at the free surface and the interface are shown in figure 2.5. It can be seen that the internal waves are short and oblique to the surface wave. In chapter 3, these typical kinematic properties of the internal waves will be shown to be in agreement with the experimental observations.

The numerical values of α's and β's as calculated by Mathematica® for this case are

$$\alpha_1 = -17.32i \ (m.s)^{-1}, \qquad \beta_1 = 0.0195 \ rad/s$$

$$\alpha_2 = -17.14i \ (m.s)^{-1}, \qquad \beta_2 = 0.0188 \ rad/s$$

As seen, α's as well as β's are nearly equal. Also, it is interesting to note that $\alpha_1/\omega_1 \approx \alpha_2/\omega_2$ in accordance with (2.20).

2.3.1 Changing Density Ratio

It is instructive to explore first the effects of a small density difference on the kinematics of the internal waves. Figure 2.6(a) shows variations of the non-dimensional internal wave numbers k_1/k_0 and k_2/k_0 with the small parameter $\delta = \Delta\rho/\rho$, where $k_i = \left|\vec{k}_i\right|$. As seen, when the density difference approaches zero, the internal wave numbers become infinitely large. Knowing that $\vec{k}_0$ remains finite at small density differences, this implies that for small density differences the internal waves are essentially deep waves in the two layers, and hence their dispersion relation is given by (Turner, 1973)

$$\omega^2 = \frac{\rho - \rho'}{\rho + \rho'} gk \tag{2.44}$$

Equation 2.44 can be obtained assuming $k \to \infty$ in (2.2). Variations of the non-dimensional internal wave frequencies ω_1/ω_0 and ω_2/ω_0 are shown in figure 2.6(b). As seen, when $\delta \to 0$, $\omega_1 \to \omega_2 \to \omega_0/2$. Taking ω_0 to be $O(1)$, this implies that ω_1 and ω_2 as well are $O(1)$ in δ. Knowing these, one can determine the orders of the wave numbers. In absence of a density difference, the dispersion relation for the surface wave is $\omega^2 = gk\tanh(kH)$. Since $\omega_0 \sim O(1)$, this implies that $\vec{k}_0 \sim O(1)$. The dispersion relations for the internal waves when $\delta \to 0$ is given by (2.44). Given that ω_1 and ω_2 are $O(1)$, $\vec{k}_1$ and $\vec{k}_2$ are found to be

$O(1/\delta)$, consistent with figure 2.6(a). These are important ordering properties and will be referred to later on.

Next, the effects of the density difference on the dynamics of the interaction are investigated. The non-dimensional variable $\alpha H/\omega_0$ is plotted as a function of ρ/ρ' in figure 2.7(a). As seen, $\alpha H/\omega_0$ is nearly constant from $\rho/\rho' = 1.00$ to 1.04. This suggests that for the given surface wave the forcing does not change considerably over the range of density ratio from 1.00 to 1.20, which corresponds to the range of density ratio in most real situations. The graph of $\alpha H/\omega_0$ decreases mildly for $\rho/\rho' > 1.04$.

Variation of the non-dimensional damping coefficient of the internal waves, β/ω_0, with ρ/ρ' is illustrated in figure 2.7(b). As ρ/ρ' approaches 1.00 from higher values, damping increases rapidly. The explicit expression for β/ω_0 around $\rho/\rho' = 1.00$ can be obtained as follows. For a deep internal wave in a two-layer fluid, the dispersion relation is given by (2.44), and β/ω_0 can be obtained from (2.36) as follows.

$$\frac{\beta}{\omega_0} = \frac{\nu k^2}{\omega_0} \tag{2.45}$$

By substituting k from (2.44) in (2.45) and noting that ω_1 and ω_2 are approximately equal to $\omega_0/2$, see figure 2.16, for instance, one can obtain the following expression for β/ω_0.

$$\frac{\beta}{\omega_0} \approx \frac{\nu\omega_0^{\,3}(1+\rho'/\rho)^2}{16g(1-\rho'/\rho)^2} \tag{2.46}$$

According to the above expression, β/ω_0 increases rapidly as the density ratio approaches 1.00, consistent with the graph of β/ω_0 in figure 2.7. From a physical point of view, this rapid growth of the dissipation rate can be explained by noting that the frequencies of the internal waves are almost constant (around $\omega_0/2$). Hence, the wavelengths of the internal

waves decrease as the density difference approaches zero. This results in a higher dissipation of the internal waves, as predicted by equation 2.46 for the deep-wave case.

From the foregoing discussion, it is expected that for values of ρ / ρ' close to unity, the internal waves may not be excited at all even at high amplitudes of the surface wave. This is consistent with the plot of the growth rate in figure 2.7(c), where the non-dimensional parameter γ / ω_0 for $a_0 = (a_0)_{max}$ is plotted against the density ratio. The quantity $(a_0)_{max}$ is the half-amplitude of the surface wave at breaking and can be obtained from Miche's (1944) equation:

$$\frac{k(a_0)_{max}}{Tanh[k(h+d)]} = \frac{\pi}{14} \tag{2.47}$$

It can be seen from figure 2.7(c) that the internal waves do not have any chance to grow for ρ / ρ' around 1.00 even when the surface wave is at breaking.

2.3.2 Changing Surface Wave Amplitude

Surface wave height has a direct effect on the growth of the internal waves. This is obvious from equation 2.40, where γ / ω_0 is an increasing function of the surface wave amplitude. According to (2.40) for the internal waves to grow, $|a_0|$ must be larger than β / α, which can be regarded as a critical surface wave amplitude below which the internal waves are suppressed due to viscosity. In the dimensionless form, the growth condition can be written as

$$\frac{|a_0|}{H} > \frac{\beta / \omega_0}{\alpha H / \omega_0} \tag{2.48}$$

Experimental verification of the above will be presented in Chapter 3.

2.3.3 Changing Depth Ratio

For a given configuration when the total depth H is fixed, changing the depth ratio of the two layers, d/h, can influence the interaction process substantially. Figure 2.8(a) shows variation of the dimensionless variable $\alpha H/\omega_0$ with d/H. As seen, $\alpha H/\omega_0$ increases rapidly from $d/H = 0$ to 0.10 but takes a mild slope thereafter. An explanation for the behavior of $\alpha H/\omega_0$ at low d/H can be made by considering that as d/H increases from zero, the interface falls into the high velocity region of the surface wave field, and hence the shear around the interface intensifies. With the hypothesis that the shear is the main cause of instability, increasing the ratio d/H leads to a higher forcing. It should be noted that α is obtained from an inviscid analysis, and hence the effect of viscosity-induced forcing at low d/H ratio is not reflected in figure 2.8(a).

Variations of β/ω_0 and $k_1 d$ with d/H are plotted in figure 2.8(b). It is observed that damping is nearly constant for $k_1 d > \pi$ (deep-water range of the internal wave) while it increases rapidly when d/H approaches zero. This behavior can be explained by looking at the boundary layer formation at the bed and the interface as a result of the internal wave motion. It is recalled that in computation of β the lower layer is assumed to be viscous. Hence, theoretically there exist two boundary layers in the lower layer, one at the bed and the other at the interface. For constant H, as d becomes large, the internal waves become deep in the lower layer, and their effects on the bed diminish. Therefore, dissipation becomes independent of the depth of the lower layer at large d/H, as indicated by figure 2.8(b). In this situation, boundary layer formation is confined to the interface. On the other hand, when d/H approaches zero, the internal wave field reaches the bed, and therefore another boundary layer is formed at the bed. The smaller d, the higher the horizontal excursion of the particles near the bed as a result of the internal wave motion, and hence the more energy dissipation, as indicated by figure 2.8(b).

Rapid dissipation of the internal waves when d/H is small inhibits their growth. Figure 2.8(c) shows variation of γ/ω_0 with d/H for $a_0 = (a_0)_{max}$. For $d/H < 0.2$, which corresponds to $k_1 d < \pi$ (intermediate-depth range of the internal waves), γ/ω_0 decreases as d/H decreases until the growth rate becomes negative, and the waves are suppressed. The experimental demonstration of this trend of the growth rate will be presented in chapter 3.

2.3.4 Changing Lower Layer Viscosity

Now, attention is turned to the effect of ν, the lower layer viscosity, on the interaction. As α is obtained from an inviscid analysis, $\alpha H/\omega_0$ is expected to be independent of the viscosity. This is indicated by figure 2.9(a), where $\alpha H/\omega_0$ is plotted as a function of $\nu/\sqrt{gH^3}$ and is seen to be constant everywhere.

Variation of β/ω_0 with $\nu/\sqrt{gH^3}$ is shown in figure 2.9(b). It is observed that β/ω_0 is a linear function of viscosity. Note that in the present problem $k_1 d$ =3.25 and $k_2 d$ =3.15, which imply that the internal waves are essentially deep-water waves. Hence β/ω_0 is given by equation 2.46, where damping is a linear function of viscosity. This explains the linearity of β/ω_0 in figure 2.9(b).

Physically, one expects that high viscosity inhibits growth of the internal waves. This is consistent with the results of the analysis in figure 2.9(c), where at high enough viscosity γ/ω_0 for $a_0 = (a_0)_{max}$ is seen to be negative, implying the internal waves decay. In chapter 3 this theoretical result will be verified experimentally.

2.3.5 Changing Surface Wave Frequency

The analysis indicates that the destabilizing effect of the surface wave alters with frequency. Figure 2.10(a) illustrates variation of $\alpha H/\omega_0$ with $k_0 H$. It is seen that when the surface wave is a shallow wave, $\alpha H/\omega_0$ increases with frequency. This trend reverses after the

forcing reaches a maximum somewhere in the intermediate-depth range; the forcing drops rapidly and approaches zero at infinite depths, where the surface wave effect on the interface diminishes.

Variation of β/ω_0 with k_0H is plotted in figure 2.10(b). It is seen that at high frequencies (high values of k_0H) β/ω_0 increases with k_0H. This can be explained as follows. As the frequencies of the internal waves are proportional to the surface wave frequency, the two internal waves become essentially deep waves in the two layers when the surface wave frequency becomes high enough. In this situation, the dissipation rate of the internal waves is given by equation 2.46, which indicates β/ω_0 is an increasing function of ω_0 and hence k_0H.

Decreasing the surface wave frequency does not always result in a lower dissipation rate for the internal waves. In fact, figure 2.10(b) indicates that at low k_0H, the dissipation increases as the surface wave frequency decreases. Again, this behavior can be explained by noting that as the frequencies of the internal waves are proportional to ω_0, for enough low surface wave frequencies the motion fields of the internal waves reach the bed. This leads to the formation of the boundary layer at the bed, which contributes to faster dissipation of the internal waves as the frequency decreases.

To see how the state of the internal waves affects the trend of their dissipation, variation of β/ω_0 with k_1d is plotted in figure 2.11. The parameter k_1d is a measure of deepness of the internal wave 1 in the lower layer and is an increasing function of the surface wave frequency. As the surface wave frequency varies, k_1d and hence the deepness of the internal wave 1 in the lower layers changes. It can be seen when k_1d is around the deep-water limit ($k_1d = 3.0$), the trend of β/ω_0 reverses as pointed out above.

From the above behaviors of $\alpha H/\omega_0$ and β/ω_0, it is expected that there will be no excitation of the internal waves at high frequencies of the surface wave. This agrees with the

results of the analysis in figure 2.10(c), where γ / ω_0 for $a_0 = (a_0)_{max}$ is seen to become negative at high $k_0 H$. From figure 2.10(c), one also can see that at low surface wave frequencies the growth rate decreases as the frequency drops. As the breaking condition of the surface wave changes with frequency, $(a_0)_{max}$ is a function of $k_0 H$ in the plot of γ / ω_0 in figure 2.10(c). To isolate the effect of the surface wave frequency from the surface wave amplitude, γ / ω_0 for $a_0 = 1.00\,cm$ is also plotted in figure 2.10(c). The graph is similar in trend to that for $a_0 = (a_0)_{\max}$, and hence the foregoing arguments are also valid for the constant a_0.

2.3.6 Changing Direction of Internal Wave 1

In section 2.2, it was mentioned that there are infinite pairs of the internal waves that can form a resonant triad with a given surface wave. Now, the question arises as to which pair will occur in a real situation. To find the answer, one should look at the growth rates of the different pairs. The pair having the highest growth rate has the best chance to appear in a real situation. Experimental verification of this point will be given in chapter 3. In the following, growth properties of the pairs are compared and the pair with maximum growth rate is identified.

Each pair is identified by the direction angle of the internal wave 1, θ_1. To study all the internal waves pairs, one needs to vary θ_1 between 0 and 360°. However, the symmetries present in the problem reduce the required range to between 0 and 90°. The symmetries come from the fact that if the pair consisting of the internal wave 1 with wave number $(k_{1,x}, k_{1,y})$ and frequency ω_1, and the internal wave 2 with wave number $(k_{2,x}, k_{2,y})$ and frequency ω_2 form a resonance triad with a given surface wave, then the two pairs $\{(k_{1,x}, -k_{1,y}), \omega_1\}, \{(k_{2,x}, -k_{2,y}), \omega_2\}$ and $\{(k_{2,x}, k_{2,y}), \omega_2\}, \{(k_{1,x}, k_{1,y}), \omega_1\}$ as well can be in resonance with the surface wave. In other words, the images of the internal waves with

respect to the surface wave and also the pair resulting from interchanging the two internal waves are the other possible solutions to the resonant triad. Furthermore, according to figure 2.17, which gives variation of $\theta_2 - 180^\circ$ with θ_1, when θ_1 varies between 0 and 90°, θ_2 sweeps the range 180° to 270°. This in conjunction with the aforementioned symmetries justifies limiting the study to the range of θ_1 from 0 to 90°.

The direction of the internal wave pair has a direct effect on the forcing. Figure 2.12(a) shows variation of $\alpha H / \omega_0$ with θ_1. As seen, $\alpha H / \omega_0$ is an increasing function of θ_1 with a maximum around $\theta_1 = 90^0$.

Variation of β / ω_0 with θ_1 is illustrated in figure 2.12(b). The damping is seen to be nearly independent of the direction of the internal wave pair. This can be explained by considering that for a given configuration β is a function of the kinematic properties of the internal waves, e.g., their frequencies. According to figure 2.16, which gives variations of the kinematic properties of the internal waves with θ_1, ω_1 and ω_2 are nearly equal to $\omega_0 / 2$ regardless of θ_1. Therefore, the dissipation is also expected to be almost constant with θ_1.

From the preceding discussion, it is expected that the growth rate would be an increasing function of the direction angle. This is in accord with the model results in figure 2.12(c), where growth rate is plotted against θ_1. It is seen that in general the growth rate increases as the internal waves become more oblique to the surface wave except for angles close to the normal. According to figure 2.12(c), the growth rate has a maximum value around $\theta_1 = 90^\circ$. To find exactly where the maximum growth rate occurs, variation of γ / ω_0 with $\left|(k_2)_x / (k_1)_x\right|$ for $a_0 = (a_0)_{max}$, where subscript x refers to x-component of wave number, is plotted in figure 2.13. It can be seen that the maximum growth rate takes place when $\left|(k_2)_x / (k_1)_x\right| = 1$, that is, when $\vec{k}_1$ and $\vec{k}_2$ are symmetric with respect to $\vec{k}_0$. At this symmetric configuration, the frequencies of the internal waves are exactly equal to $\omega_0 / 2$.

This symmetric arrangement of the internal waves about the surface wave is illustrated in figure 2.14.

From the above discussion, it is expected that in a horizontally infinite medium the internal waves appear almost perpendicular to the surface wave. A computer simulation of the wave patterns at the free surface and the interface in this situation is shown in figure 2.15.

Earlier it was stated that the internal waves are short compared to the surface wave and their frequencies are nearly half of the frequency of the surface wave. The non-dimensionalized wave numbers k_0/k_1 and k_0/k_2, where $k_i = |\vec{k}_i|$, along with the non-dimensionalized frequencies ω_1/ω_0, and ω_2/ω_0 are plotted as functions of θ_I in figure 2.16. The plots indicate that the ratios k_0/k_1 and k_0/k_2 stay around 0.1, and the ratios ω_1/ω_0 and ω_2/ω_0 around 0.5, as pointed out before. Also, it is seen that the wavelengths and frequencies of the internal waves remain nearly constant as θ_I varies.

It is interesting to look at the variation of the relative angle of propagation of the internal waves, $\theta_2 - \theta_1$, as θ_1 changes. This is shown in figure 2.17. It can be seen $\theta_2 - \theta_1 \approx 180°$, and therefore at any angle θ_1, the two waves propagate nearly in opposite directions.

2.4 SUMMARY

In this chapter, a three-dimensional analysis of the interaction in a two-layer fluid was presented. The fluid system was assumed to consist of an inviscid upper layer and a weakly viscous lower layer. Following Davis and Acrivos (1967) the model was initially formulated with the assumption of inviscid layers. The viscous damping of the internal waves was included in the analysis after obtaining the evolution equations. This technique is validated in chapter 4, where a fully viscous analysis of the interaction is presented, and the results of the two analyses are compared.

The performed analysis indicated that under certain circumstances a surface wave traveling in a two-layer fluid can excite two internal waves. It was found that the internal waves are nearly identical in frequency and wavelength, and propagate in opposite directions. The frequencies of the internal waves were found to be close to $\omega_0 / 2$, and their wavelengths an order of magnitude smaller than the surface wavelength. These are typical properties of the internal waves and are in agreement with the theoretical and experimental findings of Wen (1995), Hill and Foda (1996), and Hill (1997).

The interaction analysis indicated that variation of the amplitudes of the internal waves has the exponential form $e^{\gamma t}$ at large time. The constant γ is the growth parameter and is the sum of two terms: $\alpha|a_0|$, which is a measure of the surface wave forcing in excitation of the internal waves, and $-\beta$, which is the viscous damping term. The excitation takes place when the forcing is high enough to overcome the viscous damping, that is, when γ is positive.

The independent parameters of the system are H, d, ρ', ρ, ν, g, $|a_0|$, ω_0 (or equivalently k_0), and θ_1. To evaluate the effects of each parameter on the interaction, a typical example was considered, and a sensitivity analysis was performed by changing each independent parameter separately and observing the effects on the properties of the internal waves, in particular, their evolution. The results were presented in non-dimensional forms. The main findings are summarized below.

The surface wave forcing is most affected by the depth ratio d / H, the surface wave frequency, the direction of the internal wave pair, and the surface wave height. The density ratio does not seem to have an appreciable influence on the forcing. The forcing increases with d / H as well as the surface wave amplitude. The forcing also increases when the internal waves become more oblique to the surface wave. However, the forcing decreases

with the frequency when the surface wave is a deep wave. For a shallow-water surface wave, the trend is reversed and the forcing increases with the frequency.

With respect to the dissipation of the internal waves, the density ratio, the depth ratio, the viscosity and the surface wave frequency were found to have the biggest effect. The viscous damping of the internal wave pair is nearly independent of the propagation direction of the internal wave pair. Although the forcing is nearly independent of the density difference of the two layers, the damping grows rapidly as the density difference approaches zero. The damping has the same trend when d / H decreases. For shallow-water surface waves, the damping is a decreasing function of the surface wave frequency. For deep-water surface waves, it increases with the frequency. This is in conflict with Hill's (1997) result that for high frequencies the viscous effects are negligible for the case of a viscous layer underlying an inviscid fluid. Hill's result is also in contradiction with equation 2.46, which becomes exact as $\omega_0 \to \infty$.

The parameters that significantly influence the growth of the internal waves are the depth ratio, the density difference, the viscosity, the surface wave frequency, the direction of the internal wave pair, and the surface wave amplitude. It was found that when the depth ratio d / H or the density difference is sufficiently small, the internal waves are unable to grow. The same is true when the viscosity or the surface wave frequency is high enough. These were shown to be the results of the internal wave damping.

One important result of the three-dimensional analysis was that the internal waves have a higher growth rate when they become more oblique to the surface wave. It was shown that the growth rate is maximal when the internal waves form a symmetric configuration with respect to the surface wave. In this situation the internal waves propagate nearly perpendicular to the surface wave. Also, it was found that the growth rate is an increasing

function of the surface wave amplitude. These results are found to be in agreement with Hill's (1997) theoretical study.

The analysis also indicated that for the interaction process to lead to growth of the internal waves, the amplitude of the surface wave should be bigger than a critical value. The critical amplitude is a function of the damping. As the internal waves are more damped, the magnitude of the critical amplitude increases.

Hill (1997) in his inviscid analysis of the 3D interaction found that there are narrow bands of surface wave frequency and density ratio within which only the growth of the internal waves is possible. Also, his analysis indicated that there upper and lower bounds on the direction angle of the internal wave pair for growth. These were found to be in conflict with the results of the present study. These discrepancies will be addressed in detail in chapter 3 in light of the experimental results. Another discrepancy between the two analyses is their different predictions of the interaction in two dimensions. Hill (1997) found that there is no growth of the internal waves in an inviscid medium when the internal waves are in the same plane as the surface wave. A similar result was obtained by Wen (1995), and Hill and Foda (1996) in the study of the interaction in two dimensions. However, the present analysis and those of Jamali (1997a and b) suggest that even in a two-dimensional inviscid medium the internal waves may grow.

The differences between the results of the present analysis and those of the above authors stem from the different treatments of the second-order equations. To preclude the possibility of a secular solution at second order, Wen (1995), Hill and Foda (1996), and Hill (1997) all took the solvability condition to be the orthogonality of the forcing functions and the homogenous solution. This is correct only when the systems of equations are self-adjoint. However, the systems of equations at second order are not self-adjoint, and the correct solvability condition is obtained by requiring that the forcing functions be orthogonal to the

homogeneous solution of the adjoint system (Drazin and Reid, 1981, p 385), as sought in the present analysis.

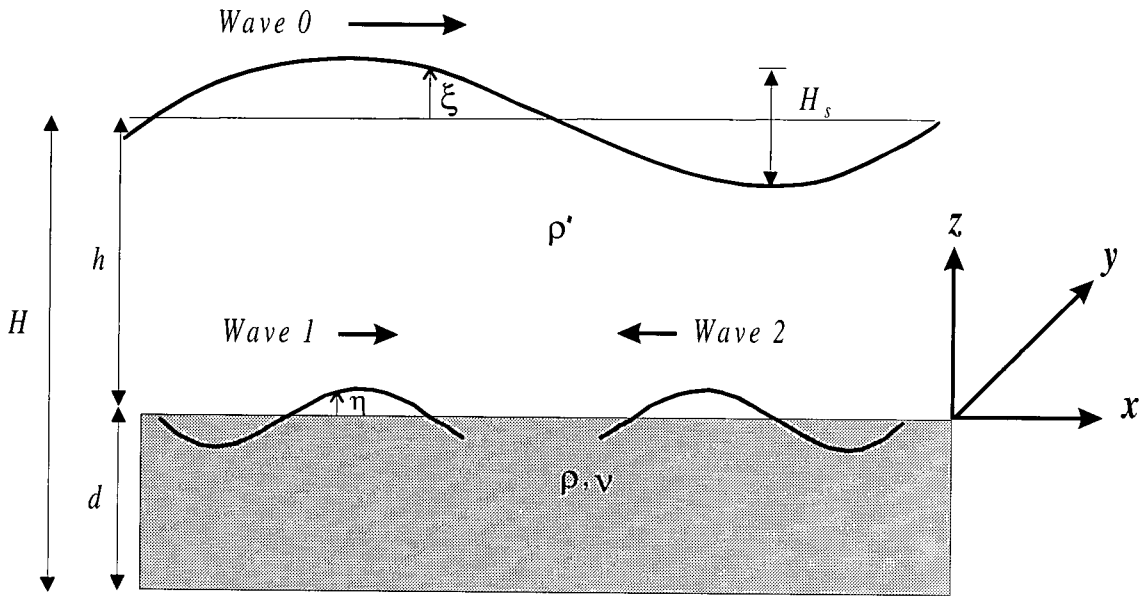

Figure 2.1 Configuration of the problem in the three-dimensional interaction analysis.

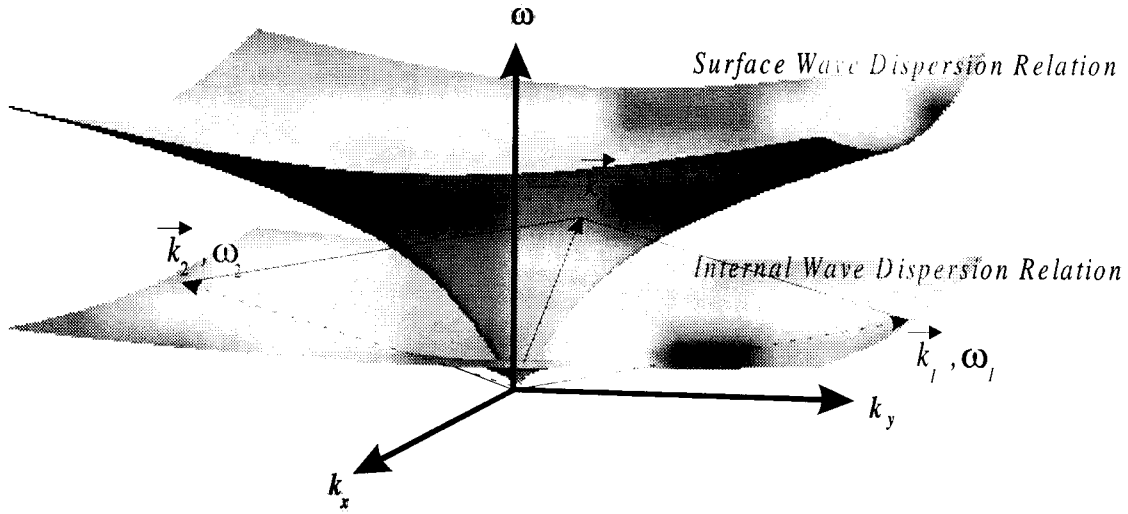

Figure 2.2 Demonstration of existence of the resonant triad in the interaction of a surface wave (denoted with subscript 0) with two internal waves (denoted with subscripts 1 and 2).

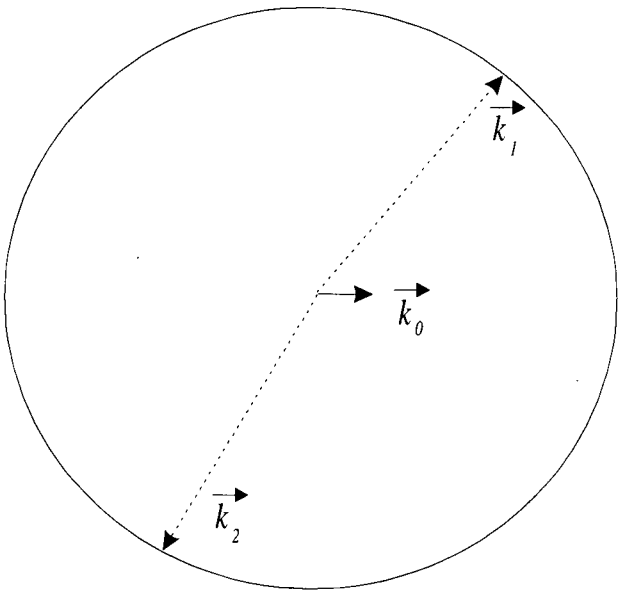

Figure 2.3 Locus of the wave numbers of the internal waves 1 and 2 in the interaction.

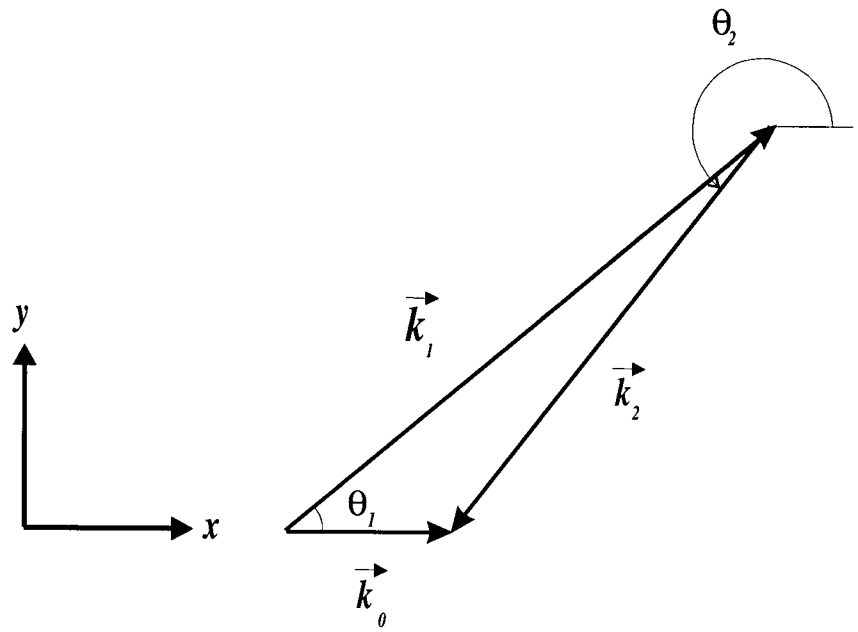

Figure 2.4 The set of two internal waves and one surface wave forming the interaction triad.

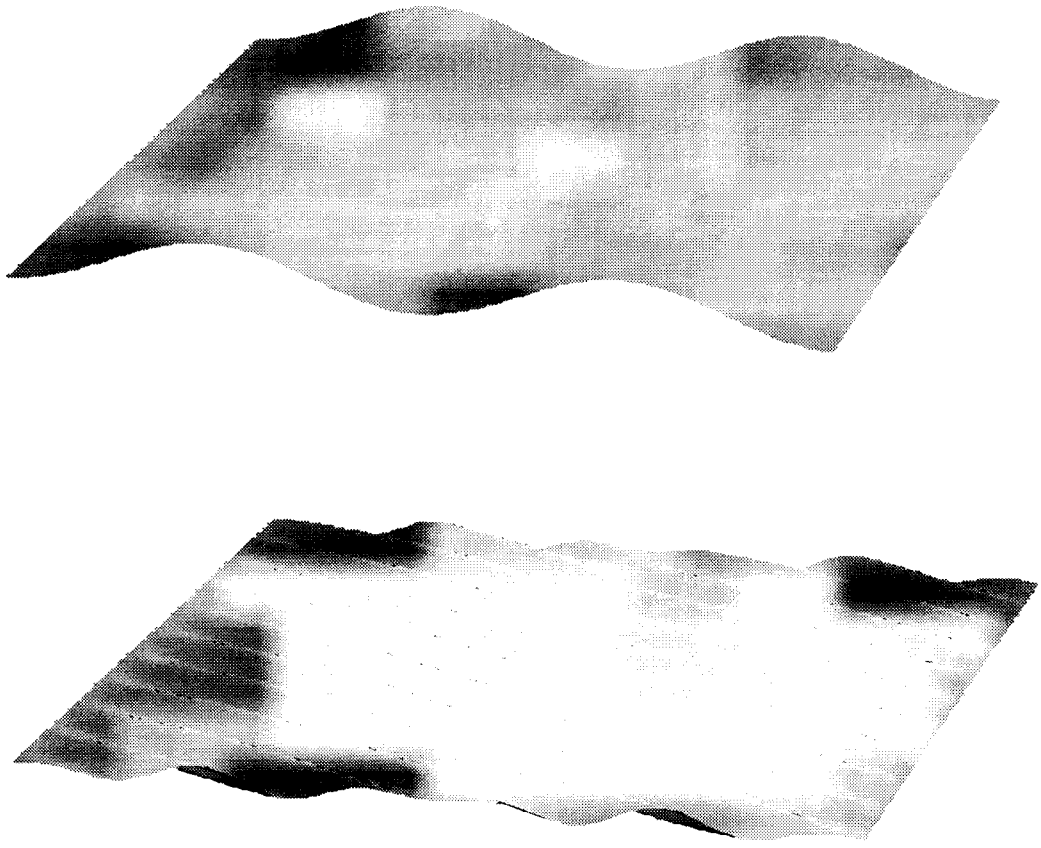

Figure 2.5 Wave patterns at the free surface and the interface at $\theta_1 = 75^\circ$.

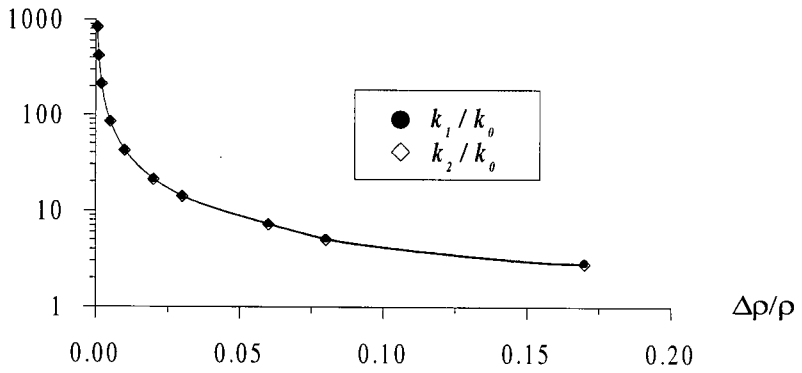

(a)

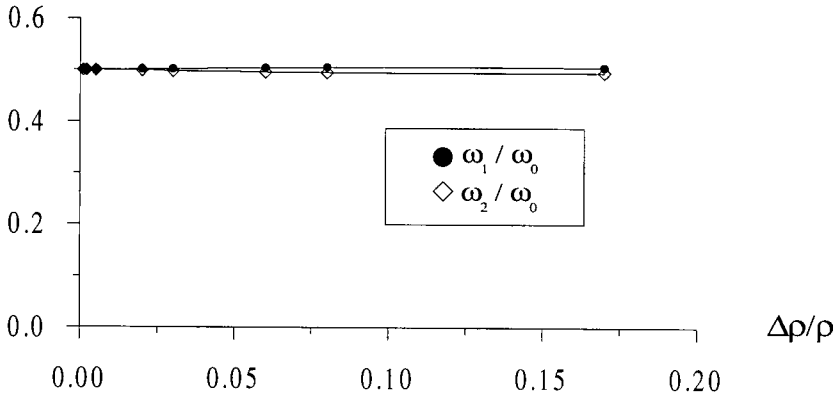

(b)

Figure 2.6 Variation of **a)** the non-dimensional internal wave numbers and **b)** non-dimensional internal wave frequencies with $\Delta\rho / \rho$.

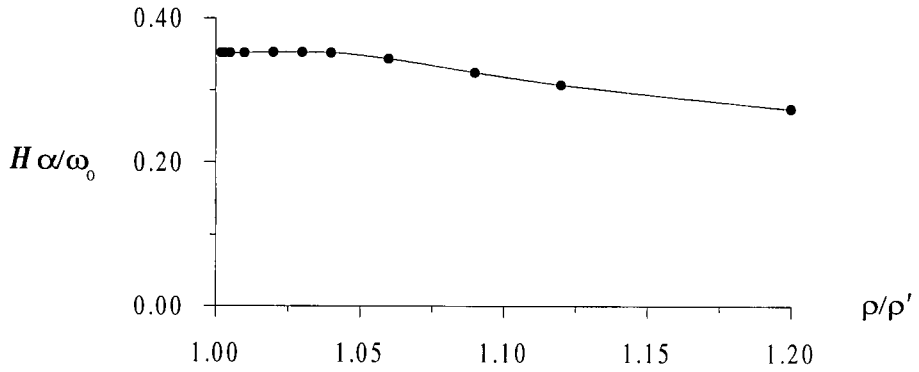

(a)

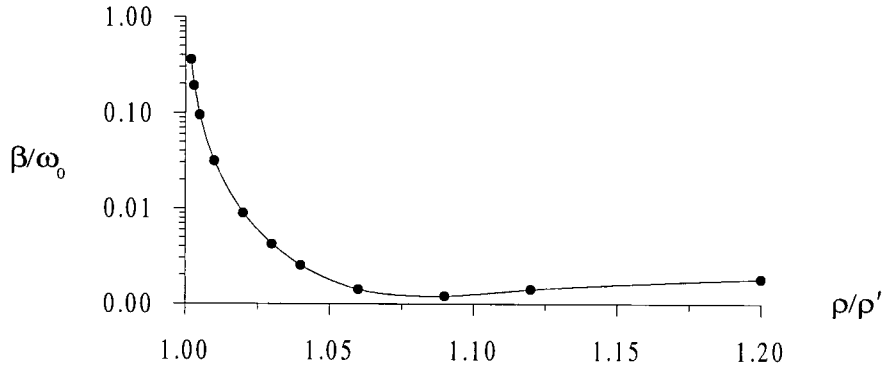

(b)

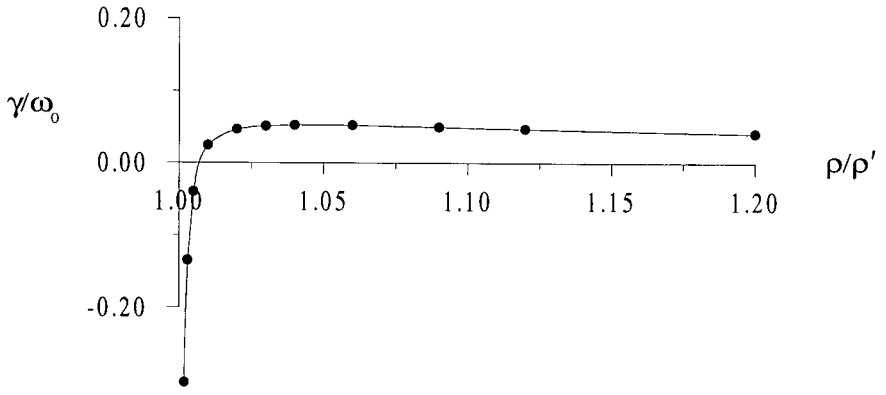

(c)

Figure 2.7 Variation of **a)** $\alpha H / \omega_0$, **b)** β / ω_0, and **c)** γ / ω_0 for $a_0 = (a_0)_{max}$ with ρ / ρ'.

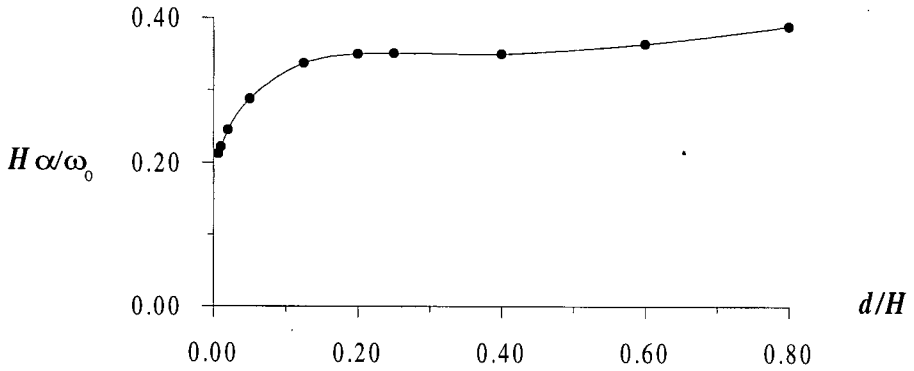

(a)

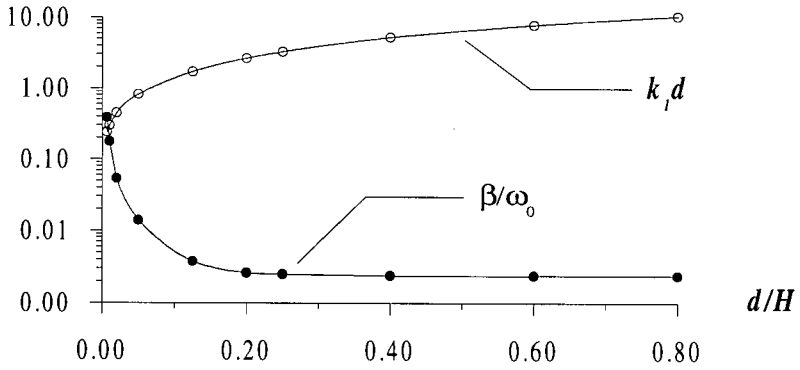

(b)

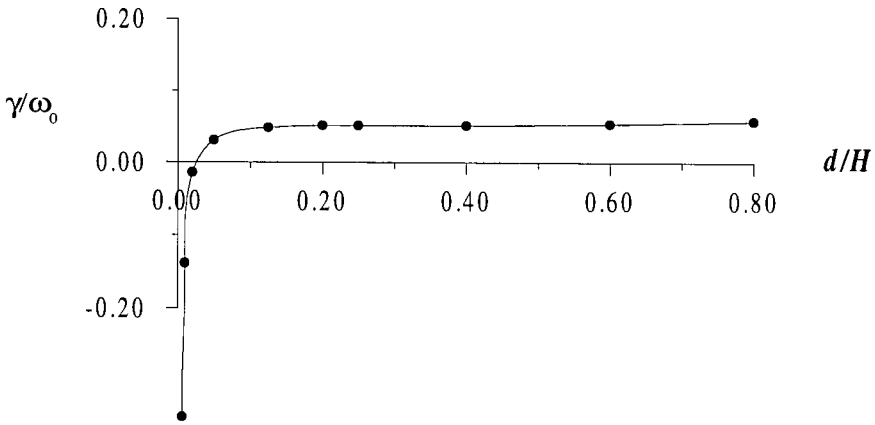

(c)

Figure 2.8 Variation of **a)** $\alpha H / \omega_0$, **b)** β / ω_0 and $k_1 d$, and **c)** γ / ω_0 for $a_0 = (a_0)_{max}$ with d / H.

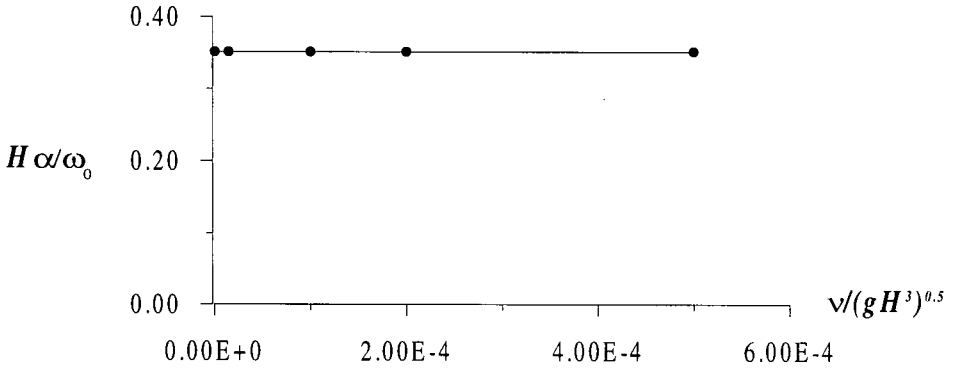

(a)

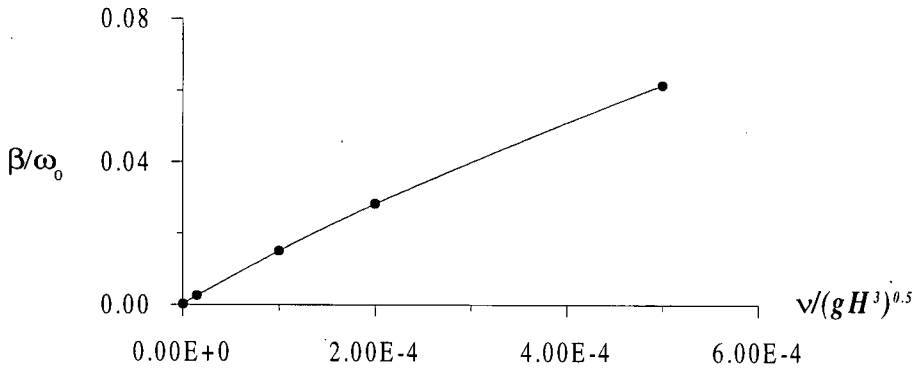

(b)

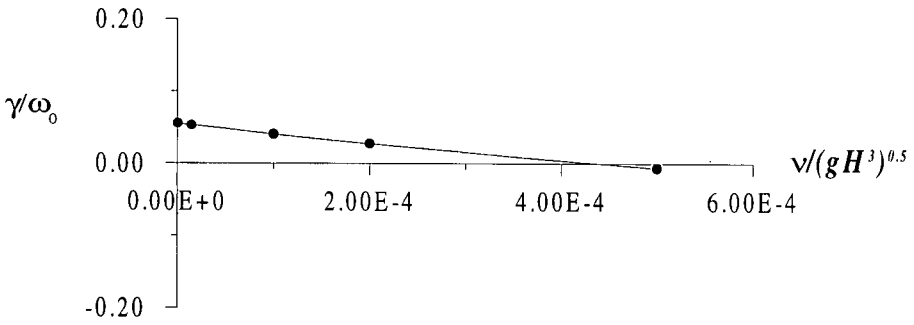

(c)

Figure 2.9 Variation of **a)** $\alpha H/\omega_0$, **b)** β/ω_0, and **c)** γ/ω_0 for $a_0 = (a_0)_{max}$ with $\nu/(gH^3)^{1/2}$.

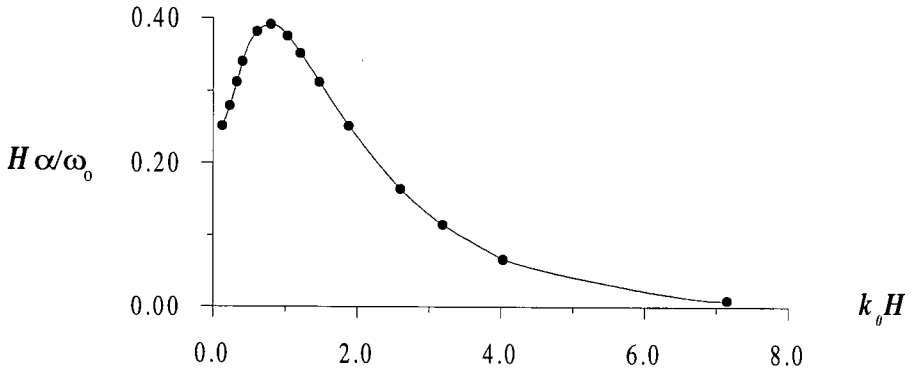

(a)

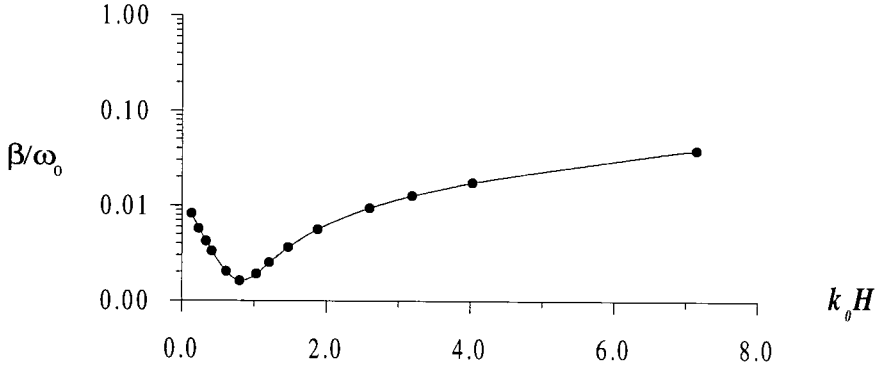

(b)

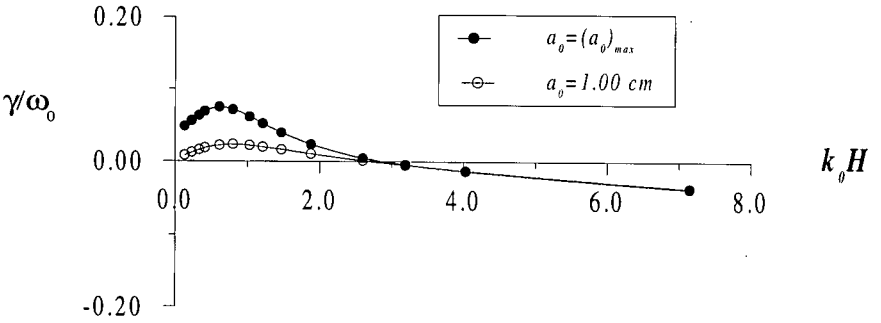

(c)

Figure 2.10 Variation of **a)** $\alpha H/\omega_0$, **b)** β/ω_0, and **c)** γ/ω_0 with k_0H.

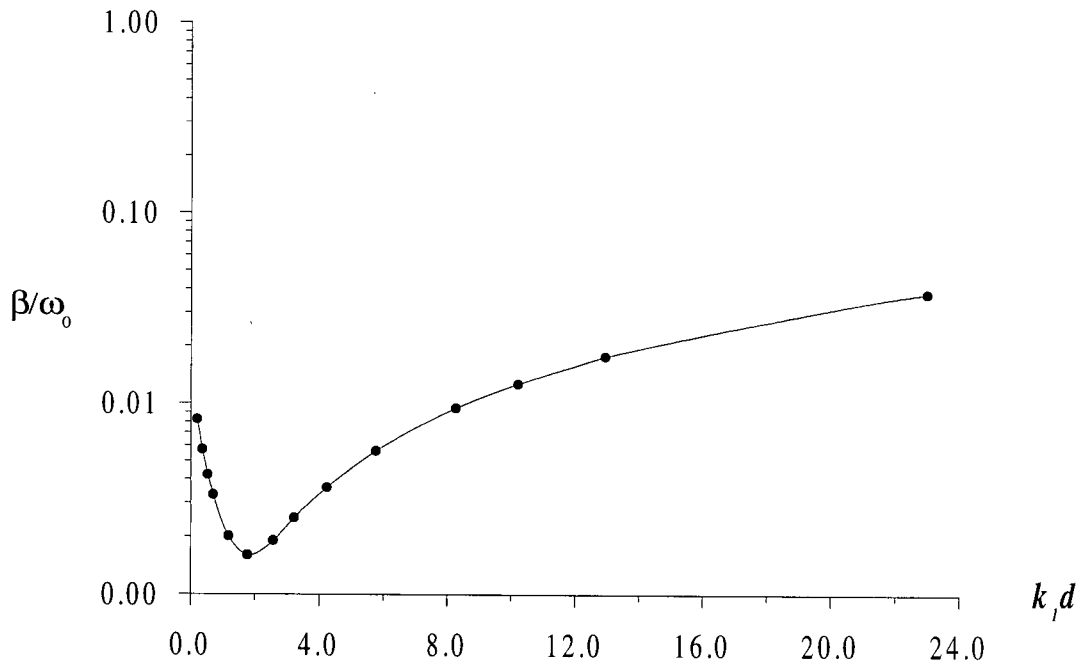

Figure 2.11 Variation of β / ω_0 with $k_1 d$.

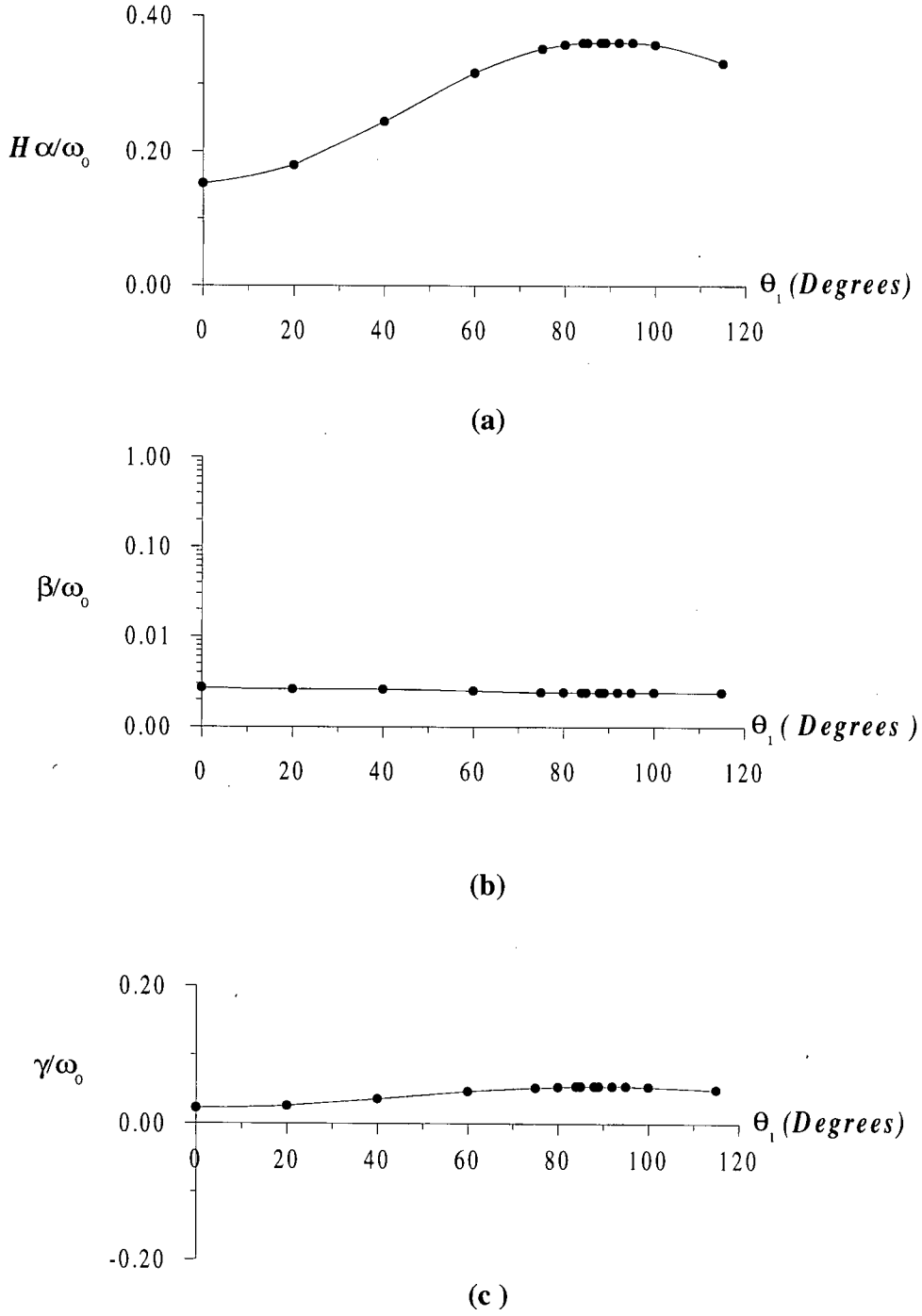

Figure 2.12 Variation of **a)** $\alpha H / \omega_0$, **b)** β / ω_0, and **c)** γ / ω_0 for $a_0 = (a_0)_{max}$ with θ_1.

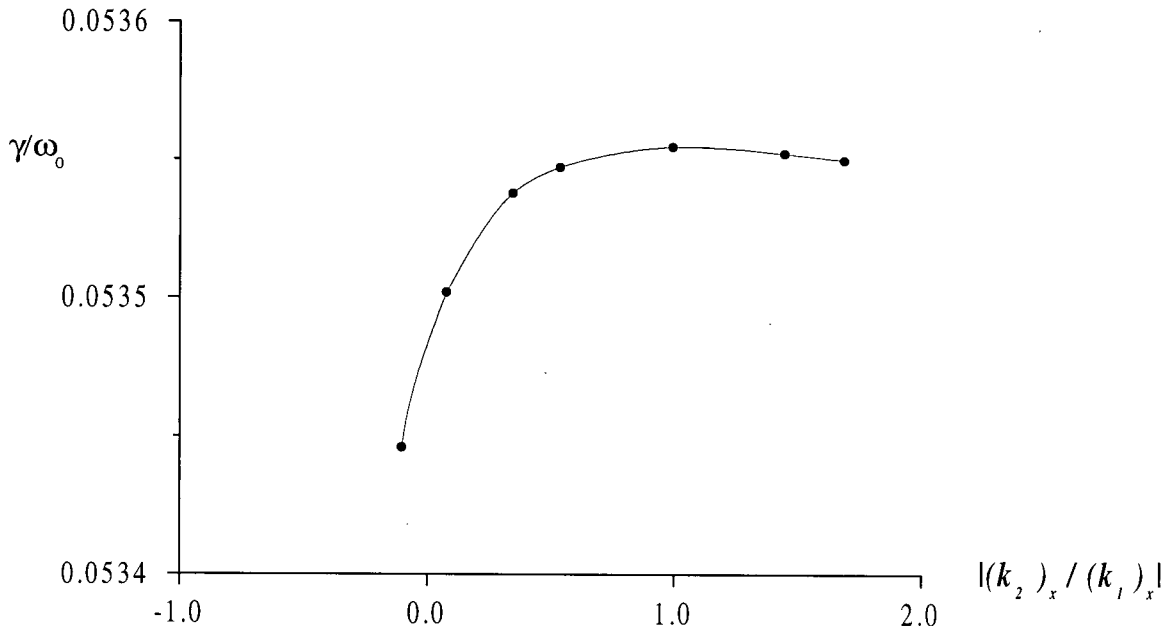

Figure 2.13 Variation of γ / ω_0 with $\left|\left(k_2\right)_x / \left(k_1\right)_x\right|$ for $a_0 = (a_0)_{max}$.

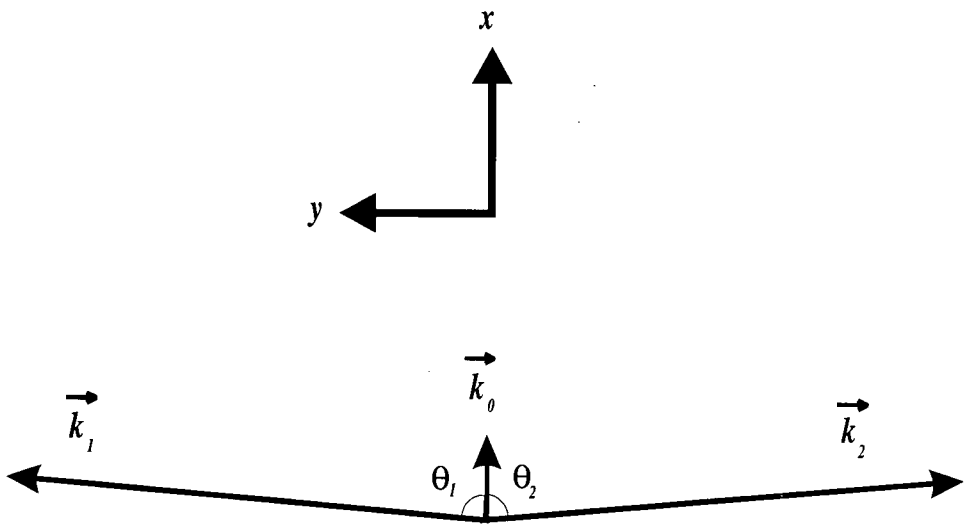

Figure 2.14 Directional configuration of the waves at the maximum growth rate, where $\theta_1 = \theta_2$.

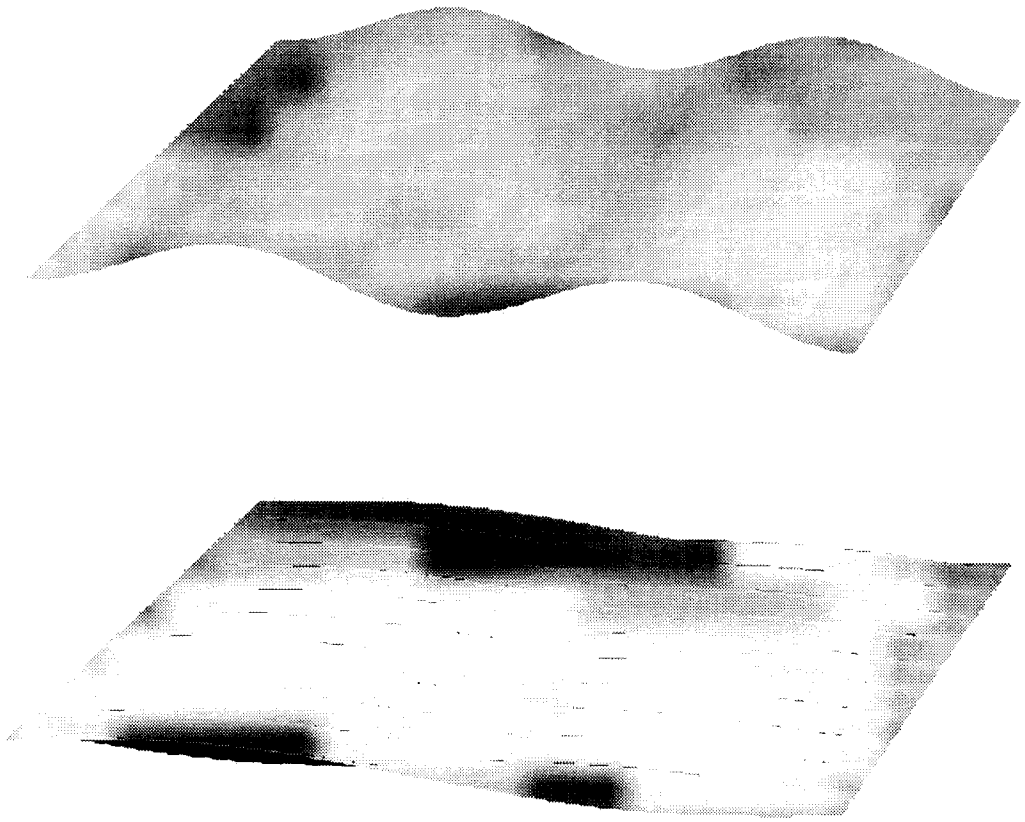

Figure 2.15 Wave patterns at the free surface and the interface at the maximum growth rate.

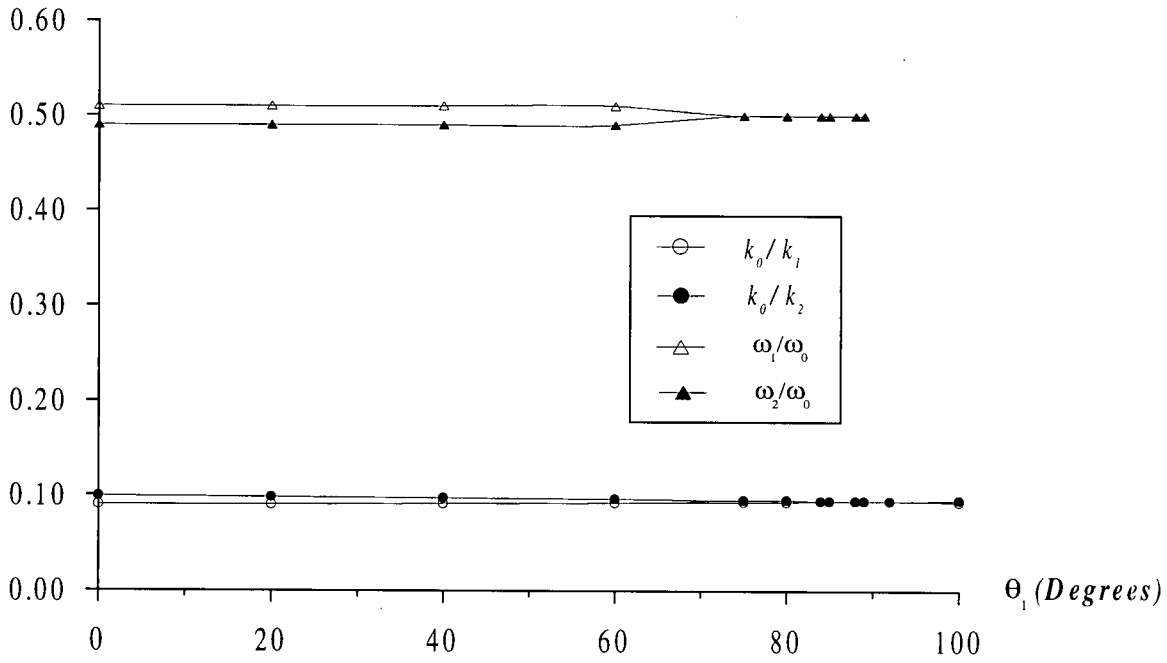

Figure 2.16 Variation of k_0/k_1, k_0/k_2, ω_0/ω_1, and ω_0/ω_2 with θ_1 .

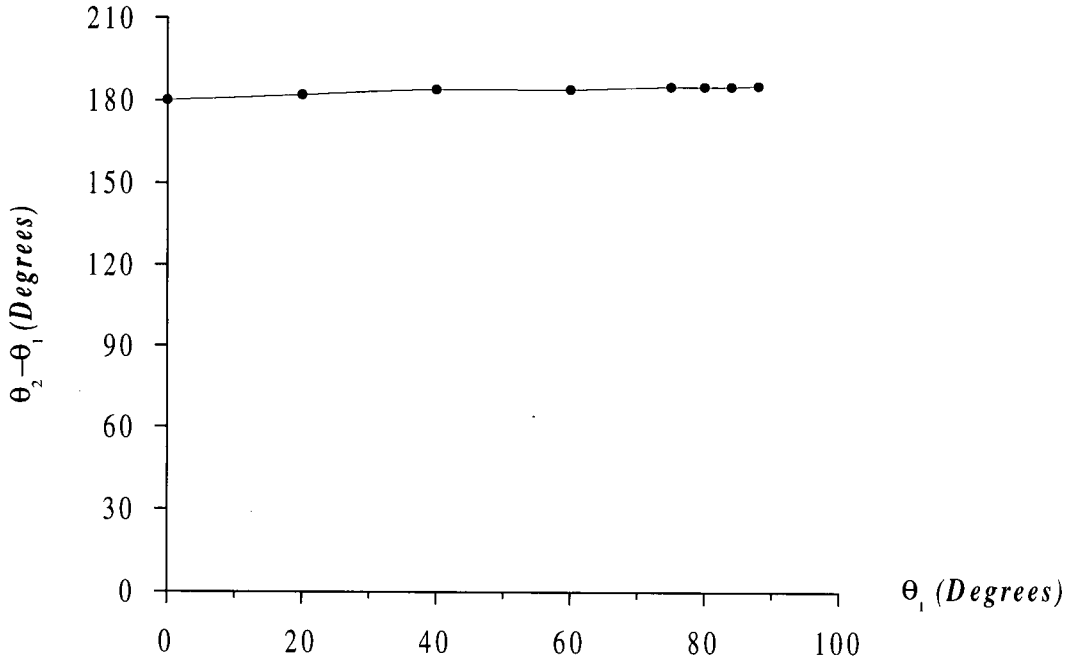

Figure 2.17 Variation of $\theta_2 - 180^\circ$ with θ_1 .

CHAPTER 3

EXPERIMENTATION

3.1 INTRODUCTION

In chapter 2, the interaction of a surface wave with two oblique, opposite-traveling internal waves was studied theoretically. It was found that the internal waves have nearly the same wave length and frequency. Their wavelengths are short compared to the surface wave, and their frequencies are nearly half of the surface wave frequency. The internal waves were found to have an exponential growth when the surface wave amplitude is bigger than a critical value. The theoretical analysis also indicated that the direction angle of the internal wave pair is an important factor in the evolution. It was shown that the more oblique the internal waves to the surface wave, the higher their growth rate. Also, it was found that the viscosity has an important role in energy dissipation of the internal waves and hence in their suppression.

In this chapter, the results of the experimental investigation of the interaction are presented. As one of the main objectives of this study has been to show the possibility of

occurrence of the interaction in a nearly inviscid medium, salt water was used as the heavier fluid in the majority of the experiments. The experiments were carried out in a laboratory wave flume at the Department of Civil Engineering, the University of British Columbia.

In the following sections, first the experimental setting is described and then the results are presented and discussed in detail. The experimental measurements are compared with the theory, and some issues raised by Hill (1997) regarding the 3D interaction are addressed.

3.2 EXPERIMENTAL SET-UP AND PROCEDURE

The experiments were carried out in a wave flume 3 meters long, 21 cm wide, and 35 cm deep. The set-up of the experiments is shown in figure 3.1. An aluminum false bottom, 5 cm deep, was used to contain the lower fluid. The false bottom had sufficiently gentle slopes at the transitions to ensure smooth surface wave motion in the flume. At one end of the flume, a perforated mat lying on a sand beach served to absorb the surface wave energy. At the other end of the flume, a wave paddle connected to a driving motor constituted the wave maker unit. The frequency and stroke of the wave maker were adjustable.

The flume was initially filled with fresh water to the desired level. Then, salt water with known density was discharged from a tank into the false bottom. The flow rate was sufficiently low to avoid mixing of the two fluids. Rodamine, a red dye, was used to visualize the saline water. The variation of the density across the interface was measured using a micro-scale conductivity probe that was profiled vertically through the two-layer fluid by a small electric motor. A video camera was used to record the experiments and to obtain the measurements of heights, frequencies and wavelengths of the surface and internal waves. The videotape of a few experiments is provided in Appendix E. The tape displays a few experiments with salt water as well as an experiment with a sediment bed.

Six series of experiments each of which was composed of several separate experiments were performed. Salt water was used as the heavier fluid in all the experiments except in series 4 where corn syrup was used instead. The density of the heavier fluid was the same within each series and ranged from about 1040 kg/m^3 to 1160 kg/m^3 between the series. Series 1, 2, and 3 served to measure mainly the kinematic properties of the internal waves. The quantities measured were wavelengths, frequencies, and direction angles of the internal waves. Also, the growth rate of the internal waves was measured in a few experiments to examine the growth properties of the internal waves as obtained by the theory in chapter 2. These series are summarized in Table 3.1. Series 4 and 5 served to investigate the effects of viscosity and surface wave amplitude on the excitation of the internal waves. These two series are summarized in Tables 3.4 and 3.5. In series 6 the effect of depth ratio on the interaction was studied. Table 3.6 outlines this series.

3.3 RESULTS AND DISCUSSION

In this section, the experimental results are presented and discussed. First, an explanation for the appearance of a three-dimensional pattern at the interface is sought. Then, the properties of the observed internal waves such as their frequencies, wavelengths and growth rate are discussed with reference to the theoretical results. Also, the effects of changing the viscosity, the depth ratio, and the surface wave amplitude on the evolution of the internal waves are explored, and the results are compared with the theory. Finally, two more phenomena observed in the wave flume are pointed out.

A simplified configuration of the fluid system is shown in figure 3.2. The total water depth is denoted by H, the upper layer depth by h, the lower layer depth by d, the surface wave height by H_s, the density of the fresh water by ρ', and the density of the heavier fluid

by ρ. The coordinate x is measured in the surface wave direction, y across the wave flume, and z vertically. The density variation across the depth is assumed to be of the form illustrated in figure 3.2, where h_ρ is half of the interface thickness.

3.3.1 3D Pattern of the Interface

In a typical experiment in the wave flume, a three-dimensional internal wave pattern was observed at the interface a few minutes after the surface wave was generated in the flume. Initially there was no interfacial wave, but as the experiment proceeded, the internal waves appeared with growing amplitude. The time of the first appearance (visibility level), the geometric properties of the pattern, and the growth rate of the internal waves were found to depend on the experimental parameters. In this section, the focus will be on the kinematic properties of the observed patterns. The growth properties of the internal waves will be discussed later.

Two successive pictures from an experiment in the wave flume are shown in figure 3.3. From the pictures as well as the companion videotape it can be seen that the observed internal wave pattern has two length-scales along the flume: a long wavelength of twice the surface wavelength, and a short wavelength. In the figure, the node and the crest of the long wavelength of the pattern are where the amplitude of the short internal waves becomes zero and maximum respectively (along the flume), and the distance between them is equal to one fourth of the wavelength.. At any point along the long wavelength, the short internal waves have the same amplitude across the flume. The pictures also indicate that the internal waves are standing across flume.

The next feature of the observed pattern is its frequency. Five successive pictures of the internal waves taken from a close view at an interval of $T_0/2$, where T_0 is the period of the surface wave, are presented in figure 3.4. It is interesting to note that at the short length-scale

the internal wave pattern is standing both across and along the flume with a period of $2T_0$, equivalent to a frequency of $\omega_0/2$. These can also be seen from the companion videotape.

In the formation of the three-dimensional pattern, the flume side-walls play a crucial role. It is recalled from chapter 2 that the internal waves have a higher growth rate when they are oblique to the surface wave. As a result, the internal waves are expected to appear as oblique waves in the flume. However, the flume has finite width, and the internal waves are reflected from the side-walls. This leads to the generation of the image internal waves $1'$ and $2'$ besides the original internal waves 1 and 2 as illustrated in figure 3.5. Since the internal waves have the same wave numbers normal to the surface wave, see the resonance conditions (2.1), the four internal waves have the same wavelength l_y across the flume. The combination of each internal wave and its image forms a wave pattern that is standing across the flume. This requires that the flume width be an integral number of the half-wavelength of the internal wave across the flume. In other words,

$$l_y = \frac{2B}{n-1} \tag{3.1}$$

where $B =$ width of the flume, equal to 21.1 cm in the experiments, and $n =$ the total number of the peaks and the troughs of the three-dimensional pattern across the flume.

Considering the above, the developed theory in chapter 2 can now be used to explain the observed phenomenon. It is shown that the combination of the original internal waves 1 and 2 and their reflections, waves $1'$ and $2'$, leads to the creation of the observed three-dimensional pattern with the mentioned properties. It is important to note that from the symmetric properties of the interaction discussed in section 2.3.6, when the surface wave is in resonance with the internal waves 1 and 2, it is in resonance with their reflections, waves $1'$ and $2'$, as well. Hence, the mechanism of generation of the three-dimensional pattern can be

summarized as in figure 3.6. The internal waves 1 and 2 are assumed to have frequencies ω_1 and ω_2, and wave numbers

$$\vec{k}_1 = (k_{1,x}, k_{1,y}) \quad \text{and} \quad \vec{k}_2 = (k_{2,x}, k_{2,y}) \tag{3.2}$$

respectively. With reference to figure 3.5, since the surface wave does not have any component in the *y*-direction

$$k_{1,y} = -k_{2,y} = 2\pi / l_y \tag{3.3}$$

where l_y is given by (3.1). The reflected internal waves $1'$ and $2'$ have frequencies ω_1 and ω_2, and wave numbers

$$\vec{k}_1' = (k_{1,x}, -k_{1,y}) \quad \text{and} \quad \vec{k}_2' = (k_{2,x}, -k_{2,y}) \tag{3.4}$$

respectively. The resonance conditions for the triad involving the image internal waves are

$$\begin{aligned} \vec{k}_0 &= \vec{k}_1' + \vec{k}_2' \\ \omega_0 &= \omega_1 + \omega_2 \end{aligned} \tag{3.5}$$

Assuming that the four internal waves have the same amplitude $\bar{b}$, the interface displacement $\eta_{\text{int}}(x, y, t)$ associated with their superposition is

$$\eta_{\text{int}}(x, y, t) = \bar{b}\left\{Sin(\vec{k}_1.\vec{x} - \omega_1 t) + Sin(\vec{k}_2.\vec{x} - \omega_2 t) + Sin(\vec{k}_1'.\vec{x} - \omega_1 t) + Sin(\vec{k}_2'.\vec{x} - \omega_2 t)\right\} \tag{3.6}$$

where $\vec{x} = (x, y)$. For convenience, the waves have been assumed to be in phase. Using the trigonometric relations, equation 3.6 can be written as

$$\begin{aligned} \eta_{\text{int}}(x, y, t) = {} & 2\bar{b}\,Sin\left(\frac{\vec{k}_1 + \vec{k}_2}{2}.\vec{x} - \frac{\omega_1 + \omega_2}{2}t\right) Cos\left(\frac{\vec{k}_1 - \vec{k}_2}{2}.\vec{x} - \frac{\omega_1 - \omega_2}{2}t\right) \\ & + 2\bar{b}\,Sin\left(\frac{\vec{k}_1' + \vec{k}_2'}{2}.\vec{x} - \frac{\omega_1 + \omega_2}{2}t\right) Cos\left(\frac{\vec{k}_1' - \vec{k}_2'}{2}.\vec{x} - \frac{\omega_1 - \omega_2}{2}t\right) \end{aligned}$$

After using the resonance conditions (2.1) and (3.5), the above is simplified to

$$\eta_{\text{int}}(x,y,t) = 2\bar{b}\,Sin\left(\frac{\vec{k}_0}{2}.\vec{x} - \frac{\omega_0}{2}t\right)\left\{Cos\left(\frac{\vec{k}_1 - \vec{k}_2}{2}.\vec{x} - \frac{\omega_1 - \omega_2}{2}t\right) + Cos\left(\frac{\vec{k}_1' - \vec{k}_2'}{2}.\vec{x} - \frac{\omega_1 - \omega_2}{2}t\right)\right\}$$

Using the sum rule for the cosines, the right hand side can be written as a product of the terms:

$$R.H.S. = 4\bar{b}\,Sin\left(\frac{\vec{k}_0}{2}.\vec{x} - \frac{\omega_0}{2}t\right)Cos\left(\frac{\vec{k}_1 - \vec{k}_1' - (\vec{k}_2 - \vec{k}_2')}{4}.\vec{x}\right)Cos\left(\frac{\vec{k}_1 + \vec{k}_1' - (\vec{k}_2 + \vec{k}_2')}{4}.\vec{x} - \frac{\omega_1 - \omega_2}{2}t\right)$$

Defining

$$k_y = \frac{2\pi}{l_y} \tag{3.7}$$

and noting that $\vec{k}_1 + \vec{k}_1' = (2k_{1,x},0)$, $\vec{k}_1 - \vec{k}_1' = (0,2k_y)$, $\vec{k}_2 + \vec{k}_2' = (2k_{2,x},0)$, and $\vec{k}_2 - \vec{k}_2' = (0,-2k_y)$, the expression for η_{int} reduces to

$$\eta_{\text{int}}(x,y,t) = 4\bar{b}\,Cos(k_y y)Sin\left(\frac{\vec{k}_0}{2}.\vec{x} - \frac{\omega_0}{2}t\right)Cos\left(\frac{k_{1,x} - k_{2,x}}{2}x - \frac{\omega_1 - \omega_2}{2}t\right) \tag{3.8}$$

By inspecting (3.8), the experimental observations can now be explained. First, attention is paid to the variation of η_{int} in the y-direction. In (3.8), the term describing the variation along y-axis, i.e., $Cos(k_y y)$, has appeared as a factor on the right hand side. Knowing that $l_y = 2\pi / k_y$ satisfies (3.1), this implies that the internal wave pattern is standing across the flume, consistent with the experimental observations.

The variations in time and x are described by the last two terms on the right hand side of (3.8). These terms are of different length and time scales. It can be shown from the ordering analysis of section 2.3.1 that $k_0/2 \sim O(1)$, and $(k_{1,x} - k_{2,x})/2 \sim O(1/\delta)$, where $\delta = \Delta\rho/\rho$ is small. Hence, there exist a long and a short scale for the variation along the x-axis. The experimental pictures in figure 3.3 clearly show these two length-scales. From the equation

the wave number of the large length-scale is $k_0/2$. This is in agreement with the measurements in figure 3.3, where the long wavelength of the internal wave pattern is seen to be twice the surface wavelength. According to equation 3.8, at the short scale the internal waves have a wave number of $(k_{1,x}-k_{2,x})/2$ along the flume. Note that in general $k_{1,x}$ and $k_{2,x}$ are of opposite sign, and hence $(k_{1,x}-k_{2,x})/2$ represents an average of the magnitudes of the x-components of $\vec{k}_1$ and $\vec{k}_2$. Defining $\bar{k}_x$ as

$$\bar{k}_x = \frac{k_{1,x}-k_{2,x}}{2} \tag{3.9}$$

it will be shown in section 3.3.2 that $\sqrt{\bar{k}_x^{\,2}+k_y^{\,2}}$ is in close agreement with the experimental measurements. In general the wave number of the internal waves across the flume, k_y, is of the same order as $\bar{k}_x$. The quantity $\sqrt{\bar{k}_x^{\,2}+k_y^{\,2}}$ is the wave number of the 3D standing wave in figure 3.4.

Now attention is turned to the time-scales of the internal waves as predicted by equation 3.8. From the ordering analysis of section 2.3.1 it can be shown that $\omega_0/2 \sim O(1)$, and $(\omega_1-\omega_2)/2 \sim O(\delta)$. Hence, there exist a long and a short scale for the time variation of the internal waves. According to (3.8), in short time-scale the internal waves have a frequency of $\omega_0/2$, consistent with the experimental observations. It is interesting to note that at the short time- and length-scale equation 3.8 can be approximated by

$$\eta_{\text{int}}(x,y,t) = 4\bar{b}\,Cos(k_y y)Cos(\bar{k}_x x)Sin\left(-\frac{\omega_0}{2}t\right) \tag{3.10}$$

indicating that the internal waves form a 3D standing internal wave (both along and across the flume) with a frequency of $\omega_0/2$, a fact clearly indicated by figure 3.4.

According to equation 3.8 in long time-scale the internal wave pattern has a frequency of $(\omega_1-\omega_2)/2$ (of order δ). Unlike the short time-scale, it is difficult to measure this time-scale accurately in the laboratory due to experimental errors. However, the long time-scale

can be identified in the videotaped experiments by observing that although the 3D standing internal wave looks stationary, it moves slowly in the surface wave direction and is unsteady in the long run, indicating a quasi-standing state.

Before leaving this section, it is worth noting that according to equation 3.8 the long wavelength of the three-dimensional pattern moves at the same speed as the surface wave. This is clear from the two successive pictures in figure 3.3, where it is seen that the internal waves with the largest amplitude and the surface wave crest move with the same speed. This can be seen by playing back slowly the companion videotape as well.

3.3.2 Wavelength of the Standing Internal Wave

The experiments in which the x and y components of the wavelength of the 3D standing internal wave, $\bar{l}_x$ and l_y, were measured are summarized in Table 3.1. In the table, the first digit in the experiment number indicates the series number. The surface wave period is denoted by T_0. For each experiment the interface half thickness h_ρ and $\Delta\rho = \rho - \rho'$ have been obtained from a regression analysis of density profile across the interface. The measured wavelength of the standing internal wave along the flume (x-axis) is denoted by $\bar{l}_x$. Note that $\bar{l}_x$ is related to $\bar{k}_x$ in equation 3.10 by

$$\bar{k}_x = 2\pi / \bar{l}_x \qquad (3.11)$$

The quantity $\bar{l}_x$ can be regarded as an average of the x-components of the wavelengths of the internal waves 1 and 2. The experimental value of l_y for each case is given in the second last column. It was calculated from (3.1) using the observed value of n, which is given in the third last column for each experiment. The experimental values of n are compared with those from the theory in section 3.3.4. In the experiments, internal wave patterns with

different n's were observed. Figure 3.7 gives pictures of some of the observed modes of the standing internal wave.

In the last column of Table 3.1, the direction angle $\bar{\theta}$ in each experiment is given for later use. Having $\bar{l}_x$ and l_y, $\bar{\theta}$ for each experiment is calculated from the following equation.

$$\bar{\theta} = ArcTan\left(\frac{\bar{k}_y}{k_x}\right) = ArcTan\left(\frac{\bar{l}_x}{l_y}\right) \tag{3.12}$$

The angle $\bar{\theta}$ can be regarded as an average of θ_1 and $\theta_2 - \pi$ in figure 3.5. Note that in general $\theta_1 \approx \theta_2 - \pi$, see figure 2.17, and hence $\bar{\theta} \approx \theta_1 \approx \theta_2 - \pi$.

A typical variation of the density across the interface in the experiments along with the corresponding regression curve is given in figure 3.8. As density had nearly *tanh* variations with z in the experiments, the regression curve in figure 3.8 was obtained from fitting equation $\rho(z) = c_1 + c_2\ tanh[c_3(z + c_4)]$ to the data points. The constants c_1, c_2, c_3, and c_4 were obtained using the least-squares method. Constant c_3 gives the parameter h_ρ in Table 3.1 for each experiment.

Having obtained $\bar{l}_x$ and l_y of the standing wave in each experiment, one then can compute the wavelength of the standing internal wave $l_{exp} = \left(\bar{l}_x^{-2} + l_y^{-2}\right)^{-1/2}$. These are tabulated in the second column of Table 3.2. In the following the theoretical wavelengths are obtained and compared with l_{exp}'s.

According to Appendix A, the dispersion relation for a wave motion in a two-layer fluid with finite depths is

$$\frac{\frac{\rho'}{\rho}(\omega^4 - g^2k^2)\tanh(kh)}{(gk\tanh(kh) - \omega^2)} + gk - \omega^2 \coth(kd) = 0 \tag{3.13}$$

Equation 3.13 is used to compute a theoretical wavelength for each experiment. These computed wavelengths are denoted by $l_{two-layer}$ and are tabulated in the third column of Table

3.2. In computation of $l_{two-layer}$, the internal wave frequency was assumed to be $\omega_0/2$. Note that in $\sqrt{\bar{k}_x^{\,2}+k_y^{\,2}}$, $\bar{k}_x$ is the average of the x-components of the wave numbers of the internal wave 1 with $\omega_1 > \omega_0/2$ and the internal wave 2 with $\omega_2 < \omega_0/2$ (see the resonance conditions 2.1), and k_y is the same in both waves. Knowing that ω_1 and ω_2 are close to $\omega_0/2$, $\sqrt{\bar{k}_x^{\,2}+k_y^{\,2}}$ can be well approximated by the wave number of an internal wave with frequency $\omega_0/2$. These theoretical wavelengths are plotted against the experimental values in figure 3.9. As seen, all the theoretical wavelengths are greater than the experimental ones. This can be explained by the fact that in the experiments the interface of the two layers was diffuse. To account for the diffusion effects, one needs to have the dispersion relation for the internal wave motion in a 2-layer, finite-depth system with a diffuse interface. Not having access to such a dispersion relation, here an attempt is made to obtain the desired theoretical wavelength approximately.

Let l_t denote the desired theoretical wavelength. l_t is a function of the diffuse-layer half thickness h_ρ, and the depths of the two layers, h and d. It can be shown that in all the experiments the standing internal wave was deep in the upper layer. Therefore, l_t can be regarded independent of the upper-layer depth, and there is no need to consider variations in h. Mathematically, one can say $l_t = l_t(h_\rho, 1/d)$ assuming the other parameters of the system remain unchanged. Using Taylor's series expansion, one can approximate $l_t(h_\rho, 1/d)$ as

$$l_t(h_\rho, 1/d) \approx l_t(0,0) + \left.\frac{\partial l_t}{\partial(1/d)}\right|_{(0,0)} \cdot\frac{1}{d} + \left.\frac{\partial l_t}{\partial h_\rho}\right|_{(0,0)} \cdot h_\rho \qquad (3.14)$$

with the assumption that h_ρ and $1/d$ are small enough. The quantity $l_t(0,0)$ is the internal wavelength when $h_\rho = 0$ and $d = \infty$. It corresponds to the internal wave motion in an infinite two-layer fluid. It is obtained from (Turner 1973, p.16)

$$\omega^2 = gk\frac{(\rho-\rho')}{(\rho+\rho')} \tag{3.15}$$

Next, the right hand side of (3.14) is rearranged to

$$\left[l_t(0,0)+\left.\frac{\partial l_t}{\partial(1/d)}\right|_{(0,0)}.\frac{1}{d}\right]+\left[l_t(0,0)+\left.\frac{\partial l_t}{\partial h_\rho}\right|_{(0,0)}.h_\rho\right]-l_t(0,0) \tag{3.16}$$

In (3.16), the first bracket is approximately the wavelength when $1/d$ is not zero, but $h_\rho = 0$. Therefore, the first bracket can be replaced with $l_{two-layer}$. The second bracket in (3.16) corresponds approximately to the wavelength of the internal wave when $1/d = 0$ but $h_\rho \neq 0$. This wavelength is denoted by $l_{diffuse}$, which is the wavelength of the internal wave in an infinite two-layer medium with a diffuse interface of *tanh* form. The appropriate dispersion relation for $l_{diffuse}$ is given by (Groen ,1948)

$$k = \left(\frac{\varepsilon_\rho . g}{2\omega^2} - h_\rho\right)^{-1} \tag{3.17}$$

where

$$\varepsilon_\rho = ln\left(\frac{\rho}{\rho'}\right) \tag{3.18}$$

Having density properties of the interface, one can use the above dispersion relation to obtain $l_{diffuse}$ with the assumption that $\omega = \omega_0 / 2$.

With the preceding approximations, (3.14) can now be replaced with

$$l_t \approx l_{two-layer} + l_{diffuse} - l_t(0,0) \tag{3.19}$$

The values of l_t obtained from (3.19) are given in the 4th column of Table 3.2. In Fig 3.10, l_t values have been compared with the experimental wavelengths. It can be seen that now a close agreement between the experiments and the theory exists.

3.3.3 Growth Rate of the Internal Waves

It is recalled from the theoretical study of chapter 2 that the amplitudes of the internal waves change exponentially at large time, i.e.,

$$b_i \sim e^{\gamma t} \tag{3.20}$$

where b_i is half of the internal wave amplitude. The parameter γ, which is an indicator of the growth rate of the internal waves, is given by equation 2.40

$$\gamma = -\beta + \alpha|a_0| \tag{2.18}$$

where $-\beta$ is the dissipation term, α is a measure of efficiency of the energy transfer between the waves, and $|a_0|$ is half of the surface wave amplitude, equal to $H_s/4$.

Among the experiments performed, two were repeated with different surface wave amplitudes. The variations of the amplitude of the standing wave with time in experiment 3-1 are plotted in figure 3.11 for the surface wave heights of 2.1 cm, 2.6 cm, 3.4 cm, and 3.6 cm. Figure 3.12 presents the similar plots for experiment 3-3 for surface wave heights of 1.6 cm, 2.7 cm, and 2.9 cm. To obtain γ for each surface wave height, the exponential function $2b_i(t) = c_1 e^{\gamma t}$ was fitted to the data points using the least-squares technique, and the result was plotted on the same graph. The regression factor r_g is indicated for each case on the graph.

An interesting result from the plots of the regression curves regards their prediction of the internal wave amplitude at $t = 0$. Although $b_i \approx 0$ at $t = 0$ was not included as a data point in any of the plotted data sets, the regression curves all nearly passed through the origin. This along with the values of r_g close to 1.00 in all the cases (> 0.99 in experiment 3.1, and ≥ 0.96 in experiment 3.3) is an indication of the exponential growth of the internal waves with time in the flume, as predicted by the theory.

Plots of γ versus $|a_0|$ for experiments 3-1 and 3-3 are given in figure 3.13. Theoretically, the relationship between γ and $|a_0|$ is linear. Hence, for each case a line was fit to the data points using the least-squares method. The slope of the line in each case gives the parameter α, see (2.18). The regression factors have been indicated on the graphs. It is interesting to note that the points corresponding to the high amplitudes lie off the line. This can be attributed to the non-linearity of the surface wave at the high amplitudes. It is recalled that the proposed theory was developed assuming nearly linear waves. Nevertheless, in the experiments increasing the amplitude of the surface wave did not affect the interfacial pattern.

Table 3.3 compares the experimental values of α obtained above with the theory. The theoretical values of α have been obtained using the three-dimensional model of chapter 2 with the assumption that the internal waves are traveling in the same direction as in the corresponding experiments. The last column in Table 3.3 gives $k_{exp}h_\rho$ where $k_{exp} = 2\pi / l_{exp}$. This parameter is a measure of significance of diffusivity of the interface in the interaction; the higher $k_{exp}h_\rho$, the bigger the effect of the diffuse layer on the motion of the internal waves and hence on the interaction.

As seen from Table 3.3, although the experimental and the theoretical values of α are of the same order of magnitude, they are not in close agreement. In fact, the theoretical values are higher. This can be explained by noting that α_{theory} has been obtained from an analysis that does not take into account the effects of a diffuse interface on the interaction. In a real situation, a diffuse interface smoothes the velocity variation at the interface and hence reduces the magnitude of the forcing for excitation of the internal waves (Davis and Acrivos, 1967), represented by the parameter α. This explanation is consistent with the experimental results presented. In Table 3.3 α_{theory} for experiment 3-1 with $k_{exp}h_\rho = 0.041$ is in a better agreement with the experimental value than α_{theory} for experiment 3-3 with a higher $k_{exp}h_\rho$.

It is expected that a more sophisticated theory that takes into account the effects of the diffuse interface on the interaction would yield a better agreement between experiment and theory.

The plots in figure 3.13 can also be used to calculate the damping parameter β in each experiment knowing that the y-intercept of the regression line in each case is equal to $-\beta$. However, the experimental values can not be compared with those from the theory. In the salt-water experiments the two layers had similar viscosities, and there existed boundary layers at the flume sides, the free surface, the interface, and the flume floor. In contrast, the proposed equation 2.33, from which β is computed, is valid only when the lower layer is much more viscous than the upper layer. In addition, since the upper layer is assumed to be inviscid, the equation does not take into account the effects of the boundary layers at the flume sides and those in the upper layer at the free surface and the interface. Note that internal wave dissipation due to the neglected boundary layers is of the same order as that by the rest.

3.3.4 Direction Angle of the Internal Waves

According to the theoretical analysis of chapter 2, the internal waves have a higher growth rate when they are more oblique to the surface wave. Hence, it is expected that in the wave flume the internal waves would occur at the maximum possible $\bar{\theta}$. First it should be noted that unlike an infinite medium, a finite-width wave flume restricts the values of k_y through equation 3.1, and hence for a given configuration the internal waves can admit only certain directions. The admissible angles $\bar{\theta}$ satisfy

$$Sin\bar{\theta} = \frac{k_y}{\bar{k}} = \frac{\pi(n-1)}{B\bar{k}} \qquad (3.21)$$

where $n \geq 1$ is an integer, and $\bar{k} = \sqrt{\bar{k}_x^{\,2} + k_y^{\,2}}$. Note that $\bar{k}$ is almost independent of the direction angle, e.g., see figure 2.16, and hence can be regarded as a constant in (3.21). The

admissible angles for $\vec{k}_1$ are shown schematically in figure 3.14. Note that the y-component of $\vec{k}_1$ at each angle is a multiple of π / B as dictated by equation 3.1. According to equation 3.21, a higher growth rate requires a bigger n. However, since $Sin(\bar{\theta}) \leq 1$, and hence

$$\frac{\pi(n-1)}{B\bar{k}} \leq 1, \tag{3.22}$$

n can not be unbounded. For a given configuration the maximum value of n which satisfies (3.22) gives the highest growth rate. Denoting this maximum value by $n_{\max}$, the internal waves are expected to appear with $n = n_{\max}$ in the wave flume. In the following the observed n's are compared with the calculated $n_{\max}$'s.

To compute $n_{\max}$, one needs to have $\bar{k}$ for each experiment. The value of $\bar{k}$ can be calculated theoretically. However, since the exact dispersion relation for wave motion in a two-layer system with diffuse interface is not known, the experimental data are used to compute $\bar{k}$. This minimizes the error in calculating $n_{\max}$. Having the experimental values of $\bar{l}_x$ and l_y, $\bar{k}$ is obtained from

$$\bar{k} = \sqrt{(2\pi / \bar{l}_x)^2 + (2\pi / l_y)^2} \tag{3.23}$$

The final results indicate that for all the experiments the calculated value of $n_{\max}$ coincided with the observed n. This clearly shows that the internal waves have occurred at the maximum possible angle in the wave flume in order to acquire the highest growth rate.

3.3.5 Effect of Viscosity on the Interaction

To study the effect of viscosity on the interaction, two experiments with salt water were repeated with diluted corn syrup. The experiments with corn syrup are denoted as series 4. The syrup mixture had a density of 1.160 gr/cm^3 and its viscosity was approximately $22\times10^{-6} m^2/\text{sec}$, 20 times greater than the viscosity of water. In Table 3.4, the

corresponding corn syrup and salt water experiments are grouped together for comparison. The time t_1 gives the time when the internal waves became first visible for cases with excitation of the internal waves, and the time t_{exp} gives duration of the experiment for cases without excitation of the internal waves. The measurements indicate that the experiments with the corn syrup did not result in appearance of the internal waves. However, the experiments with the salt water, with the same or even smaller surface wave amplitude, led to generation of the internal waves in a time interval shorter than the duration of the corresponding corn syrup experiment. Note that a smaller surface wave amplitude means lower forcing for excitation of the internal waves. These experimental findings are in agreement with the theoretical results in figure 2.9(c), which indicates that growth rate is a decreasing function of viscosity. In chapter 4, by introducing a new interaction model, the subject of interaction in a highly viscous medium is studied. The analysis takes into account both forcing and dissipating effects of the viscosity on the interaction.

3.3.6 Effect of Surface Wave Amplitude on the Interaction

According to the theoretical analysis of chapter 2, the growth rate is an increasing function of the surface wave amplitude, see equation 2.40. The analysis also suggests that there exists a critical wave amplitude for excitation of the internal waves. To examine these results, two experiments with salt water were repeated for a different surface wave height. These experiments are tabulated in Table 3.5, where the corresponding tests are grouped together. Experiments 5-4 and 5-6 were performed immediately after experiments 5-3 and 5-5 respectively, and hence the thickness of the diffuse interface layer did not change appreciably between the consecutive experiments.

It is clear from the measurements that increasing the surface wave amplitude has led to the appearance of the internal waves in the flume. In experiment 5-3 the internal waves didn't

appear during the six-minute experiment. However, increasing the height of the surface wave from 1.9 cm to 2.5 cm brought about enough forcing to cause the appearance of the internal waves in 3.7 minutes. Also in experiment 5-5 the internal waves didn't appear during the 7.3-minute experimentation, but increasing the height of the surface wave from 3.8 cm to 4.3 cm resulted in the appearance of the internal waves in 3.0 minutes. These experimental results confirm the theoretical findings.

3.3.7 Effect of Depth Ratio on the Interaction

To explore the effect of depth ratio on the interaction, two experiments with the identical configuration except in the depth ratio were performed. These experiments are summarized in Table 3.6. The parameter $k_{exp}d$ is a measure of deepness of the standing internal wave in the lower layer. In experiment 6-1, $k_{exp}d$ is equal to 2.7, which indicates that the internal waves are in the intermediate-depth range. According to theoretical results of figure 2.8, when the internal waves are in this range, decreasing the depth ratio reduces the growth ratio. This is in agreement with the experimental results in Table 3.6. According to measurements, the time for the first appearance of the internal waves has increased from 1.2 minutes in experiment 6-1 with $d/H = 0.16$ to 3.5 minutes in experiment 6-2 with $d/H = 0.09$. Therefore, the growth rate has decreased by lowering the depth ratio, in accord with the theoretical result. It should be mentioned that the thickness of the diffuse layer was almost the same in these experiments.

3.3.8 Comparison with Hill (1997)

In his experiments with the fresh water and the mineral oil, Hill (1997) observed the same three-dimensional internal wave pattern as in here. However, in his experiments only the mode $n = 2$ was observed. This can be attributed to the high density-difference between the

two fluids ($\Delta\rho = 0.176$) in his experiments. Theoretically, when the density difference becomes larger while the other parameters are kept constant, the internal waves tend to become longer (e.g., see equation 3.15 for the deep-water wave case). This leads to a longer standing wave across the flume and hence a smaller n, see (3.22). From this discussion it can also be concluded that for the sufficiently high density-difference the two-dimensional interaction, which corresponds to $n = 1$, is possible provided viscosity does not inhibit the growth. Besides the high density-difference, viscosity of the mineral oil seems to be an important factor for the absence of the higher modes in Hill's (1997) experiments.

According to Table 3.1, the present experiments led to the appearance of the standing internal waves with n's ranging from 3 to 7. In his study, Hill (1997) did not address the possibility of occurrence of higher modes nor the fact that the pattern was the result of the reflection of the internal waves.

In comparing the experimental growth rates with the theoretical values, Hill (1997) used the results of his inviscid analysis and neglected the effects of the high viscosity of the mineral oil on the evolution of the internal waves. This can be a partial explanation to the lack of a close agreement between the measured growth rates and the theoretical values in his study.

In his theoretical study, Hill (1997) found that the growth of internal waves is confined to narrow bands of density ratio and surface wave frequency. His analysis also indicated that there are close upper and lower bounds on the direction angles of the internal waves. Hill (1997, p.105) concludes:

> "The net effect of these various bounds was that instability of the internal waves, i.e., internal wave growth, was found to be a very selective process, occurring under very specific conditions."

These findings of Hill (1997) are addressed below in light of the experimental results.

First, reference is made to the direction angles of the internal waves. According to table 3.1, the values of $\bar{\theta}$ in the experiments ranged between 43° and 83°. These values have been plotted against k_0H in figure 3.15(a). The range of $\bar{\theta}$ observed in the experiments indicates the internal waves can grow within a wide range of the direction angle, and their evolution is not confined to specific bounds. It is also interesting to note that in Table 3.1 the range of density ratio over which the instability was observed is not narrow either. The instability took place at all density ratios tested, i.e., 1.04, 1.07, 1.12, 1.16.

Next, the range of the surface wave frequency within which the internal waves were excited is considered. The non-dimensional parameter k_0H is a measure of the deepness as well as the frequency of the surface wave. In the experiments, k_0H varies between 0.50 and 1.80, see figure 3.15(a) or (b). Given that a surface wave is shallow when $k_0H \approx 0.3$, and deep when $k_0H \approx 3.0$, it is clear that the instability is not restricted to a narrow band of the surface wave frequency.

In figure 3.15(b) the parameter d/H in each experiment has been plotted against k_0H. It is seen that the range of the tested depth ratios is not narrow either. The parameter d/H varies between 0.09 and 0.33 in the experiments.

From the preceding discussions, it is concluded that the process of excitation of the internal waves is not restricted to very specific conditions and may occur within a wide range of each parameter. It should be noted that the actual ranges of the parameters for instability in the wave flume might be wider than the tested ones.

3.3.9 Other Experimental Observations

Two more phenomena observed in the wave flume are worth mentioning here. These are the long-term behavior of the internal waves and the occasional excitation of some harmonic internal waves besides the sub-harmonic ones. These are discussed below.

As discussed in section 3.3.4, the internal waves grew exponentially in the wave flume. However, this process did not continue forever. At some stage the internal waves stopped growing further and reached a temporary equilibrium state with a large amplitude. This phenomenon which is visible in the companion videotape was accompanied by some mixing of the layers. The stabilization process was also detected by Hill (1997) in his measurements of the interface displacement. The phenomenon can be explained by considering that it occurred when the internal waves had become quite large in amplitude and hence were highly non-linear. For a non-linear wave the dispersion relation is a function of the amplitude. This implies that the resonance conditions (2.1), initially satisfied by the weakly non-linear waves, did not hold, and hence the waves were not in exact resonance any more. However, since the triad was still close to resonance, the interface oscillated with a constant, large amplitude similar to the motion of a simple oscillator subject to a forcing which has a frequency close to the natural frequency of the oscillator (see, for example, Clough and Penzien, 1993). After this stable period, the internal waves started decaying very slowly. In long term the internal waves seemed to have a cyclic slow growth and decay. However, due to mixing of the layers the long-term process was not clearly visible in the wave flume.

The next observed phenomenon is the occasional excitation of harmonic standing internal waves in the flume. These waves, in the form of narrow strips riding on the sub-harmonic internal waves, are shown in the first picture ($n = 3$) of figure 3.7. They were two-dimensional standing waves across the flume and were occasionally excited simultaneously with the sub-harmonic internal waves. However, they had shorter wavelengths than the sub-harmonic waves, and their amplitudes remained quite small, implying that these waves are less unstable than the sub-harmonic ones. In each experiment, the harmonic standing wave appeared with a n different from that of the standing sub-harmonic wave.

3.4 SUMMARY

The results of an experimental investigation of the interaction in a laboratory flume were presented. The study consisted of six series of experiments. The common phenomenon observed in all the experiments was the generation of a three-dimensional internal wave pattern at the interface. This was shown to be the result of the reflection of the excited internal waves from the flume sidewalls. The observations also indicated that the internal wave pattern had two length- and two time-scales. At the large length-scale the pattern had a wavelength of twice the surface wavelength and at the short length-scale it had the form of a three-dimensional standing internal wave. At the short time-scale, the frequency of the interface oscillation was half of the frequency of the surface wave, and at the long time-scale, the short length-scale (three-dimensional standing internal wave) was moving slowly along the flume. All of these observations were explained theoretically.

The wavelength of the 3D standing internal wave was measured in each experiment. It was found that the diffusivity of the interface has a direct affect on the wavelength. In comparing the measured wavelengths with the theory, a closer agreement was obtained when the thickness of the diffuse interface was taken into account in the computation of the theoretical values.

To study the evolution of the internal waves, the amplitude of the standing internal wave was measured with time in a few experiments. The measurements confirmed the theoretical result that the internal waves have an exponential growth in time. However, in terms of the growth rate, a close agreement between the experimental and theoretical values was not obtained although the values were of the same order of magnitude. This was attributed to the diffusivity of the interface in the experiments. As the interface becomes diffuse, the velocity profile across the interface smoothes out leading to less interface shear and hence less forcing

for excitation of the internal waves, which results in a lower growth rate. The explanation was in agreement with the experimental results as the measured growth rates were less than those from the two-layer theory presented in chapter 2.

According to the three-dimensional model, the more oblique the internal waves to the surface wave, the higher their growth rate. This result was confirmed by the experimental measurements as in the wave flume the internal waves occurred at the maximum possible angle from the surface wave.

According to the theoretical studies of Wen (1995) and Hill and Foda (1996) viscosity has a destabilizing effect on the interaction. However, the three-dimensional analysis of chapter 2 indicates the growth rate of the internal waves decreases with the viscosity of the lower layer. This was found in agreement with the experimental results as replacing the salt water with a viscous mixture (diluted corn syrup) resulted in the disappearance of the internal waves in the wave flume.

The effects of the surface wave amplitude and the depth ratio on the interaction process were also examined in the laboratory. According to the three-dimensional analysis of chapter 2, the growth rate increases with the surface wave amplitude, and there is a critical surface wave amplitude below which the internal waves can not grow. These results were verified by the experimental measurements. Also, the theoretical result that when the internal waves are not deep in the lower layer, the growth rate decreases as the depth ratio d / H reduces was found to be in agreement with the experimental observations.

Also, reference was made to the work of Hill (1997). Hill's (1997) theoretical analysis indicated that there are narrow bands of the surface wave frequency, the direction angle of the internal waves, and the density ratio of the layers only within which the internal waves can grow. These results were found in conflict with the experimental results as no specific

bounds on the interaction process were found. The interaction took place in the laboratory flume over wide ranges of the parameters.

Finally, two more phenomena observed in the wave flume were discussed. These were the long-term behavior of the internal waves and the occasional excitation of some harmonic internal waves besides the sub-harmonic ones.

Exp. No.	H (cm)	d (cm)	H_s (cm)	T_0 (sec)	$\Delta\rho$ gr/cm^3	h_ρ (cm)	$\bar{l}_x$ (cm)	n	$l_y^{\perp}$ (cm)	$\bar{\theta}$ (deg)
1-1	16.4	3.9	2.2	0.96	0.040	0.26	17.3	5	10.6	58
1-2	16.5	3.9	2.8	0.80	0.039	0.19	15.6	7	7.0	65
1-3	16	3.9	2.0	0.90	0.040	0.29	20.8	6	8.4	68
1-4	16.5	3.9	3.0	0.84	0.040	0.24	40.1	7	7.0	80
1-5	16.3	3.8	2.4	1.11	0.040	0.27	26.8	4	14.1	62
1-6	16.5	3.8	2.7	1.19	0.041	0.34	67.3	4	14.5	77
1-7	15.8	3.8	3.5	1.30	0.041	0.35	20.1	3	21.1	43

Exp. No.	H (cm)	d (cm)	H_s (cm)	T_0 (sec)	$\Delta\rho$ gr/cm^3	h_ρ (cm)	$\bar{l}_x$ (cm)	n	$l_y^{\perp}$ (cm)	$\bar{\theta}$ (deg)
2-1	16.0	4.1	3.0	1.21	0.041	0.51	44.0	4	14.1	72
2-2	16.7	4.1	3.0	1.33	0.040	0.52	32.8	3	21.1	57
2-3	17.2	4.1	3.7	1.56	0.040	0.43	84.7	3	21.1	76
2-4	19.8	4.1	3.5	1.57	0.040	0.54	85.0	3	21.1	76
2-5	19.0	4.1	3.3	1.24	0.040	0.54	55.8	4	14.1	75
2-6	18.8	4.1	3.5	1.13	0.041	0.57	18.1	4	14.1	52
2-7	19.1	4.1	3.5	1.10	0.041	0.61	17.0	5	10.6	58
2-8	18.7	4.1	2.3	0.89	0.040	0.55	19.4	7	7.0	70
2-9	13.0	4.2	2.6	1.15	0.040	0.45	26.7	4	14.1	62
2-10	12.9	4.2	2.7	0.91	0.040	0.45	32.0	6	8.4	75
2-11	13.2	4.2	2.4	0.97	0.040	0.53	35.0	6	8.4	76

Exp. No.	H (cm)	d (cm)	H_s (cm)	T_0 (sec)	$\Delta\rho$ gr/cm^3	h_ρ (cm)	$\bar{l}_x$ (cm)	n	$l_y^{\perp}$ (cm)	$\bar{\theta}$ (deg)
3-1	12.7	4.1	3.6	1.01	0.071	0.11	27.5	3	21.1	52
3-2	13.2	3.5	2.3	0.79	0.071	0.24	16.4	4	14.1	49
3-3	13.2	3.4	2.7	0.72	0.072	0.25	20.4	5	10.6	62
3-4	12.8	3.3	2.2	0.67	0.072	0.24	28.4	6	8.4	73
3-5	13.2	3.6	2.6	0.69	0.071	0.12	15.2	5	10.6	55
3-6	16.3	3.6	2.8	0.97	0.072	0.28	21.4	3	21.1	45
3-7	17.2	3.6	3.2	0.78	0.072	0.28	15.6	5	10.6	55
3-8	17.1	3.6	2.2	0.70	0.072	0.30	74.6	6	8.4	83
3-9	17.2	3.6	2.3	0.68	0.072	0.30	16.8	6	8.4	63
3-10	16.5	3.6	4.0	1.12	0.072	0.30	64.0	3	21.1	71

$^{\perp}$ $l_y = 2B/(n-1)$, where B is the flume width equal to 21.1 cm.

Table 3.1 Summary of the experimental series 1, 2, and 3.

Experiment No.	l_{exp} *(cm)*	$l_{two\text{-}layer}$ *(cm)*	l_t *(cm)*	*Observed n*
1-1	9.0	11.1	9.4	5
1-2	6.4	7.6	6.4	7
1-3	7.8	9.8	8.2	6
1-4	6.9	8.6	7.1	7
1-5	12.5	14.5	12.7	4
1-6	13.8	16.5	14.8	4
1-7	14.6	19.1	17.2	3
2-1	13.4	17.0	14.3	4
2-2	17.8	20.0	16.9	3
2-3	20.5	25.7	23.0	3
2-4	20.5	26.0	22.6	3
2-5	13.6	17.8	14.4	4
2-6	11.1	15.1	11.9	4
2-7	9.0	12.3	8.8	5
2-8	6.6	9.7	6.3	7
2-9	12.5	15.6	12.9	4
2-10	8.2	10.1	7.3	6
2-11	8.2	11.5	8.4	6
3-1	16.7	20.1	19.0	3
3-2	10.7	13.1	11.3	4
3-3	9.4	11.1	9.4	5
3-4	8.1	9.7	8.1	6
3-5	8.7	10.3	9.3	5
3-6	15.0	18.5	16.6	3
3-7	8.8	12.9	11.0	5
3-8	8.4	10.6	8.6	6
3-9	7.5	10.0	8.0	6
3-10	20.0	23.0	20.8	3

Table 3.2 Experimental and theoretical wave lengths and observed n's. The theoretical n's are the same as the observed ones.

Experiment No.	α_{exp} $(sec\text{-}cm)^{-1}$	α_{theory} $(sec\text{-}cm)^{-1}$	$k_{exp}\, h_\rho$
3-1	0.104	0.139	0.041
3-3	0.114	0.202	0.168

Table 3.3 Experimental and theoretical values of α.

Experiment No.	*Lower Layer*	*H (cm)*	*d (cm)*	*H_s (cm)*	*T_0 (sec)*	*n*	*$\Delta\rho$ gr/cm^3*	*t_{exp} (min)*	*t_1 (min)*
4-1	Corn Syrup	13.0	3.3	2.9	0.64	-	0.160	7.3	-
5-1	Salt Water	13.0	3.3	2.9	0.64	3	0.160	-	2.0
4-2	Corn Syrup	17.3	3.7	3.4	0.64	-	0.160	9.0	-
5-2	Salt Water	17.3	3.7	3.2	0.64	3	0.160	-	6.5

Table 3.4 Experiments for evaluation of effects of viscosity.

Experiment No.	*H (cm)*	*d (cm)*	*H_s (cm)*	*T_0 (sec)*	*n*	*$\Delta\rho$ gr/cm^3*	*t_{exp} (min)*	*t_1 (min)*
5-3	13.0	3.0	1.9	0.64	-	0.160	6.0	-
5-4	13.0	3.0	2.5	0.64	3	0.160	-	3.7
5-5	17.0	3.0	3.8	0.64	-	0.160	7.3	-
5-6	17.0	3.0	4.3	0.64	3	0.160	-	3.0

Table 3.5 Experiments for evaluation of effects of surface wave amplitude.

Experiment No.	*H (cm)*	*d (cm)*	*H_s (cm)*	*T_0 (sec)*	*n*	*$\Delta\rho$ gr/cm^3*	*k_{exp} d*	*t_{exp} (min)*	*t_1 (min)*
6-1	17.0	2.7	3.6	0.70	4	0.120	1.3	-	1.2
6-2	17.0	1.5	3.6	0.70	5	0.120	0.9	-	3.5

Table 3.6 Experiments for evaluation of effects of depth ratio.

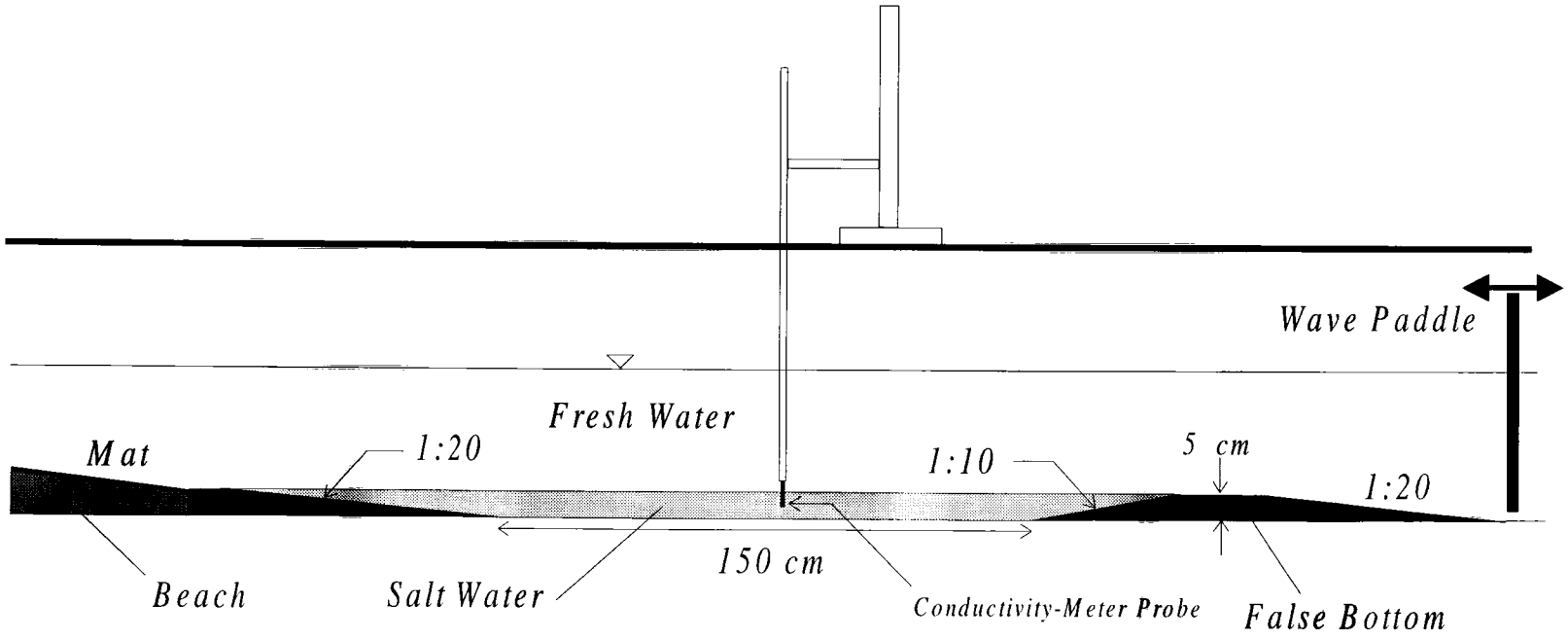

Figure 3.1 Experimental set-up.

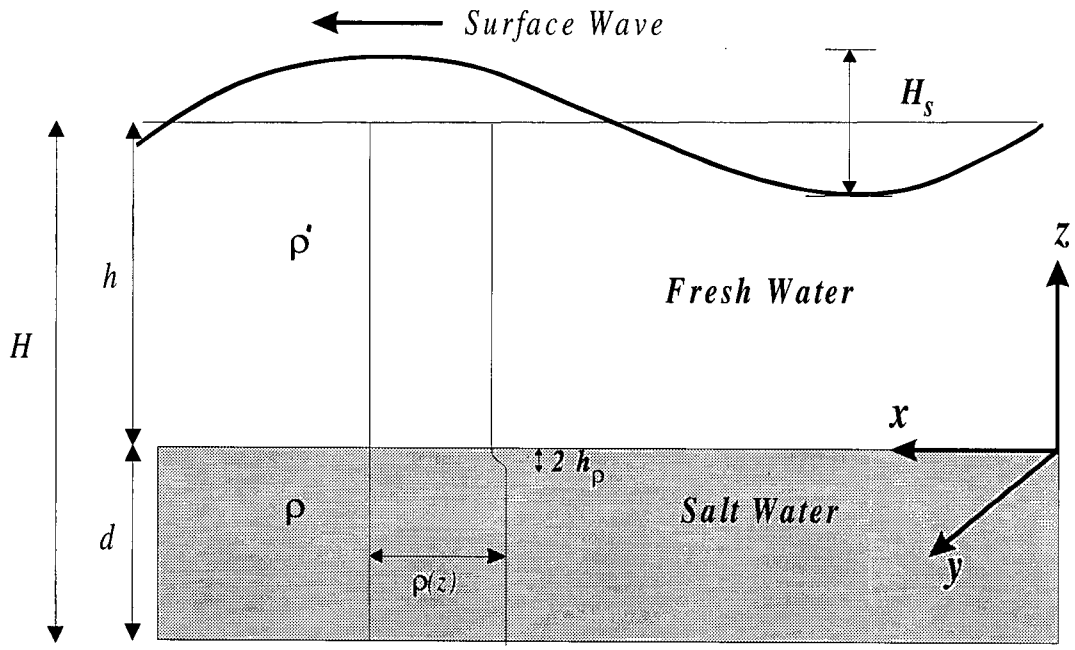

Figure 3.2 Configuration of the problem in the experiments.

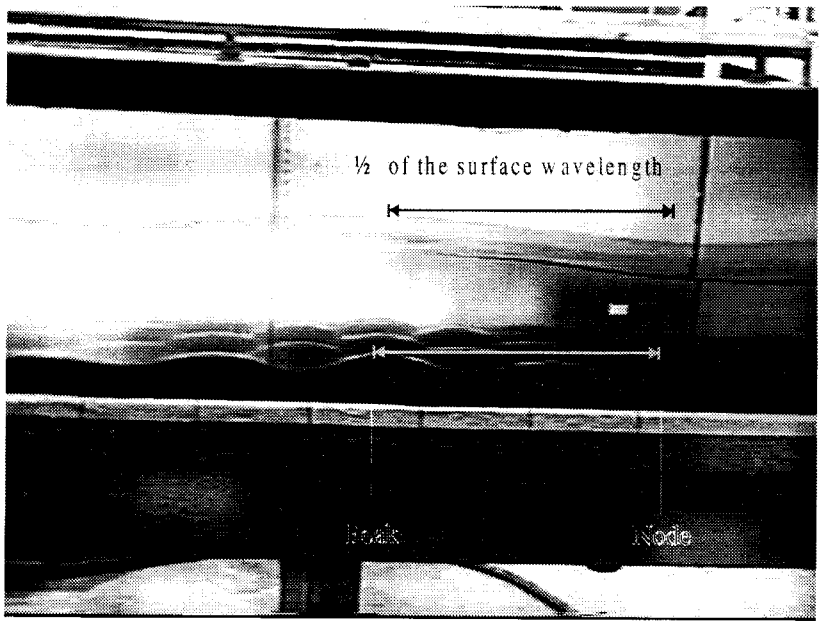

(a)

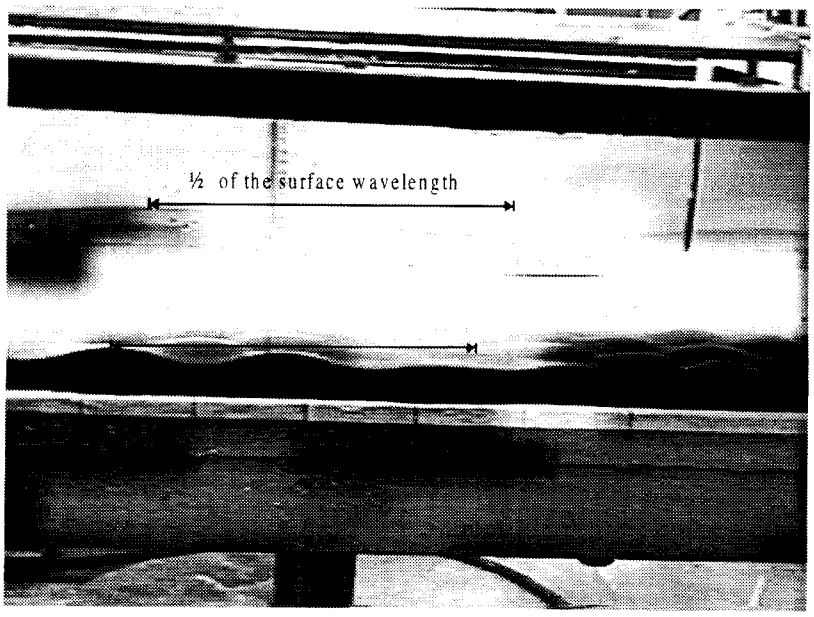

(b)

Figure 3.3 Two successive pictures of the surface and internal wave motion in the flume.

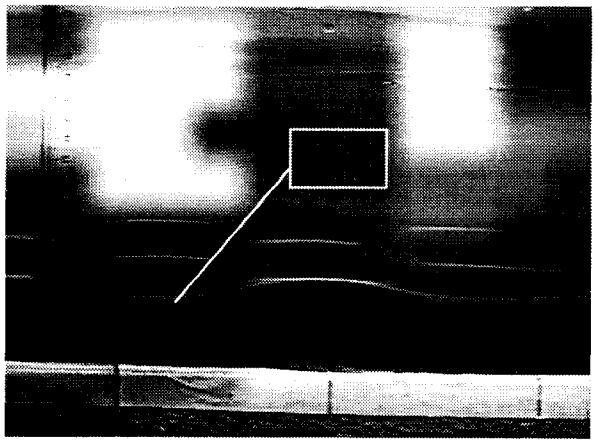

$t = 0$

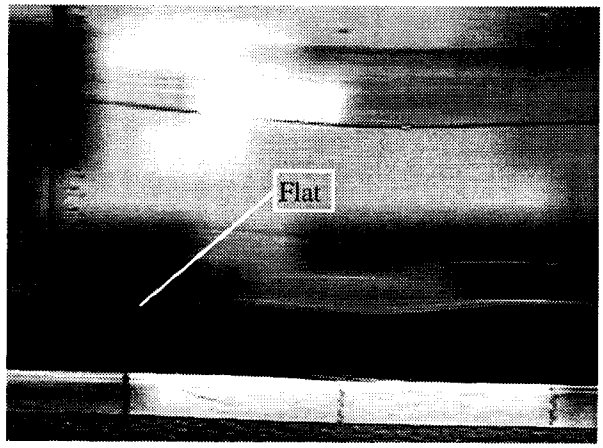

$t = T_0 / 2$

$t = T_0$

Figure 3.4 Variation of the 3D standing internal wave during two surface wave periods.

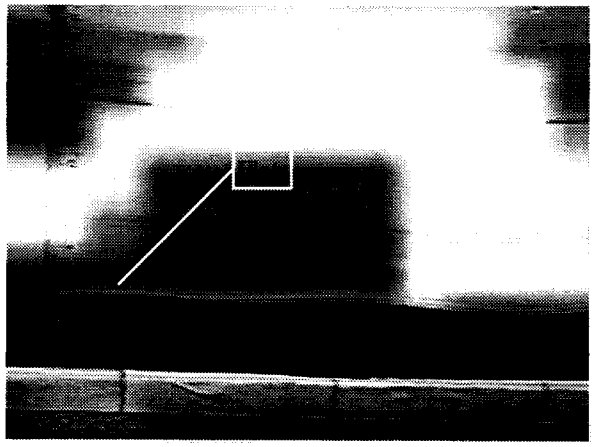

$t = 3T_0 / 2$

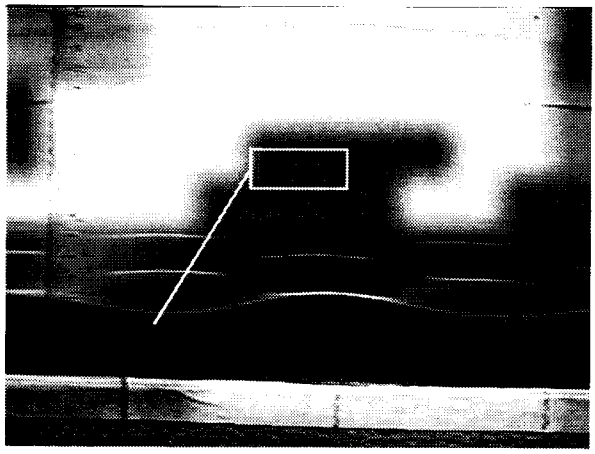

$t = 2T_0$

Figure 3.4 Continued

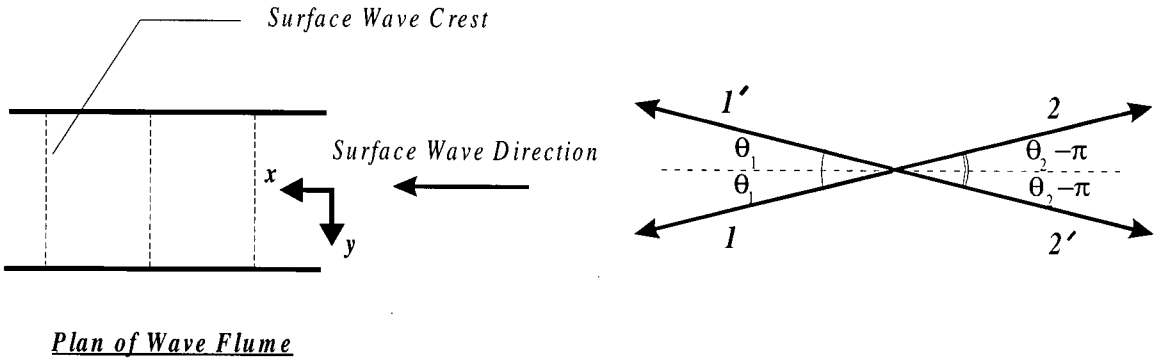

Plan of Wave Flume

Figure 3.5 The four waves comprising the observed 3D standing wave pattern. Waves 1′ and 2′ are the reflections of waves 1 and 2 from the side-walls respectively.

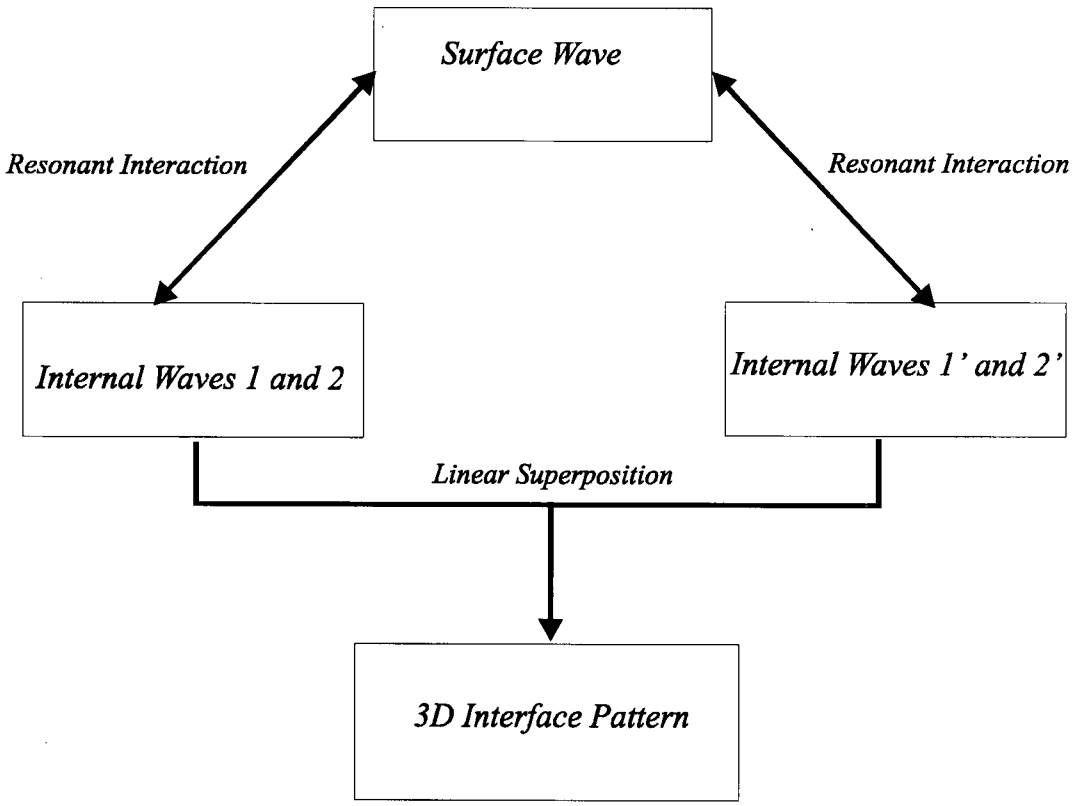

Figure 3.6 Mechanism of generation of the 3D standing wave at the interface.

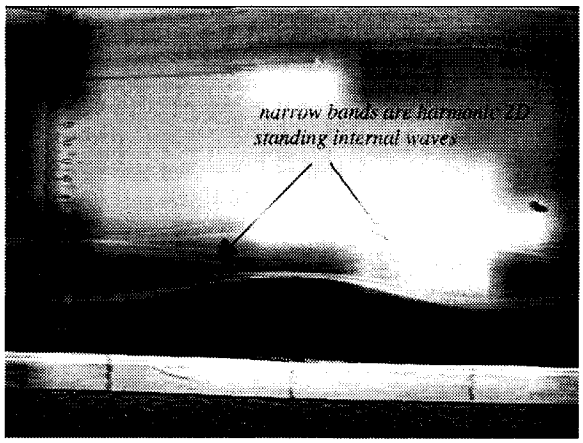

n=3

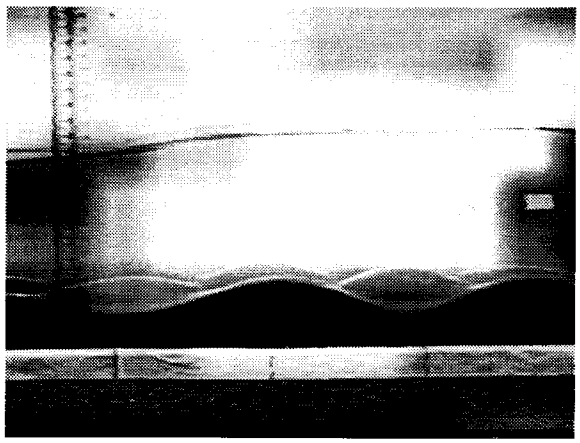

n=4

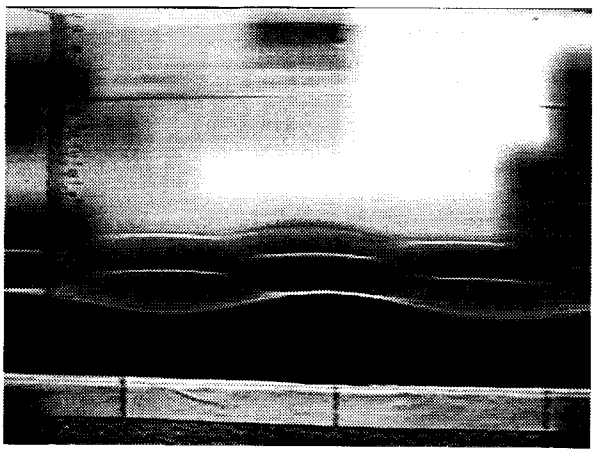

n=5

Figure 3.7 Top-side views of 3D standing internal waves with different n's.

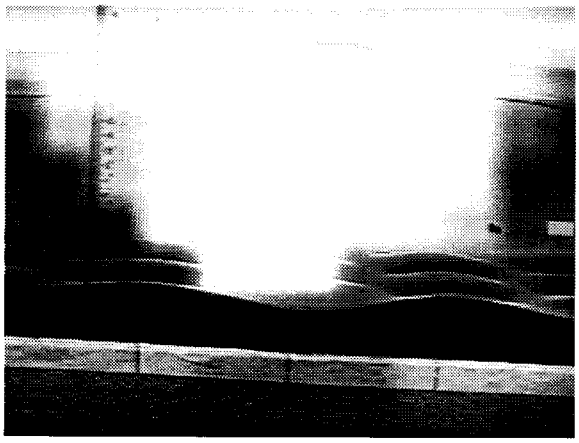

n=6

Figure 3.7 Continued.

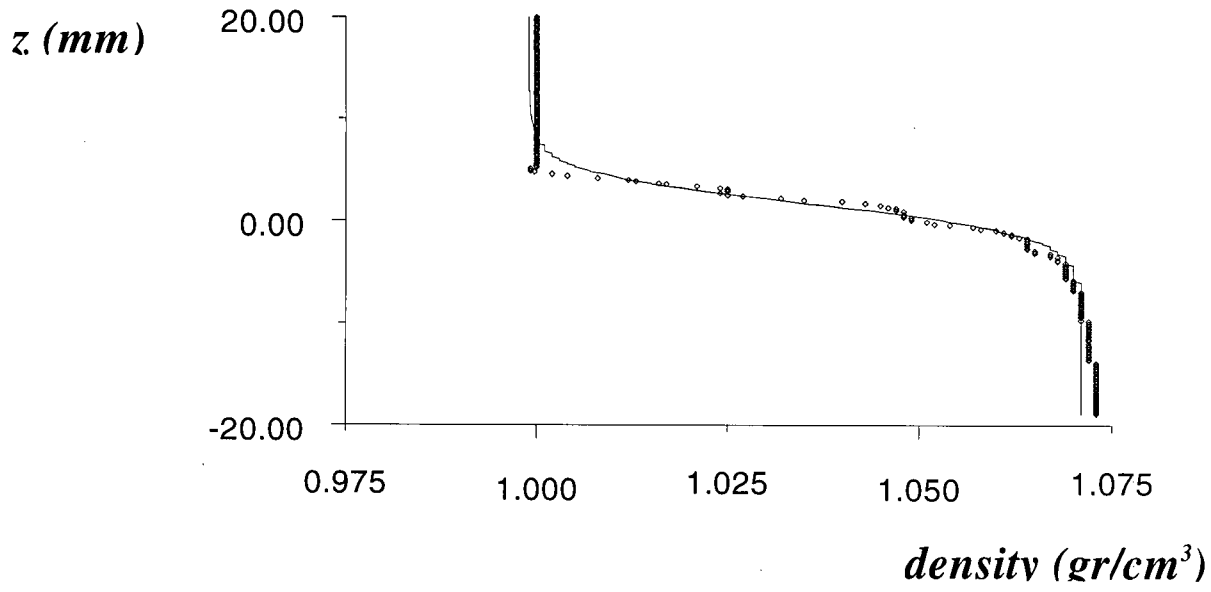

Figure 3.8 Typical density variation across the interface in the experiments.

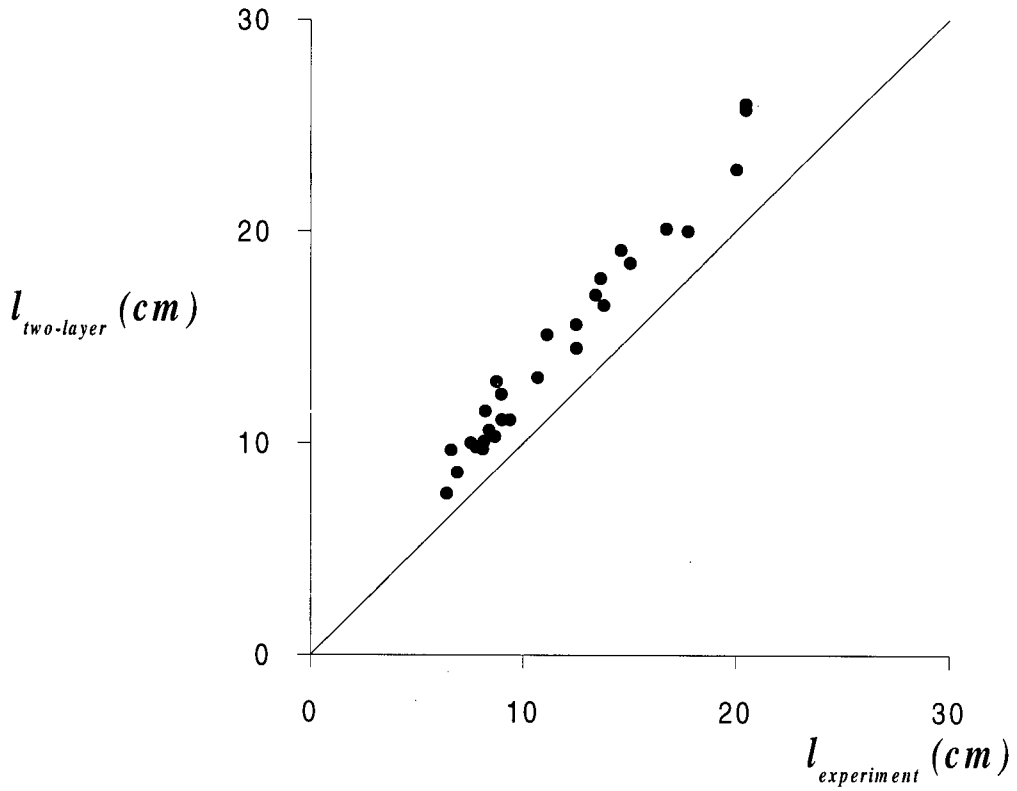

Figure 3.9 Comparison of the theoretical wave lengths $l_{two-layer}$ with the measured values $l_{\exp}$.

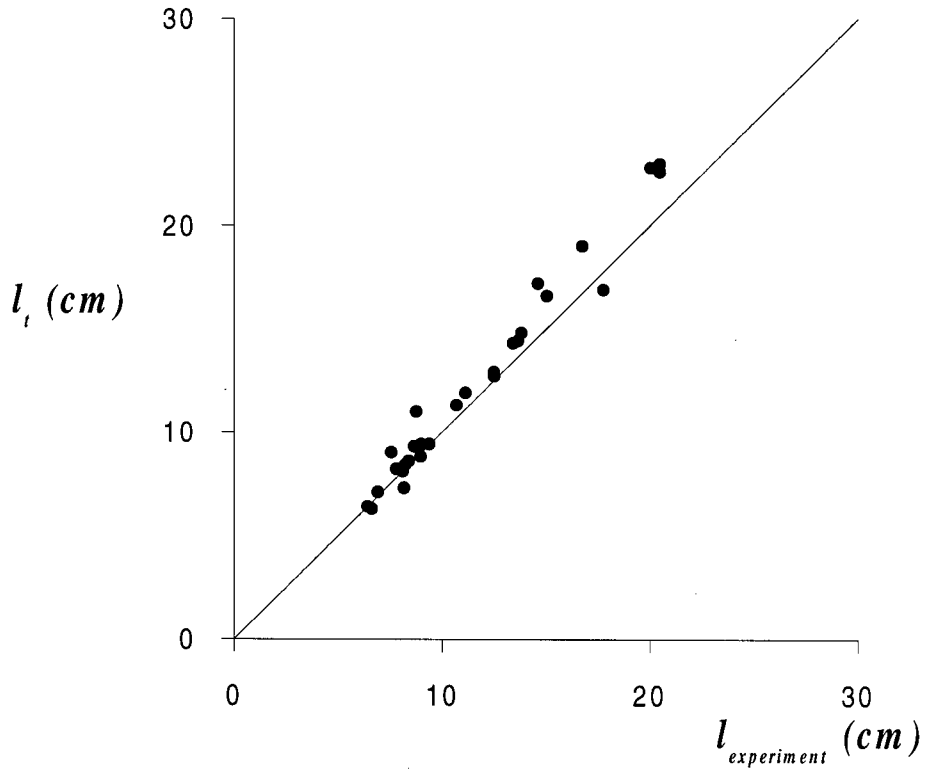

Figure 3.10 Comparison of the theoretical wave lengths l_t with the measured values $l_{\exp}$.

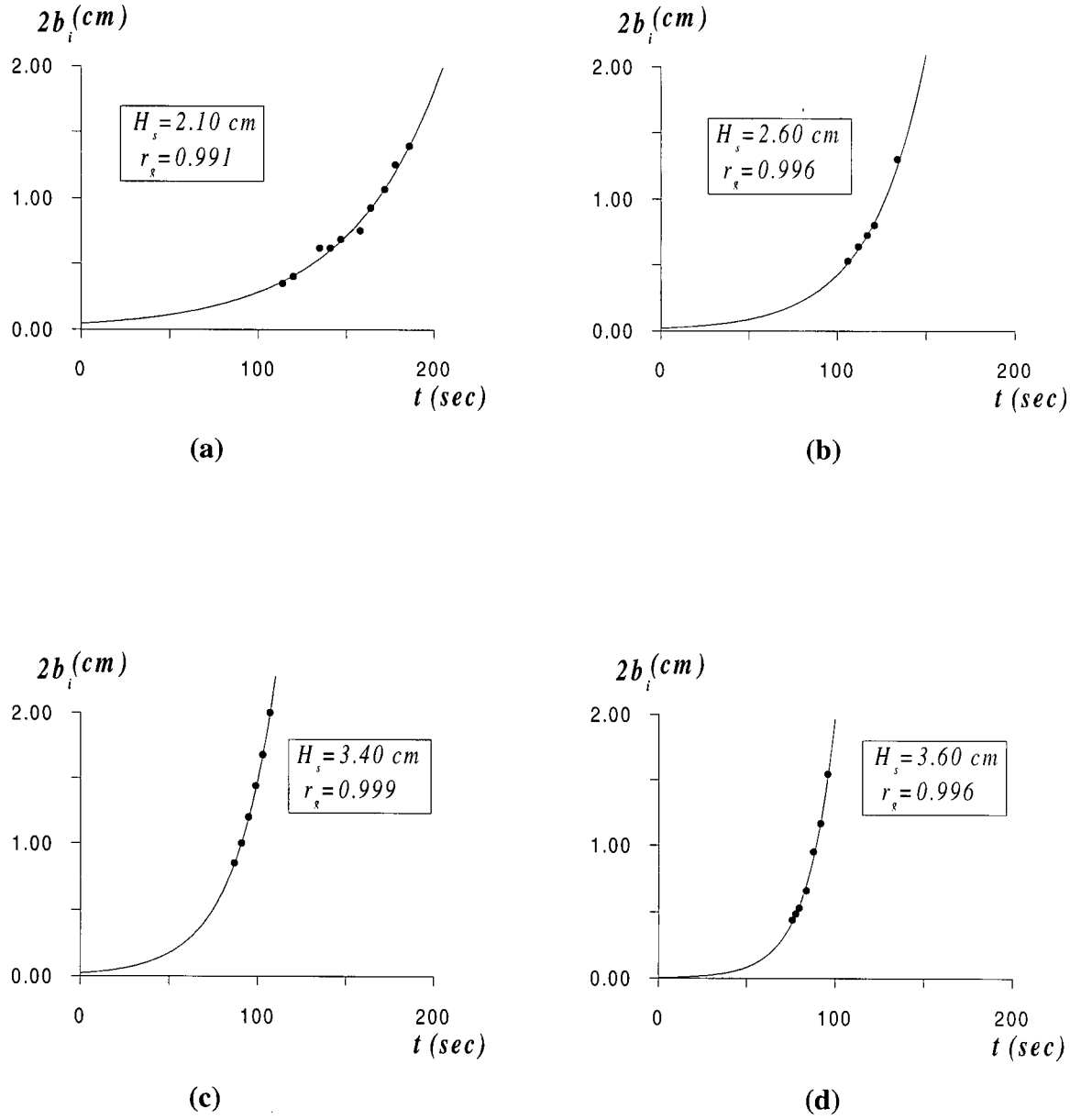

Figure 3.11 Time variation of the amplitude of the standing internal wave in experiment 3-1 for a) $H_s = 2.10\ cm$, b) $H_s = 2.60\ cm$, c) $H_s = 3.40\ cm$, and d) $H_s = 3.60\ cm$.

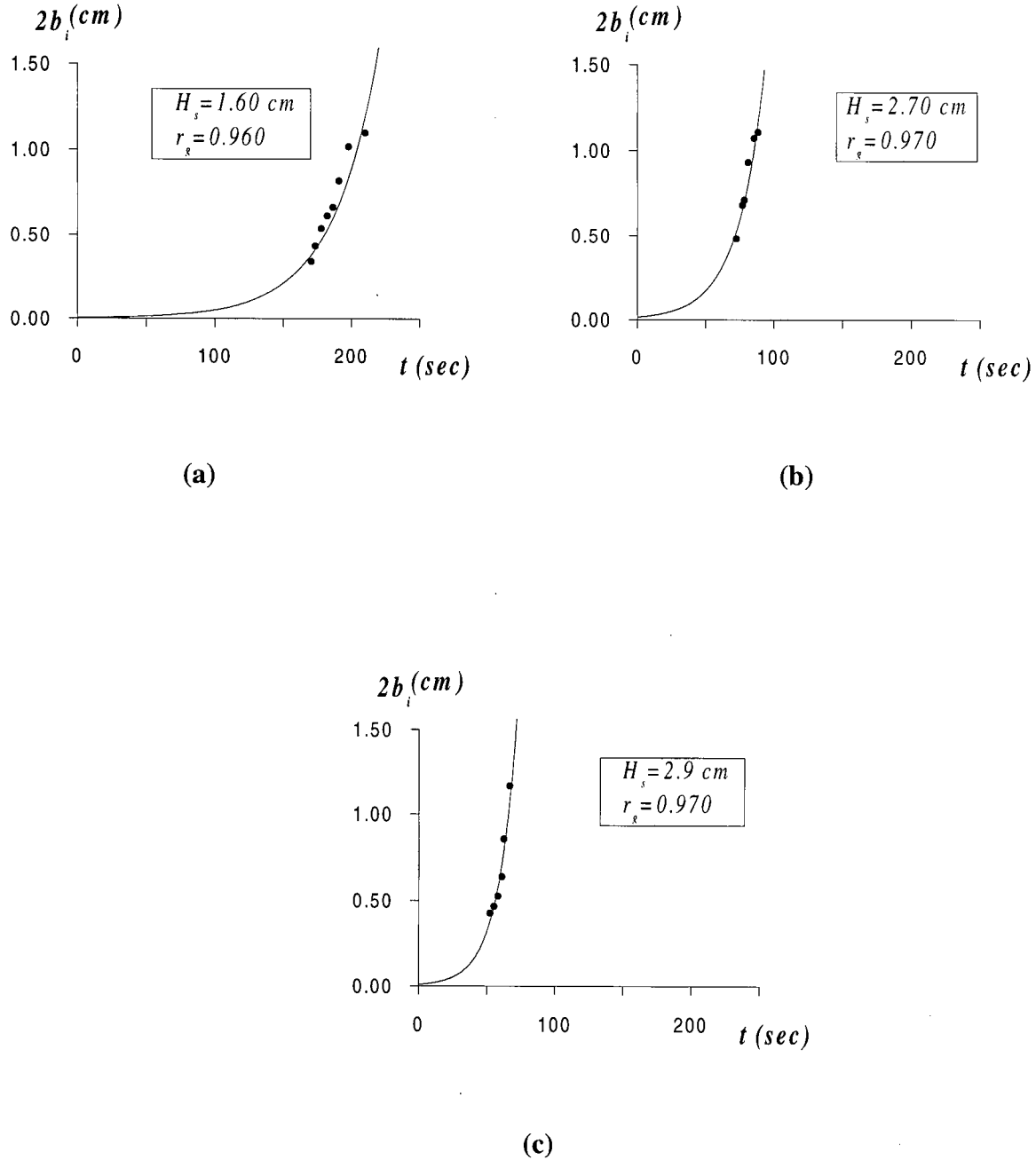

Figure 3.12 Time variation of the amplitude of the standing internal wave in experiment 3-3 for **a)** $H_s = 1.60\ cm$, **b)** $H_s = 2.70\ cm$, and **c)** $H_s = 2.90\ cm$.

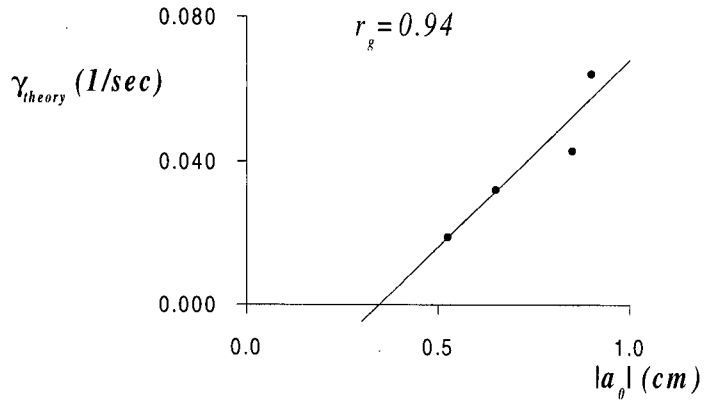

(a)

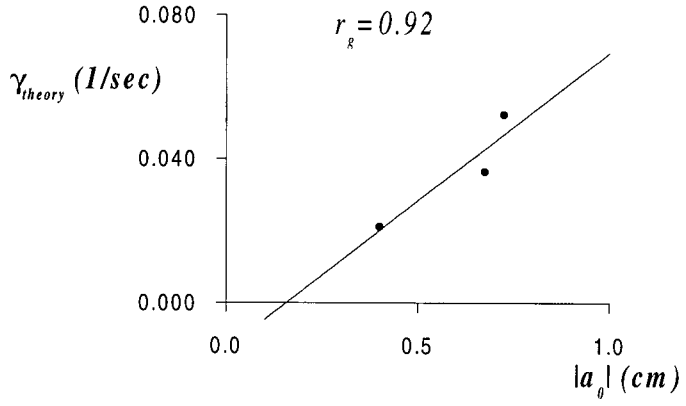

(b)

Figure 3.13 Variation of γ with $|a_0|$ in experiments **a)** 3-1 and **b)** 3-3.

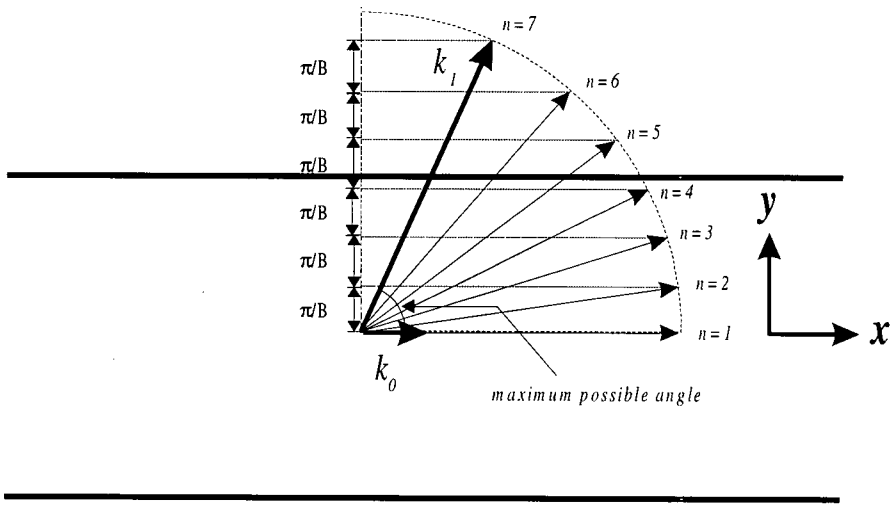

Figure 3.14 Admissible directions of internal wave 1 in the wave flume.

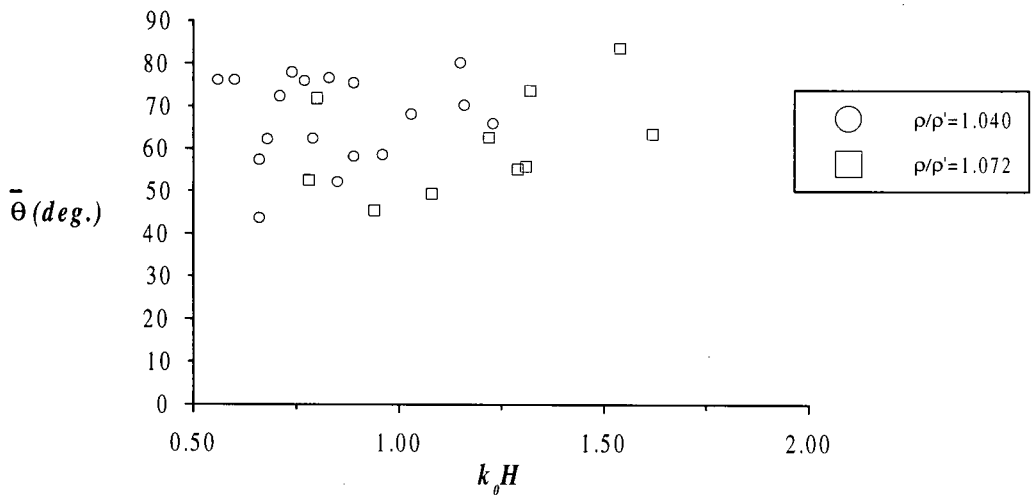

(a)

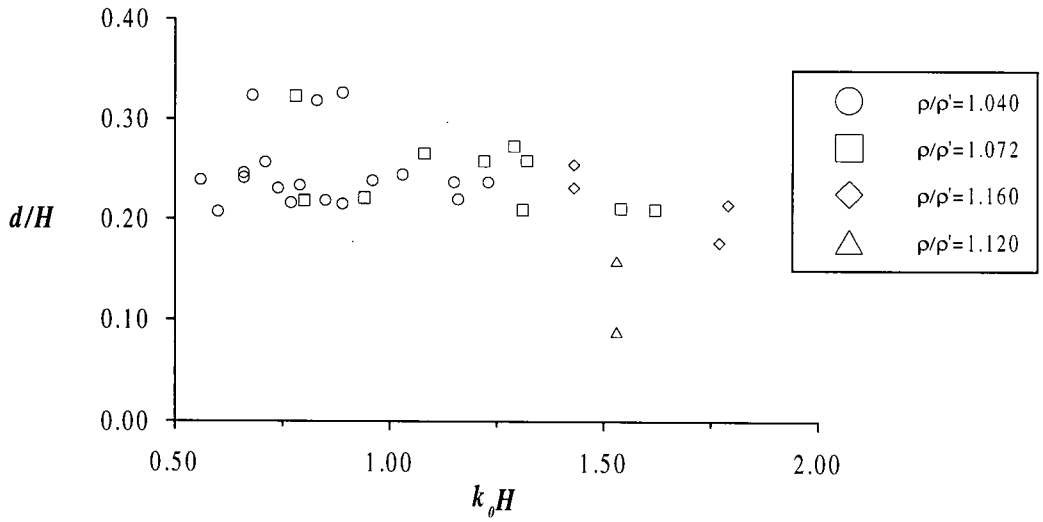

(b)

Figure 3.15 Plots of the experimental values of **a)** $\overline{\theta}$ and **b)** d/H as functions of $k_0 H$.

CHAPTER 4

TWO-DIMENSIONAL VISCOUS ANALYSIS OF INTERACTION

4.1 INTRODUCTION

In this chapter, the interaction is studied theoretically in two dimensions based on a fully viscous analysis. In the three-dimensional analysis of the interaction in chapter 2 the forcing role of viscosity was neglected in the formulation of the problem, and only the damping effect of viscosity was considered in the analysis. In this chapter both effects of viscosity on the interaction, particularly in a highly viscous medium, are taken into account in the analysis. It is worth noting that according to the experimental results, the two-dimensional interaction may not be realistic. However, as the formulation of the problem in two dimensions is much simpler than in three dimensions, and both roles of viscosity in the interaction are still simulated, the viscous interaction is studied in two dimensions.

A technique that is capable of handling both low and high viscosity of the lower layer is used to find the evolution equations. The results for a typical problem are presented and compared with those from the three-dimensional model in chapter 2. It will be shown that the two models are asymptotically equivalent when viscosity of the lower layer approaches zero.

A main finding of the present analysis regards the relative significance of the viscous damping and the viscosity-induced forcing in the interaction process. It is shown that when the lower layer is highly viscous, the viscous damping dominates the interaction process and inhibits growth of the internal waves even at large surface wave heights. This is far different from the results of the viscous analyses of Hill and Foda (1996) and Wen (1995), whose theoretical analysis indicated that viscosity enhances excitation of the interfacial waves.

4.2 GOVERNING EQUATIONS

Consider the fluid system shown in figure 4.1. It consists of an inviscid upper layer and a viscous lower layer. The depth of the upper layer is denoted by h, depth of the lower layer by d, and the corresponding densities by ρ' and ρ. The lower layer is assumed to have a kinematic viscosity of ν. The surface wave is denoted as wave 0 and the two opposite-traveling internal waves as waves 1 and 2.

With the assumption of inviscid, incompressible fluids and an irrotational flow, the velocity field in the upper layer can be described by

$$u' = \frac{\partial \phi}{\partial x}$$
$$w' = \frac{\partial \phi}{\partial z} \qquad (4.1)$$

where ϕ is a potential function. In the lower layer, the velocity field can be described by a stream function ψ.

$$u = \frac{\partial \psi}{\partial z}$$
$$w = -\frac{\partial \psi}{\partial x} \tag{4.2}$$

Definition of the stream function in the lower domain leads to automatic satisfaction of the continuity equation.

In the upper layer, the continuity equation is described by

$$\nabla^2 \phi = 0 \tag{4.3}$$

and the momentum equations are given by unsteady Bernoulli equation.

$$\rho' \phi_t + \frac{1}{2}\rho'(\phi_x^2 + \phi_z^2) + p' + \rho' g z = C(t) \tag{4.4}$$

where p' is the pressure in the upper layer, and the subscripts refer to the corresponding derivatives. In the lower layer, the momentum equations can be written as

x-Momentum $$\rho \psi_{zt} + p_x - \rho \nu \nabla^2 \psi_z = \rho(\psi_x \psi_{zz} - \psi_z \psi_{zx}) \tag{4.5}$$

z-Momentum $$\rho \psi_{xt} - p_z - \rho \nu \nabla^2 \psi_x - \rho g = \rho(\psi_x \psi_{xz} - \psi_z \psi_{xx}) \tag{4.6}$$

Elimination of p from the above equations results in the well-known vorticity equation.

$$\nabla^2 \psi_t - \nu \nabla^4 \psi = \psi_x \nabla^2 \psi_z - \psi_z \nabla^2 \psi_x \tag{4.7}$$

The advection term makes the above equation nonlinear.

The above field equations are subject to the boundary conditions at the free surface, the two-layer interface, and the solid bed. At the free surface, there is one dynamic and one

kinematic boundary condition. The dynamic boundary condition is resulted from the assumption of the atmospheric pressure at the free surface. Implementing $p' = 0$ in the Bernoulli equation, equation (4.4), results in

$$\rho'\phi_t + \frac{1}{2}\rho'(\phi_x^2 + \phi_z^2) + \rho' gz = C(t), \qquad z = h + \xi(x,t) \qquad (4.8)$$

where $\xi(x,t)$ is the displacement of the free surface. The kinematic boundary condition can be expressed as

$$\xi_t - \phi_z = -\phi_x \xi_x, \qquad z = h + \xi(x,t) \qquad (4.9)$$

which ensures that the fluid particles do not leave the air-fluid boundary.

At the two-layer interface, there are two kinematic and two dynamic boundary conditions. The kinematic B.C.'s are

$$\eta_t - \phi_z = -\phi_x \eta_x, \qquad z = \eta(x,t) \qquad (4.10)$$

and

$$\eta_t + \psi_x = -\psi_z \eta_x, \qquad z = \eta(x,t) \qquad (4.11)$$

where $\eta(x,t)$ is the displacement of the interface. The dynamic boundary conditions, with reference to figure 4.2, can be expressed as

$$\hat{\tau} = 0, \qquad z = \eta(x,t) \qquad (4.12)$$

$$\hat{\sigma}_{22} + p' = 0, \qquad z = \eta(x,t) \qquad (4.13)$$

The first equation comes from the fact that the upper layer can not carry any shear stress, and thus the shear stress along the interface should be zero. The second one states that the normal stress to the interface should be continuous across the boundary. One can use stress

transformation rules and write $\hat{\tau}$ and $\hat{\sigma}_{22}$ in these equations in terms of σ_{11} , σ_{22} and τ, which are components of the stress tensor in x-z directions. The transformation rules in terms of the interface displacement are

$$\hat{\sigma}_{22} = \sigma_{22}\frac{1}{1+\eta_x^2} - 2\tau\frac{\eta_x}{1+\eta_x^2} + \sigma_{11}\frac{\eta_x^2}{1+\eta_x^2} \tag{4.14}$$

$$\hat{\tau} = \tau\frac{\eta_x^2 - 1}{1+\eta_x^2} - (\sigma_{22} - \sigma_{11})\frac{\eta_x}{1+\eta_x^2} \tag{4.15}$$

Using the above expressions for $\hat{\sigma}_{22}$ and $\hat{\tau}$, and the Bernoulli equation for p' at the interface, one can rewrite (4.12) and (4.13) as

$$\tau\frac{\eta_x^2 - 1}{1+\eta_x^2} - (\sigma_{22} - \sigma_{11})\frac{\eta_x}{1+\eta_x^2} = 0 \tag{4.16}$$

$$\sigma_{22}\frac{1}{1+\eta_x^2} - 2\tau\frac{\eta_x}{1+\eta_x^2} + \sigma_{11}\frac{\eta_x^2}{1+\eta_x^2} - \rho'(\phi_t + \frac{1}{2}(\phi_x^2 + \phi_z^2) + g\eta) + C(t) = 0 \tag{4.17}$$

Next, equation 4.2 and the constitutive laws between stress and rate of strain in the lower layer, i.e.,

$$\begin{aligned} \sigma_{11} &= -p + 2\mu u_x && \text{(a)} \\ \sigma_{22} &= -p + 2\mu w_z && \text{(b)} \\ \tau &= \mu(w_x + u_z), && \text{(c)} \end{aligned} \tag{4.18}$$

are used to rewrite equations 4.16 and 4.17 in terms of ψ and p (lower layer pressure).

$$\mu(\psi_{zz} - \psi_{xx})(\eta_x^2 - 1) + 4\mu\psi_{xz}\eta_x = 0, \qquad z = \eta(x,t) \tag{4.19}$$

$$\{-p-2\mu\psi_{xz}-2\mu(-\psi_{xx}+\psi_{zz})\eta_x+(-p+2\mu\psi_{zx})\eta_x^2\}/(1+\eta_x^2)-$$
$$\rho'(\phi_t+\frac{1}{2}(\phi_x^2+\phi_z^2)+gz)+C(t)=0$$
$$, \qquad z=\eta(x,t) \qquad (4.20)$$

Equations 4.19 and 4.20 are the appropriate forms of the dynamic boundary conditions at the interface for later use.

The set of boundary conditions for the problem becomes complete with knowing that at the solid bed, the horizontal and vertical velocities vanish. These conditions can be written as

$$\psi_x = 0, \qquad z=-d \qquad (4.21)$$

$$\psi_z = 0, \qquad z=-d \qquad (4.22)$$

Equations 4.3 to 4.7 along with boundary conditions 4.8 to 4.11, and 4.19 to 4.22 are the governing equations for the fluid flow in the two-layer system.

4.3 FORMULATION OF THE WEAKLY NONLINEAR WAVE INTERACTION

In a weakly nonlinear interaction analysis, it is assumed that the amplitudes of the interacting waves are small enough to allow truncation of the governing equations at order ε^2, where ε is a typical non-dimensionalized wave amplitude. In the following this assumption is used to simplify the governing non-linear equations.

Simplification of the equations starts with the free surface boundary conditions, i.e., equations 4.8 and 4.9. These equations are transferred from the unknown free surface to $y=h$ using the Taylor's series expansions of the equations at the undisturbed surface. The

resulting equations are truncated at $O(\varepsilon^2)$, and, as a result, the kinematic boundary condition at the free surface reduces to

$$\xi_t + \phi_x \xi_x - \phi_z - \phi_{zz}\xi = 0, \qquad z = h \qquad (4.23)$$

and the dynamic boundary condition at the free surface to

$$\rho'\phi_t + \frac{1}{2}\rho'(\phi_x^2 + \phi_z^2) + \rho' g h - C(t) + \rho'(\phi_{tz} + g)\xi = 0, \qquad z = h \qquad (4.24)$$

To eliminate $\xi(x, t)$ from the equations, the above two equations can be combined. As a result, the following equation is obtained after some simplification.

$$\phi_{tt} + g\phi_z = \left\{-\frac{1}{2}(\phi_x^2 + \phi_z^2) + \frac{1}{g}\phi_t\phi_{zt}\right\}_t - \{\phi_x\phi_t\}_x, \qquad z = h \qquad (4.25)$$

which is correct to $O(\varepsilon^2)$. Similarly, the Taylor's series expansions of the kinematic and dynamic boundary conditions at the interface, truncated at $O(\varepsilon^2)$, yield

$$\eta_t - \phi_z = \phi_{zz}\eta - \phi_x\eta_x, \qquad z = 0 \qquad (4.26)$$

$$\eta_t + \psi_x = -\psi_{xz}\eta - \psi_z\eta_x, \qquad z = 0 \qquad (4.27)$$

$$(\psi_{zz} - \psi_{xx}) = 4\psi_{xz}\eta_x - (\psi_{zzz} - \psi_{xxz})\eta, \qquad z = 0 \qquad (4.28)$$

$$p - C(t) + 2\rho\nu\psi_{xz} + p_z\eta + \rho'(\phi_t + g\eta) = 2\rho\nu\psi_{xx}\eta_x - 2\rho\nu(\psi_{zz}\eta)_x - \rho'\left\{\frac{1}{2}(\phi_x^2 + \phi_z^2) + \phi_{zt}\eta\right\}, \qquad z = 0 \qquad (4.29)$$

Again, the above equations are correct to $O(\varepsilon^2)$.

Equations 4.3, 4.5 to 4.7, 4.9, 4.25 to 4.28, 4.21 and 4.22 are used to perform a weakly nonlinear interaction analysis of the problem. Note that in all these equations except 4.29, all the linear terms are gathered on the left-hand side, separated from the nonlinear terms on the

right hand side. In equation 4.29, the term $p_z\eta$ on the left side produces one linear and one nonlinear term at O(ε^2).

Next, it is assumed that three waves, one surface and two opposite-traveling internal waves, form a resonant triad. The following kinematic conditions of resonance ensure effective and continuous energy transfer between the three waves.

$$\begin{aligned} \omega_0 &= Re[\,\omega_1\,] + Re[\,\omega_2\,] \\ k_0 &= k_1 + k_2 \end{aligned} \tag{4.30}$$

where ω's are the frequencies; k's are the wave numbers; and subscript 0 refers to the surface wave (traveling in the positive x-direction), and subscripts 1 and 2 refer to the positively and negatively traveling internal waves respectively. In the above equations all the frequencies and wave numbers can be complex numbers, except ω_0, which is real. Given ω_0, (4.30) and the linear dispersion relations for waves 0, 1, and 2 form a system of algebraic equations from which all the wave numbers and frequencies can be determined.

The wavelengths of the internal waves computed from the above kinematic relations turn out to be small compared to that of the surface wave, consistent with the experimental observations. This point will be demonstrated later in the numerical example. Considering the fact that the dissipation in short waves is much higher than the long waves, one can simplify the analysis by neglecting the attenuation of the surface wave with space; therefore k_0 is assumed to be real in 4.30. One consequence of this simplification is that k_1 and k_2 also turn out to be real from the calculations.

Next, the solution to the governing equations is expanded as power series in terms of the amplitudes of the waves. For the surface displacement, it is assumed

$$\xi(x,t) = \xi_0(x,t) + \xi_1(x,t) + \xi_2(x,t) + \sum_{i=0}^{2}\sum_{j=i}^{2}\xi_{ij}(x,z,t) + O(\varepsilon^3) + c.c. \tag{4.31}$$

where

$$\xi_i(x,t) = a_i\, e^{i\vartheta_i}, \qquad i = 0,1,2 \tag{4.32}$$

and for the interface displacement

$$\eta(x,t) = \eta_0(x,t) + \eta_1(x,t) + \eta_2(x,t) + \sum_{i=0}^{2}\sum_{j=i}^{2}\eta_{ij}(x,z,t) + O(\varepsilon^3) + c.c. \tag{4.33}$$

where

$$\eta_i(x,t) = b_i\, e^{i\vartheta_i}, \qquad i = 0,1,2 \tag{4.34}$$

In the above equations, the single-indexed terms such as η_i are first-order terms, and the double-indexed terms such as η_{ij} are second-order terms. The quantity ϑ_i is $k_i x - \omega_i t$, $i = 0$ to 2, and c.c. denotes complex conjugate. The a_i's and b_i's, $i = 0$ to 2, are half of the amplitudes of the waves at order ε (linear order) respectively at the free surface and at the interface.

Similarly, the following forms are assumed for ϕ, ψ and p.

$$\phi(x,t) = \phi_0(x,z,t) + \phi_1(x,z,t) + \phi_2(x,z,t) + \sum_{i=0}^{2}\sum_{j=i}^{2}\phi_{ij}(x,z,t) + O(\varepsilon^3) + c.c. \tag{4.35}$$

$$\psi(x,t) = \psi_0(x,z,t) + \psi_1(x,z,t) + \psi_2(x,z,t) + \sum_{i=0}^{2}\sum_{j=i}^{2}\psi_{ij}(x,z,t) + O(\varepsilon^3) + c.c. \tag{4.36}$$

$$p(x,t) = \tilde{p}(z) + p_0(x,z,t) + p_1(x,z,t) + p_2(x,z,t) + \sum_{i=0}^{2}\sum_{j=i}^{2}p_{ij}(x,z,t) + O(\varepsilon^3) + c.c. \tag{4.37}$$

In (4.37), $\tilde{p}(z)$ represents the zeroth-order pressure, which is the static pressure in absence of any motion in the system.

In a medium with weakly nonlinear waves in resonance, energy is exchanged continuously among the triad in a time-scale much longer than the characteristic wave period. Therefore, it is justifiable to follow the method proposed by Bogoliubov and Mitropolski (1958) and assume that at $O(\varepsilon)$ the waves have amplitudes which are weak functions of time as follows.

$$\frac{da_i}{dt} = O(\varepsilon^2), \qquad i = 0,1,2 \qquad (4.38)$$

$$\frac{db_i}{dt} = O(\varepsilon^2), \qquad i = 0,1,2 \qquad (4.39)$$

More precisely, the following forms for the variation of a_i's and b_i's with time are assumed.

$$\frac{da_0}{dx} = O(b_1 b_2) \qquad \text{(a)}$$

$$\frac{db_1}{dx} = O(a_0 \bar{b}_2) \qquad \text{(b)} \qquad (4.40)$$

$$\frac{db_2}{dx} = O(a_0 \bar{b}_1) \qquad \text{(c)}$$

where symbol $^-$ indicates complex conjugate. This technique was first adapted by Benny (1964) from Bogoliubov and Mitropolski's works on nonlinear oscillations and was applied to wave interaction problems. The above assumptions simplify the solution and result in the appearance of time-derivatives of the amplitudes in the governing equations at second order.

After the above assumptions are incorporated into the perturbation scheme, the complete solution of the problem can be obtained by solving the resulting equations order by order. However, here in a weakly nonlinear interaction analysis, only the solution up to $O(\varepsilon^2)$ is needed. First, zero-th and first order solutions are obtained. In order to develop expressions for the variation of a_i's and b_i's, $i = 0$ to 2, with time, one then needs to carry on to second order. At this order, the equations are inhomogeneous with the time variation of the

amplitudes of the waves appearing in the forcing functions. The sets of governing equations have secular solutions at this order unless a solvability condition is imposed on the forcing functions. As it will be seen later, this solvability condition gives the desired equations for the variation of the amplitudes of the surface and internal waves with time.

4.3.1 Zeroth-order Solution

At zeroth-order

$$C(t) = \rho' g h \tag{4.41}$$

$$\tilde{p}(z) = g(\rho' h - \rho z) \tag{4.42}$$

The above expression for $\tilde{p}(z)$ corresponds to the pressure distribution in the system in absence of any motion.

4.3.2 First-order Solution (linear theory)

The field equations at $O(\varepsilon)$, with subscripts dropped, are

$$\nabla^2 \phi = 0 \tag{4.43}$$

in the upper layer, and

$$\nabla^2 \psi_t - \nu \nabla^4 \psi = 0 \tag{4.44}$$

in the lower layer. Similarly, the corresponding boundary conditions are

$$\phi_{tt} + g\phi_z = 0 \quad , \qquad z = h \tag{4.45}$$

$$\xi_t = \phi_z , \qquad z = h \tag{4.46}$$

$$\eta_t = \phi_z , \qquad z = 0 \tag{4.47}$$

$$\eta_t = -\psi_x, \qquad z = 0 \qquad (4.48)$$

$$p + 2\rho\nu\psi_{xz} - \rho g\eta + \rho'(\phi_t + g\eta) = 0\ , \qquad z = 0 \qquad (4.49)$$

$$\rho\psi_{zt} + p_x - \rho\nu\nabla^2\psi_z = 0, \qquad z = 0 \qquad (4.50)$$

$$\psi_{zz} - \psi_{xx} = 0, \qquad z = 0 \qquad (4.51)$$

$$\psi_z = 0, \qquad z = -d \qquad (4.52)$$

$$\psi_x = 0, \qquad z = -d \qquad (4.53)$$

Solution to the above set of differential equations for a wave with wave number k and frequency ω is given in Appendix C.

4.3.3 Second-order Solution

Substitution of 4.31 to 4.37 in the governing equations and collection of $O(\varepsilon^2)$ terms result in sets of linear partial differential equations (PDE's) with associated boundary conditions. A close inspection of these equations in conjunction with the kinematic relations of (4.30) shows possibility of resonance (or semi-resonance as explained later) as the secular terms in the solutions may appear at this order.

For instance, in the set of PDE's at $O(a_0\bar{b}_1)$, the forcing functions, which are due to nonlinear coupling of waves 1 and 0, have terms some of which are in phase with the solution to the homogenous problem. This means the nonlinear coupling of waves 1 and 0 is in resonance with wave 2, and therefore the secular terms could appear in the solution of the interaction problem at $O(a_0\bar{b}_1)$.

To illustrate the above point, the governing equations at $O(a_0\bar{b}_1)$ are derived. First, the following convenient form for the linear solution to the motion of wave 2 is assumed.

$$\begin{aligned}
\eta_2(x,t) &= b_2 e^{i\vartheta_2} \\
\xi_2(x,t) &= b_2 \hat{\xi}_2 e^{i\vartheta_2} \\
\phi_2(x,z,t) &= b_2 \hat{f}_2(z) e^{i\vartheta_2} \\
\psi_2(x,z,t) &= b_2 \hat{g}_2(z) e^{i\vartheta_2} \\
p_2(x,z,t) &= b_2 r\hat{p}_2(z) e^{i\vartheta_2}
\end{aligned} \tag{4.54}$$

The quantities $\hat{\xi}_2$, $\hat{p}_2(z)$, $\hat{f}_2(z)$, and $\hat{g}_2(z)$ can be easily determined from the appropriate relations in Appendix C. The governing equations at order $a_0\bar{b}_1$ are

$$\nabla^2\phi_{01} = 0, \qquad 0 < z < h \tag{4.55}$$

$$\begin{aligned}
&\nabla^2(\psi_{01})_t - \nu\nabla^4\psi_{01} = \\
&\quad \left\{(\psi_0)_x \nabla^2(\bar{\psi}_1)_z + (\bar{\psi}_1)_x \nabla^2(\psi_0)_z - (\psi_0)_z \nabla^2(\bar{\psi}_1)_x - (\bar{\psi}_1)_z \nabla^2(\psi_0)_x\right\} \\
&\quad + \left\{-\frac{db_2}{dt}\left(\frac{d^2\hat{g}_2(z)}{dz^2} - k_2{}^2\hat{g}_2(z)\right)e^{i\vartheta_2}\right\}
\end{aligned}$$

$$, \qquad -d < z < 0 \tag{4.56}$$

$$\begin{aligned}
&(\phi_{01})_{tt} + g(\phi_{01})_z = \\
&\quad \left\{-(\phi_0)_x(\bar{\phi}_1)_x - (\phi_0)_z(\bar{\phi}_1)_z + 1/g(\phi_0)_t(\bar{\phi}_1)_{zt} + 1/g(\bar{\phi}_1)_t(\phi_0)_{zt}\right\}_t \\
&\quad + \left\{-(\phi_0)_x(\bar{\phi}_1)_t - (\bar{\phi}_1)_x(\phi_0)_t\right\}_x + \left\{2\frac{db_2}{dt} i\omega_2 \hat{f}_2(z) e^{i\vartheta_2}\right\}
\end{aligned}$$

$$, \qquad z = h \tag{4.57}$$

$$(\eta_{01})_t - (\phi_{01})_z = \left\{-(\phi_0)_x\bar{\eta}_1 - (\bar{\phi}_1)_x\eta_0\right\}_x + \left\{-\frac{db_2}{dt}e^{i\vartheta_2}\right\}, \qquad z = 0 \tag{4.58}$$

$$(\eta_{01})_t + (\psi_{01})_x = \left\{-(\psi_0)_z\bar{\eta}_1 - (\bar{\psi}_1)_z\eta_0\right\}_x + \left\{-\frac{db_2}{dt}\ e^{i\vartheta_2}\right\}, \qquad z = 0 \tag{4.59}$$

$$(\psi_{01})_{zz} - (\psi_{01})_{xx} =$$
$$\{4(\psi_0)_{xz}(\overline{\eta}_1)_x + 4(\overline{\psi}_1)_{xz}(\eta_0)_x + [(\psi_0)_{xxz} - (\psi_0)_{zzz}]\overline{\eta}_1 + [(\overline{\psi}_1)_{xxz} - (\overline{\psi}_1)_{zzz}]\eta_0\}$$

$$, \qquad z = 0 \qquad (4.60)$$

$$p_{01} + 2\rho\nu(\psi_{01})_{xz} + \rho'[(\phi_{01})_t + g\eta_{01}] - \rho g\eta_{01} =$$
$$\rho\{2\nu(\psi_0)_{xx}(\overline{\eta}_1)_x + 2\nu(\overline{\psi}_1)_{xx}(\eta_0)_x - 2\nu[(\psi_0)_{zz}\overline{\eta}_1 + (\overline{\psi}_1)_{zz}\eta_0]_x$$
$$- r[(\phi_0)_x(\overline{\phi}_1)_x + (\phi_0)_z(\overline{\phi}_1)_z + (\phi_0)_{zt}\overline{\eta}_1 + (\overline{\phi}_1)_{zt}\eta_0]$$
$$+ [\nu\nabla^2(\psi_0)_x - (\psi_0)_{xt}]\overline{\eta}_1 + [\nu\nabla^2(\overline{\psi}_1)_x - (\overline{\psi}_1)_{xt}]\eta_0] - \rho\hat{f}_2(z)\frac{db_2}{dt}e^{i\vartheta_2}$$

$$, \qquad z = 0 \qquad (4.61)$$

$$\rho(\psi_{01})_{zt} + (p_{01})_x - \rho\nu\nabla^2(\psi_{01})_z =$$
$$\rho\{(\psi_0)_x(\overline{\psi}_1)_{zz} + (\overline{\psi}_1)_x(\psi_0)_{zz} - (\psi_0)_z(\overline{\psi}_1)_{zx} - (\overline{\psi}_1)_z(\psi_0)_{zx}\}$$
$$- \rho\frac{d\hat{g}_2(z)}{dz}\frac{db_2}{dt}e^{i\vartheta_2}$$

$$, \qquad -d < z < 0 \qquad (4.62)$$

$$(\psi_{01})_x = 0, \qquad z = -d \qquad (4.63)$$

$$(\psi_{01})_z = 0, \qquad z = -d \qquad (4.64)$$

where single indices 0 and 1 refer to waves 0 and 1 respectively. In the above equations, symbol $^-$ denotes complex conjugate. Note that equation 4.61 has been included here just to give the expression for p_{01} in (4.62). Using the kinematic relations of resonance, equations 4.56 to 4.62 are simplified to

$$\nabla^2(\psi_{01})_t - \nu\nabla^4\psi_{01} = B_0(z)e^{\Delta\omega_2 t}e^{i\vartheta_2} + \left\{-\frac{db_2}{dt}\left(\frac{d^2\hat{g}_2(z)}{dz^2} - k_2{}^2\hat{g}_2(z)\right)e^{i\vartheta_2}\right\}$$

$$-d < z < 0 \qquad (4.65)$$

$$(\phi_{01})_{tt} + g(\phi_{01})_z = B_1\, e^{\Delta\omega_2 t} e^{i\theta_2} + \left\{ 2\frac{db_2}{dt} i\omega_2 \hat{f}_2(z) e^{i\vartheta_2} \right\}, \qquad z = h \qquad (4.66)$$

$$(\eta_{01})_t - (\phi_{01})_z = B_2\, e^{\Delta\omega_2 t} e^{i\theta_2} + \left\{ -\frac{db_2}{dt} e^{i\vartheta_2} \right\}, \qquad z = 0 \qquad (4.67)$$

$$(\eta_{01})_t + (\psi_{01})_x = B_3\, e^{\Delta\omega_2 t} e^{i\theta_2} + \left\{ -\frac{db_2}{dt}\, e^{i\vartheta_2} \right\}, \qquad z = 0 \qquad (4.68)$$

$$(\psi_{01})_{zz} - (\psi_{01})_{xx} = B_4\, e^{\Delta\omega_2 t} e^{i\vartheta_2}, \qquad z = 0 \qquad (4.69)$$

$$p_{01} + 2\rho\nu(\psi_{01})_{xz} + \rho'[(\phi_{01})_t + g\eta_{01}] - \rho g \eta_{01} = \rho B_5\, e^{\Delta\omega_2 t} e^{i\vartheta_2} - \rho'\hat{f}_2(z)\frac{db_2}{dt} e^{i\vartheta_2},$$

$$z = 0 \qquad (4.70)$$

$$\rho(\psi_{01})_{zt} + (p_{01})_x - \rho\nu\nabla^2(\psi_{01})_z = \rho B_6\, e^{\Delta\omega_2 t} e^{i\vartheta_2} - \rho\frac{d\hat{g}_2(z)}{dz}\frac{db_2}{dt} e^{i\vartheta_2},$$

$$-d < z < 0 \qquad (4.71)$$

where $\Delta\omega_2 = Im[\omega_0 + \omega_1 - \omega_2] = Im[\omega_1 - \omega_2]$, and $e^{\Delta\omega_2 t}$ is an unbalanced term in the equations. The functions $B_0(z)$ and $B_6(z)$ are known functions having $a_0\bar{b}_1$ as their common factor. Similarly, the constants B_i's, $i = 1, 2, ..., 5$, are known multiples of $a_0\bar{b}_1$. Due to their excessive lengths, B_i's, $i = 0, 1, ..., 6$, are not presented here. The term $e^{\Delta\omega_2 t}$ has appeared in the above equations because unlike the real part, the imaginary part of $\omega_0 - \bar{\omega}_1 - \omega_2$ does not vanish in the above equations. However, the internal waves have close complex frequencies, so $\Delta\omega_2$ is small compared to ω_2. This will be shown later in the numerical example. In the inviscid limit of the interaction, the frequencies do not have imaginary parts, and therefore $\Delta\omega_2 = 0$ exactly.

Next, equation 4.71 is used to eliminate p_{01} from equation 4.70. This gives

$$2\rho\nu(\psi_{01})_{xxz} - \rho(\psi_{01})_{zt} + \rho\nu\nabla^2(\psi_{01})_z + \rho'[(\phi_{01})_{xt} + g(\eta_{01})_x] - \rho g(\eta_{01})_x =$$
$$\rho[B_5(ik) - B_6]\, e^{\Delta\omega_2 t} e^{i\vartheta_2} + \left(-\rho' ik_2 \hat{f}_2(z) + \rho\frac{d\hat{g}_2}{dz}\right)\frac{db_2}{dt} e^{i\vartheta_2}$$
$$, \qquad z = 0 \qquad (4.72)$$

Equations 4.55, 4.63 to 4.69, and 4.72 establish a complete set of PDE's and corresponding boundary conditions at order $(a_0\bar{b}_1)$.

When $\Delta\omega_2 = 0$, i.e., when the waves interact in an inviscid medium, the forcing functions can be of the form that produces secular terms $te^{i\vartheta_2}$ in the solution. These secular terms grow wildly in t and destroy uniformity of the perturbation series. To avoid this, one needs to place a condition on the form of the forcing functions. Applying this solvability condition to the set of equations gives an equation in which db_2/dt is expressed as a function of $a_0\bar{b}_1$. Similarly, one can get db_1/dt and da_0/dt from imposing proper conditions on the form of the forcing functions at order $(a_0\bar{b}_2)$ and $(b_1 b_2)$ respectively. These equations for t-derivatives of the amplitudes can be solved to give a_0, b_1 and b_2 as functions of time, and hence the time variations of the waves can be determined.

In the present case, where due to viscosity $\Delta\omega_2$ is not zero but is close to it, the forcing functions can cause close-resonance behavior in the solution. This again leads to a solution that grows in time and hence destroys uniformity of the perturbation scheme, similar to the case $\Delta\omega_2 = 0$. To avoid this, a technique similar to that used by Rott (1970) in analyzing the undamped motion of a double-pendulum close to internal resonance is employed. Closeness of $\Delta\omega_2$ to zero implies that $e^{\Delta\omega_2 t}$ does not vary much with time compared to $e^{i\vartheta_2}$, and therefore it can be approximated as a constant. With this approximation, the problem can be treated as an undamped wave interaction, although viscous effects are present in the equations. Since for both weak and heavy viscosity $\Delta\omega_2$ is close to zero, the technique is valid for a broad range of damping.

Next, it is assumed that the solution to the problem at $O(a_0\bar{b}_1)$ has the following form.

$$\eta_{01}(x,t) = \hat{\eta}_{01}\, e^{i\vartheta_2} + c.c.$$
$$\phi_{01}(x,z,t) = f_{01}(z)e^{i\vartheta_2} + c.c. \qquad (4.73)$$
$$\psi_{01}(x,z,t) = g_{01}(z)e^{i\vartheta_2} + c.c.$$

After substituting the above forms in equations 4.55, 4.63 to 4.69, and 4.72; and neglecting all complex conjugate parts for the moment, the following equations are derived after elimination of $\hat{\eta}_{01}$.

$$f_{01}''(z) - k_2^2\, f_{01}(z) = 0, \qquad 0 < z < h \qquad (4.74)$$

$$g_{01}''''(z) - (k_2^2 + \lambda_2^2)g_{01}''(z) + k_2^2\lambda_2^2 g_{01}(z) = \frac{-B_0(z)}{\nu} e^{\Delta\omega_2 t} + \left\{\frac{1}{\nu}\frac{db_2}{dt}\left(\frac{d^2\hat{g}_2(z)}{dz^2} - k_2{}^2\hat{g}_2(z)\right)\right\}$$
$$, \qquad -d < z < 0 \qquad (4.75)$$

$$-\omega_2^2\, f_{01}(z) + g\, f_{01}'(z) = B_1\, e^{\Delta\omega_2 t} + \left\{2\frac{db_2}{dt} i\omega_2 \hat{f}_2(z)\right\}, \qquad z = h \qquad (4.76)$$

$$i k_2\ g_{01}(z) + f_{01}'(z) = (B_3 - B_2)\, e^{\Delta\omega_2 t}, \qquad z = 0 \qquad (4.77)$$

$$g_{01}''(z) + k_2^2\ g_{01}(z) = B_4\, e^{\Delta\omega_2 t}, \qquad z = 0 \qquad (4.78)$$

$$\left\{\nu[-3k_2^2 g_{01}'(z) + g_{01}'''(z)] + i\omega_2 g_{01}'(z) + r\omega_2 k_2 f_{01}(z) - (r-1)gk_2\frac{f_{01}'(z)}{\omega_2}\right\} =$$
$$\left(B_5(ik_2) - B_6 + (r-1)g\frac{k_2}{\omega_2}B_2\right)e^{\Delta\omega_2 t} + \left(-rik_2\hat{f}_2(z) + \frac{d\hat{g}_2}{dz} + (1-r)g\frac{k_2}{\omega_2}\right)\frac{db_2}{dt}$$
$$, \qquad z = 0 \qquad (4.79)$$

$$g_{01}(z)=0, \qquad z=-d \qquad (4.80)$$

$$g'_{01}(z)=0, \qquad z=-d \qquad (4.81)$$

where the primes refer to the derivatives with respect to z.

The set of equations corresponding to c.c. parts of equations 4.55, 4.63 to 4.69, and 4.72 is in fact the complex conjugate of the above system of equations and hence its solution will be the complex conjugate of the solution to the above equations. As a result, the complex conjugate system does not need a separate treatment.

The above set of ordinary differential equations and associated boundary conditions do not yield a uniform solution unless a solvability condition as discussed in Appendix D is imposed on the forcing functions, which are gathered on the right hand sides. This solvability condition ensures that at $O(a_0\bar{b}_1)$ the original problem has a solution of the form $e^{i\vartheta_2}$ and not of the secular form $t\,e^{i\vartheta_2}$. Applying the solvability condition from Appendix D to the forcing functions gives the following equation.

$$\frac{db_2}{dt}=\alpha_2 e^{\Delta\omega_2 t}a_0\bar{b}_1 \qquad (4.82)$$

where α_2 is a known constant.

Similarly, if the above procedure is carried out for the governing equations at $O(a_0\bar{b}_2)$ and $O(b_1b_2)$, the following relations for db_1/dt and da_0/dt are obtained.

$$\frac{db_1}{dt}=\alpha_1 e^{\Delta\omega_1 t}a_0\bar{b}_2 \qquad (4.83)$$

$$\frac{da_0}{dt}=\alpha_0 e^{\Delta\omega_0 t}b_2b_1 \qquad (4.84)$$

where α_1 and α_0 are known constants; and $\Delta\omega_1 = Im[\,\omega_2 - \bar{\omega}_1\,]$ and $\Delta\omega_0 = Im[\,\omega_1 + \omega_2\,]$. Mathematica® was extensively used to simplify the expressions for the interaction coefficients α_0, α_1 and α_2. However, even after exhaustive algebraic simplifications, the expressions are still too long to be presented here. Simultaneous solution of (4.82) to (4.84) gives the amplitudes of the waves as functions of time.

Considering the fact that the surface wave has much more energy than the internal waves, one can simplify the analysis by assuming that the surface wave amplitude does not change with time, or a_0 is constant. Hence, from now on, equation 4.84 is neglected and a_0 is treated as a constant in (4.83) and (4.82).

Now, an attempt is made to obtain an approximate, but useful, solution for $b_1(t)$ based on the above approximations. By combining (4.82) and (4.83), the following second-order differential equation in terms of $b_1(t)$ is obtained.

$$b_1''(t) - (\beta_1 - \beta_2)b_1'(t) - (\alpha_1\bar{\alpha}_2 a_0\bar{a}_0)b_1(t) = 0 \tag{4.85}$$

where

$$\beta_i = -Im[\,\omega_i\,], \qquad i = 1,2 \tag{4.86}$$

The quantity β_i is the damping coefficient of internal wave i. It is obtained from the linear wave theory and is a positive number. The exact solution to (4.85) is

$$b_1(t) = C_1 e^{\left(\frac{(\beta_1-\beta_2)+\sqrt{\Delta}}{2}\right)t} + C_2 e^{\left(\frac{(\beta_1-\beta_2)-\sqrt{\Delta}}{2}\right)t} \tag{4.87}$$

where

$$\Delta = (\beta_1 - \beta_2)^2 + 4\alpha_1\bar{\alpha}_2|a_0|^2$$

The constants C_1 and C_2 are determined from the amplitudes of the internal waves at $t=0$. Assuming $Re[\alpha_1\overline{\alpha}_2]>0$, the second term in the solution diminishes rapidly with time and hence can be neglected. This assumption will be verified later in the numerical example. Also, as the internal waves have close kinematic properties, $(\beta_1-\beta_2)^2$ is nearly zero and hence $\Delta\approx 4\alpha_1\overline{\alpha}_2|a_0|^2$. As a result, the approximate solution to $b_1(t)$ at large t is

$$b_1(t)\approx C_1 e^{\left(\frac{(\beta_1-\beta_2)}{2}+\alpha|a_0|\right)t} \tag{4.88}$$

where

$$\alpha=\sqrt{\alpha_1\overline{\alpha}_2} \tag{4.89}$$

with $Re[\alpha]>0$. From (4.88) and (4.34), the interface displacement due to internal wave 1 is

$$\eta_1(x,t)\approx C_1 e^{\left(\frac{(\beta_1-\beta_2)}{2}+\alpha|a_0|\right)t} e^{i(k_1x-\omega_1 t)} \tag{4.90}$$

or

$$\eta_1(x,t)\approx C_1 e^{\left(\frac{(\beta_1-\beta_2)}{2}-\beta_1+Re[\overline{\alpha}]|a_0|\right)t} e^{i\{k_1x-(Re[\omega_1]-Im[\alpha]|a_0|)t\}} \tag{4.91}$$

as $\omega_1=Re[\omega_1]-i\beta_1$. The first term on the right hand side of (4.91) is exponential, and the second is oscillatory in time. Note that according to (4.91), the frequency of internal wave 1 is shifted because of viscosity. Defining γ as in chapter 2 and denoting the shifted frequency by Ω, one has

$$\Omega_1=Re[\omega_1]-Im[\alpha]|a_0| \tag{4.92}$$

$$\gamma=-\beta+Re[\alpha]|a_0| \tag{4.93}$$

where

$$\beta = \frac{(\beta_1 + \beta_2)}{2} \tag{4.94}$$

is the average of the damping coefficients of the two internal waves. Note that β and $Re[\alpha]$ are both positive real numbers.

The solution of $b_2(t)$ yields the same expression for γ, but a little different expression for Ω_2:

$$\Omega_2 = Re[\omega_2] - Im[\bar{\alpha}]|a_0| \tag{4.95}$$

According to the above expressions, both the growth rates and shifted frequencies are functions of the surface wave amplitude; the higher a_0, the higher the growth rates and the more shifted the frequencies. The form of γ in (4.93) is very similar to that obtained in chapter 2.

4.4 NUMERICAL EXAMPLE AND DISCUSSION

Consider the case where $d = 4.0\ cm$, $H = 16.0\ cm$, $\rho' = 1.00\ gr/cm^3$, $\rho = 1.12\ gr/cm^3$, $\omega_0 = 7.85\ rad/s$, $g = 9.81\ m/s^2$, $\nu = 5\times10^{-4}\ m/s^2$, and $a_0 = 2.5\ cm$. The kinematic viscosity of the lower layer is 500 times bigger than the kinematic viscosity of water, and the amplitude of the surface wave corresponds to the breaking point.

From simultaneous solution of the kinematic relations of resonance and the dispersion relations, one can obtain

$$k_0 = (7.654 + 0.092\,i)\ rad/m,$$

$$k_1 = 36.15\ rad/m, \qquad \omega_1 = (4.21 - 0.75\,i)\ rad/s,$$

$$k_2 = -28.49\ rad/m, \qquad \omega = (3.64 - 0.63\,i)\ rad/s$$

The interaction analysis yields the following values for α_1 and α_2.

$$\alpha_1 = 3.55 - 1.42i \ (m.sec)^{-1}, \qquad \alpha_2 = -15.85 - 3.92i \ (m.sec)^{-1}$$

With the frequencies and wave numbers determined, the assumptions in the formulation and the solution of the viscous interaction problem can be examined. First, from the above results it is observed the imaginary part of k_0 is very small compared to the real part. This justifies neglecting the imaginary part of k_0 in the analysis. Also, $\Delta\omega_1 = -\Delta\omega_2 = \beta_2 - \beta_1$ is very small compared to the frequency of wave 1 or 2. Therefore, the main assumption in the viscous model to take $e^{\Delta\omega_1 t}$ and $e^{\Delta\omega_{21} t}$ constant in comparison to the time variation of $e^{-i\omega_1 t}$ and $e^{-i\omega_2 t}$ is also validated. Finally, from the above values $Re[\alpha_1\overline{\alpha}_2] > 0$, consistent with the assumption to neglect the second term in (4.87). Note that these results are not specific to this example and are typical of the interaction.

In the following, the results of the viscous model are compared with those of the three-dimensional analysis in chapter 2. In particular, attention is paid to the two opposite roles of viscosity in the interaction. Viscosity can enhance growth of the internal waves through production of higher shear at the interface. At the same time, however, it dampens the internal waves. The net effect of viscosity on the interaction is determined by the combination of these two counteracting roles.

As discussed in the previous chapters, $Re[\alpha]|a_0|$ is a measure of the surface wave forcing for excitation of the internal waves, and β is a measure of the dissipation rate of the internal waves. Figure 4.3(a) shows variations of $Re[\alpha]a_0/\omega_0$ from the two analyses with the non-dimensionalized viscosity $\nu/(gH^3)^{1/2}$. In derivation of the results of the three-dimensional model, it has been assumed that the interaction is two-dimensional and therefore $\theta_1 = \theta_2 = 0$. For a viscosity of $5\times10^{-4}\ m/s^2$, $\nu/(gH^3)^{1/2}$ is about 2.5×10^{-3}. It is seen the results of the three-dimensional analysis are valid only for low values of $\nu/(gH^3)^{1/2}$. As the three-

dimensional model has an inviscid formulation with regard to the calculation of the parameter α, the values of $Re[\alpha]a_0/\omega_0$ according to this model is a constant. Of interest is that according to the viscous analysis $Re[\alpha]a_0/\omega_0$ increases with $\nu/(gH^3)^{1/2}$ at high viscosity. In other words, the surface wave forcing increases with viscosity. However, it will be shown that the damping effect of viscosity on the interaction is much more important than its forcing effect. Figure 4.3(a) also indicates that as expected the viscous model is asymptotic to the three-dimensional model when $\nu \to 0$. This can be considered as a check of the long calculations in the two analyses.

Variations of β/ω_0 with the non-dimensional viscosity according to the two analyses are shown in figure 4.3(b). As seen, the two graphs are asymptotically identical when $\nu \to 0$ and remain still close together at large viscosity. Also, it can be seen that β/ω_0 increases almost linearly with viscosity.

According to the preceding discussions, a larger viscosity gives rise to a higher surface wave forcing as well as a higher damping of the internal waves. It is interesting to examine the net effect of viscosity on the growth rate. In figure 4.3(c), γ/ω_0 is plotted as a function of $\nu/(gH^3)^{1/2}$. It is seen that the viscous model predicts that an increase in viscosity reduces the growth rate considerably from a positive value at $\nu = 0$ to a negative value, which means decay, at high viscosity. This can be explained by noting that although both forcing and damping increase with viscosity, damping rises faster. The net effect will then be a reduction in the growth rate.

The preceding result is in direct conflict with the findings of Wen (1995), and Hill and Foda (1996). Based on their analyses of the interaction in a viscous medium, these authors found that for the range of the real fluids, presence of viscosity is necessary for excitation and growth of the internal waves. However, the present study indicates that the net effect of viscosity is to suppress the instability. To resolve the issue, experiments with both salt water

and diluted corn syrup as the lower layer were performed in a wave flume. The results of these experiments have been presented in section 3.3.6. The experimentation indicated that for the cases in which the internal waves were excited in the salt-water experiments, no instability were observed in the corresponding corn syrup experiments. This verifies the results of the present study regarding the significance of the dissipation role of viscosity in the interaction.

Another interesting result from figure 4.3(c) is that both the viscous and the three-dimensional models have predicted nearly the same values of γ at large viscosity. This can be explained by noting that from figures 4.3(a) and 4.3(b), the damping term in equation 4.93 at large viscosity is much bigger than the forcing term and thus $-\beta$ will be the dominant term in the equation. Considering that both models have predicted nearly the same damping β / ω_0 for the internal waves, the closeness of the two curves in figure 4.3(c) at large viscosity is explained.

As discussed earlier, viscosity also affects the frequencies of the internal waves. Figure 4.4 shows variation of non-dimensional frequency, $Re[\omega_1] / \omega_0$, and non-dimensional shifted frequency, Ω_1 / ω_0, of wave 1 with $\nu / (gH^3)^{1/2}$. Note that ω_1 is obtained from the linear theory. As seen, the shifted frequency deviates more and more from the linear theory as viscosity increases. It is also interesting to note that $Re[\omega_1] / \omega_0$ does not change much with viscosity and remains approximately equal to $1/2$.

4.5 SUMMARY

The three-dimensional model in chapter 2 considered only the dissipating effect of viscosity on the interaction. In this chapter a theoretical model that took into account both forcing and damping effects of viscosity was developed. Given the complexity of the viscous

formulation, the analysis was restricted to two dimensions. In contrast with the three-dimensional model, developed for a weak viscosity of the lower layer, the current model is not restricted in its ability to handle high viscosity.

Comparison was made with the results of Wen (1995) and Hill and Foda (1996) regarding the viscous interaction. These authors found that growth of the internal waves is critically dependent on presence of viscosity. However, the present study indicates that the net effect of viscosity on the interaction process is to suppress the internal waves. The model results showed that both surface wave forcing and viscous damping of the internal waves increase with viscosity, but the net effect is a decrease in the growth rate. This was shown to agree with the results of the corn syrup experiments in chapter 3.

It was shown that as expected the viscous model is asymptotic to the three-dimensional model when $\nu \rightarrow 0$. This can be considered as a check of the long calculations in the two analyses.

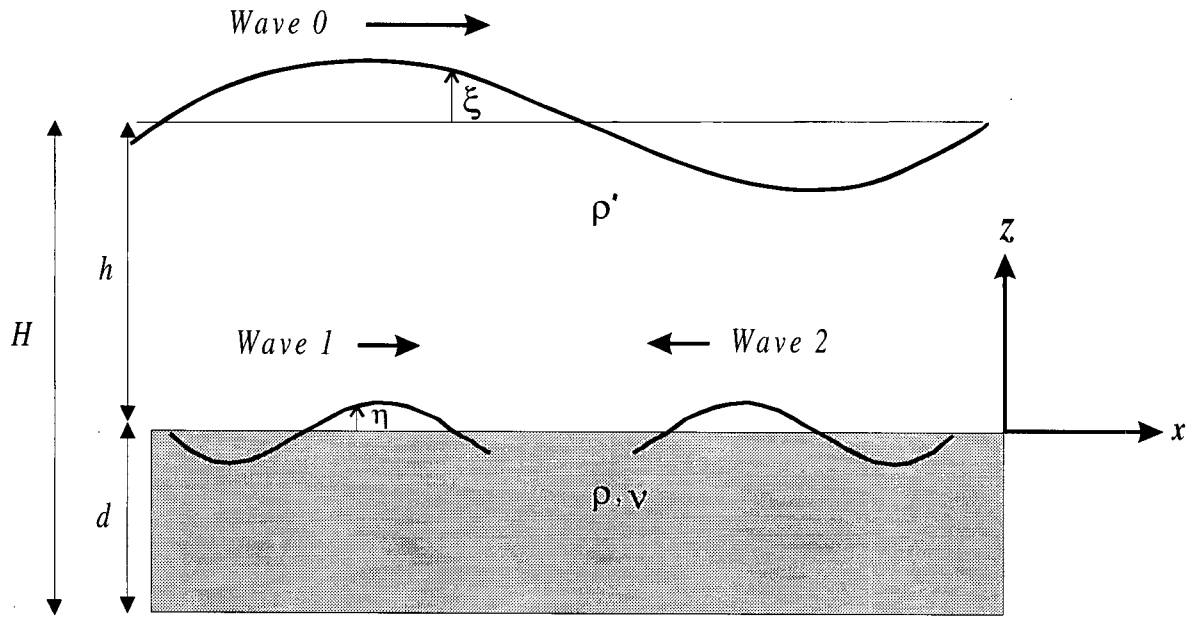

Figure 4.1 Configuration of the problem.

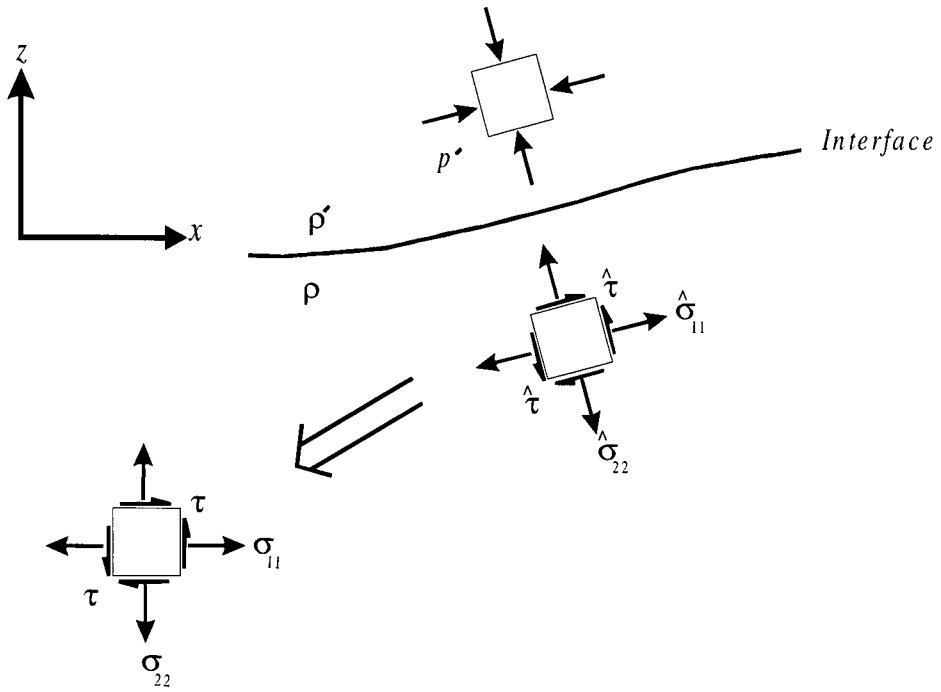

Figure 4.2 Stresses on a fluid element at the interface.

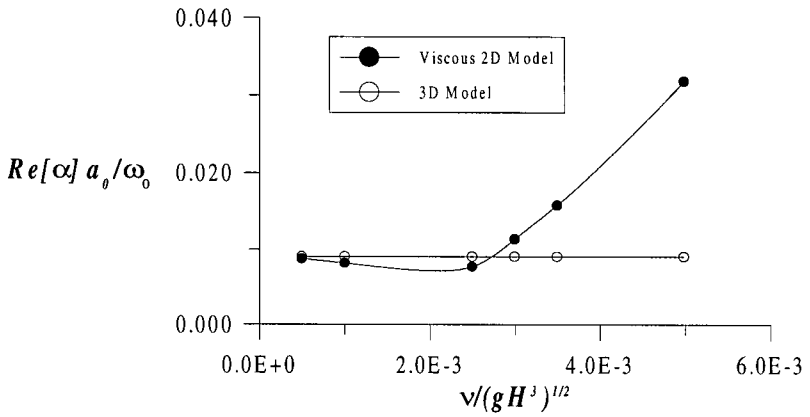

(a)

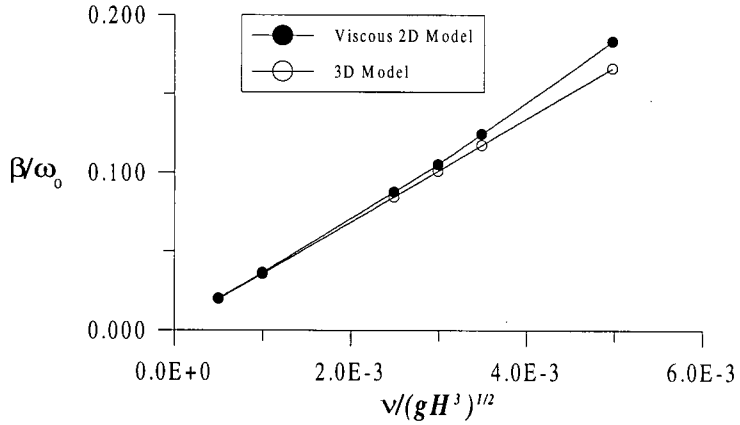

(b)

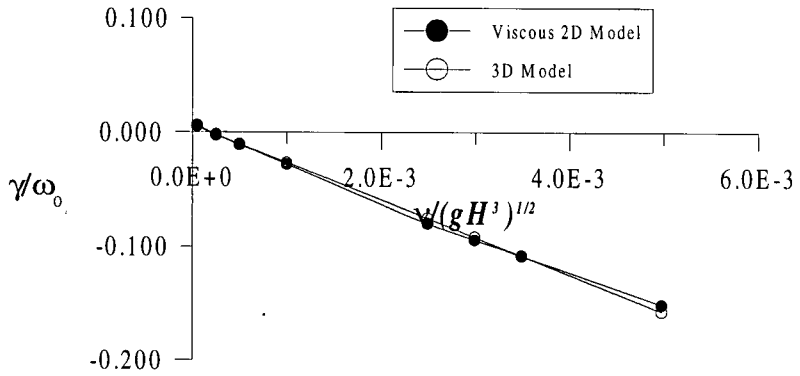

(c)

Figure 4.3 Variation of **a)** $\mathrm{Re}[\alpha]a_0/\omega_0$, **b)** β/ω_0, and **c)** γ/ω_0 with $\nu/(gH^3)^{1/2}$.

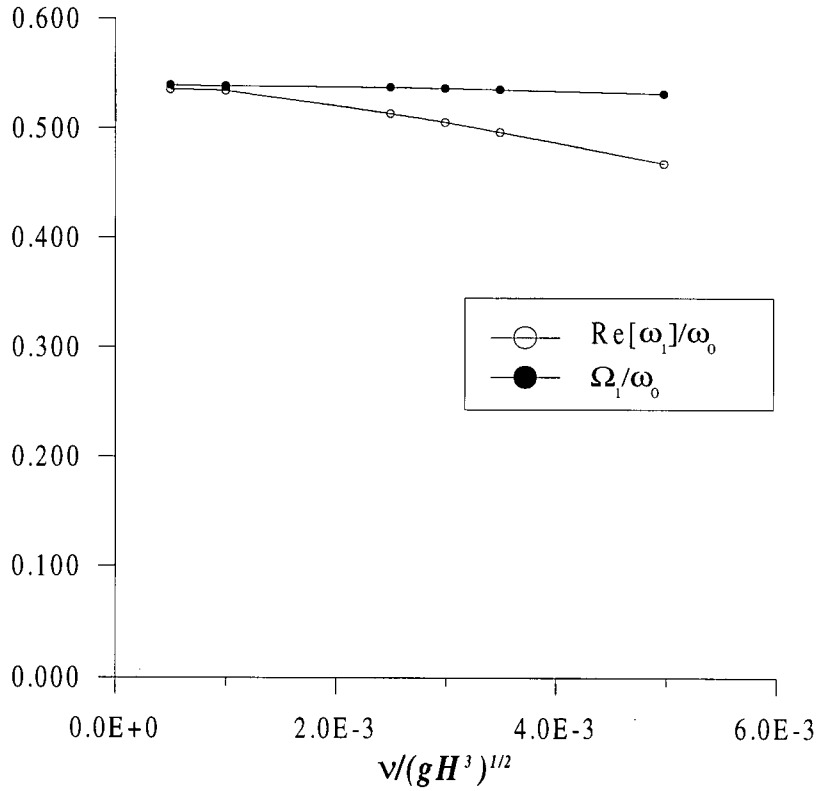

Figure 4.4 Variation of $Re[\omega_1]/\omega_0$ and Ω_1/ω_0 with $\nu/(gH^3)^{1/2}$.

CHAPTER 5

CONCLUSIONS AND RECOMMENDATIONS

5.1 INTERACTION IN A WEAKLY VISCOUS MEDIUM

The interaction between a surface and two internal waves in a weakly viscous medium was studied theoretically and experimentally in chapters 2 and 3 respectively. In the following, a summary of the study is given.

5.1.1 Theoretical Study

A conventional wave interaction analysis of the problem was presented in chapter 2. The three-dimensional two-layer fluid system was assumed to consist of an inviscid upper layer and a weakly viscous lower layer. Viscosity was neglected initially in the formulation of the problem, but after deriving the evolution equations the damping effect of viscosity on the internal waves was taken into account. The analysis indicated that under certain

circumstances a surface wave traveling in a two-layer fluid can excite two internal waves. The internal waves are much shorter than the surface wave and propagate nearly in opposite directions. The frequencies of the internal waves were found to be almost half of the frequency of the surface wave. These results are in accord with the previous theoretical and experimental studies as well as the present experimental investigation.

The interaction analysis indicated that the amplitudes of the internal waves vary as $e^{\gamma t}$ at large time. The growth parameter γ is the sum of two terms: $\alpha|a_0|$, which is the forcing term, and $-\beta$, which is the viscous damping term. The excitation takes place when the forcing is high enough to overcome the viscous dissipation of the internal waves, that is, when γ is positive.

To evaluate the effects of each system parameter on the interaction, a typical example was chosen, and a sensitivity analysis was performed by changing each independent parameter separately and observing the effects on the properties of the internal waves, in particular, on their evolution. The study indicated that the surface wave forcing is most affected by the depth ratio d / H, the surface wave frequency, the direction of the internal wave pair, and the surface wave height. The density ratio does not seem to have an appreciable influence on the forcing. The forcing increases with the surface wave amplitude and the obliqueness of the internal waves.

In terms of dissipation of the internal waves, the density ratio, the depth ratio, the viscosity and the surface wave frequency were found to have the biggest effect on the interaction. Unlike the forcing, the viscous damping of the internal wave pair was found to be nearly independent of the propagation directions of the internal waves. The results also indicated that the damping increases as the density difference or the depth ratio d / H approaches zero. The damping is large also when the surface wave frequency or the viscosity is high.

The parameters that significantly influence the growth rate of the internal waves are the depth ratio, the density difference, the viscosity, the surface wave frequency, the direction of the internal wave pair, and the surface wave amplitude. It was found that when the depth ratio d / H or the density difference is sufficiently small, the internal waves are unable to grow. The same is true when the viscosity or the surface wave frequency is high enough. These were shown to be the results of the high viscous damping of the internal waves.

One important finding of the three-dimensional analysis was that the internal waves have a higher growth rate when they become more oblique to the surface wave. It was shown that the growth rate becomes maximal when the internal waves form a symmetric arrangement with the surface wave and have exactly a frequency of $\omega_0 / 2$. In this situation, the internal waves propagate nearly perpendicular to the surface wave. Also, it was found that the growth rate is an increasing function of the surface wave amplitude, and for excitation the amplitude of the surface wave has to be bigger than a critical value.

Comparisons were made with the theoretical study of Hill (1997) on the subject. In his inviscid analysis of the three-dimensional interaction, Hill (1997) found that there are narrow bands of surface wave frequency and density ratio only within which the growth of the internal waves is possible. Furthermore, he found that there are close upper and lower bounds on the direction angle of the internal wave pair. These were found to be in conflict with the present three-dimensional results as well as the experimental findings. Another discrepancy between the two analyses is their different predictions of the interaction in two dimensions. Hill (1997) found that in an inviscid medium there is no growth of the internal waves when the internal waves are in the same plane as the surface wave. However, the results of the present analysis and those of Jamali (1997a and b) suggest that even in two dimensions the internal waves may grow in an inviscid medium.

The differences between the results of the present analysis and those of Hill (1997) stem from their different treatments of the second-order equations. To preclude the possibility of a secular solution at second order, Hill (1997) sought the solvability condition to be the orthogonality of the forcing functions and the homogenous solution. This is correct only when the system of equations is self-adjoint. However, in the current problem the systems of equations at second order are not self-adjoint, and the correct solvability condition is obtained by requiring that the forcing functions be orthogonal to the homogeneous solution of the adjoint system (Drazin and Reid, 1981, p 385) as adopted in the present work.

5.1.2 Experimental Study

In chapter 3, the results of an experimental investigation of the interaction were presented. The common phenomenon observed in all the experiments was the generation of a three-dimensional internal wave pattern at the interface. This was shown to be the result of the reflection of the excited internal waves from the flume side-walls. The observations also indicated that the internal wave pattern had two length- and two time-scales. At the long scale the pattern had a wavelength of twice the surface wavelength and at the short scale it had the form of a three-dimensional standing internal wave. At the short time-scale the frequency of the interface oscillation was half of the frequency of the surface wave. At the long time-scale the 3D standing internal wave was moving along the flume. All of these observations were clearly explained by the theory.

The wavelength and the amplitude of the standing internal wave were measured in a number of experiments. It was found that the diffusivity of the interface has a direct effect on the wavelength and evolution of the internal waves. A closer agreement between the theory and the experiments was achieved when the thickness of the diffuse interface was taken into account to obtain the theoretical wavelengths. However, in terms of the growth rate, the

experimental and theoretical values were not in close agreement. This was attributed to the diffusivity of the interface in the experiments, which is not taken into account in the theoretical analysis. A diffuse interface reduces the surface wave forcing for excitation of the internal waves and hence leads to a lower growth rate once the interface becomes diffuse. The explanation was found consistent with the experimental results. The experiments also clearly confirmed the theoretical result that the internal waves grow exponentially with time.

According to the three-dimensional model, the more oblique the internal waves to the surface wave, the higher their growth rate. This result was supported by the experimental measurements, which showed that the internal waves occurred at the maximal possible angle from the surface wave.

The effects of surface wave amplitude on the interaction process were investigated experimentally. The results confirmed the theoretical result that the growth rate increases with the surface wave amplitude, and that there is a critical surface wave amplitude below which the internal waves can not grow.

Reference was made to the work of Hill (1997). Hill's (1997) theoretical analysis indicated that there are narrow bands of the surface wave frequency, the direction angle of the internal waves, and the density ratio of the layers only within which the internal waves can grow. These results were found in disagreement with the experimental results as no specific bounds were found on the interaction process. The interaction took place in the laboratory flume over wide ranges of the experimental parameters. Also, in the experiments different modes of the standing internal wave were observed. The values of the observed modes range from $n = 3$ to $n = 7$. However, Hill (1997) did not address the possibility of occurrence of higher modes nor the fact that the pattern was the result of the reflection of the internal waves.

The effect of viscosity on the interaction has been a central issue in the past theoretical studies. The three-dimensional analysis of chapter 2 indicates that an increase in the viscosity of the lower layer causes a reduction in the growth rate of the internal waves. This result was supported by the experiments as the replacement of the salt water with the corn syrup in the laboratory flume resulted in the suppression of the internal waves. The experiments also confirmed the results of the viscous analysis in chapter 4 that the combined forcing and damping effect of viscosity on the interaction is to reduce the growth rate of the internal waves.

Finally, two more phenomena observed in the wave flume were addressed. These were the long-term behavior of the internal waves and the occasional excitation of some harmonic internal waves besides the sub-harmonic ones.

5.2 INTERACTION IN A HIGHLY VISCOUS MEDIUM

The three-dimensional model in chapter 2 considered only the damping effect of viscosity on the interaction. In chapter 4 a fully viscous model of the interaction that took into account both forcing and damping effects of viscosity was developed. The model had a fully viscous formulation, and due to its complexity its development was restricted to two dimensions. The viscous model placed no restriction on the viscosity of the lower layer.

Wen (1995) and Hill and Foda (1996) found that for the range of real fluids growth of the internal waves in two dimensions is critically dependent on presence of viscosity. However, the viscous study in chapter 4 indicated that the net effect of viscosity is to suppress the internal waves and inhibit their growth. According to the results both surface wave forcing and viscous damping increase with viscosity. However, the damping rises much faster than the surface wave forcing, and hence the net effect of a higher viscosity is to decrease the

growth rate. The experiments with the corn syrup presented in chapter 3 are in agreement with this theoretical result. It is worth mentioning that like Hill (1997), Wen (1995) and Hill and Foda (1996) obtained the evolution equations by requiring the forcing functions be orthogonal to the homogeneous equations at second order. This was shown earlier to be incorrect and can provide a partial explanation for the discrepancy between the results of the present viscous analysis and those of Wen (1995), and Hill and Foda (1996).

5.3 RECOMMENDATIONS

In many real situations, the water body is stratified into two layers and is subject to the action of the surface waves. For instance, in many lakes and muddy coastal regions a layer of fluid mud is present beneath the clear water, and the surface waves continuously disturb the interface of the two layers. Similarly, in many stratified estuaries and oceans the water body is almost two-layer, and the interface oscillates under the influence of the surface waves. The current study has considerable applications in mixing studies of two-layer fluids subject to large surface waves. Reference is made to the companion videotape for the experiments with salt water and with a sediment bed. Both sets of experiments led to the same instability phenomenon. In the experiment with the sediment bed, after a fluid-like layer of suspended sediments formed above the bed shortly following the generation of the surface wave in the flume, a three-dimensional standing internal wave was observed at the interface of the fresh water and the fluidized sediment.

The study indicates that the interaction of a surface wave with two sub-harmonic internal waves growing from the background noise is a strong mechanism for instability of the interface. The results suggest that the interface becomes easily susceptible to this type of instability under conditions that are commonly realized in nature. The degree of mixing of

the two layers after the initial growth of the internal waves depends on the energy content of the surface wave; the bigger the surface waves, the faster the energy transfer and the higher the mixing.

The phenomenon of the interaction between a surface and two internal waves has not yet been explored in all aspects although the understanding has improved considerably. There are a number of sub-areas that still demand further studies. These include, i) study of the effects of a diffuse interface on the interaction, in particular, on the forcing, ii) prediction of the long-term behavior of the growing internal waves and the corresponding mixing, and iii) derivation of simple equations to describe the interaction process.

In nearly all the physical situations, whether in the laboratory or in nature, there is always a diffuse layer present at the interface of the fluid layers. The experiments indicated that this diffuse interface reduces the forcing and changes the kinematic properties of the internal waves. To have a better understanding of the phenomenon in the real situations, the diffusivity of the interface has to be taken into account in the theoretical modeling of the problem although this adds considerable complexity to the problem.

In all the theoretical studies of the problem so far, the problem was formulated assuming the amplitudes of the waves are small. However, with the growth of the internal waves their amplitudes increase in time until at some point the preceding assumption breaks down. Analysis of the phenomenon beyond this point requires a more sophisticated theory as the internal waves are finite-amplitude waves and hence non-linear processes are more significant than before. In this regard, in the experiments that were allowed to continue for a long time it was observed that the internal waves do not have an exponential behavior in the long run, see the companion videotape. The observations indicate that after the initial stage during which the exponential growth occurs and leads to the substantial amplitudes of the internal waves, the waves stop growing and stabilize. However, in a longer run their

amplitudes seem to undergo a slow decay and growth with time although due to mixing of the layers this was not clearly visible. The stabilization phenomenon was also observed in Hill's (1997) experiments. An explanation for the stabilization behavior of the internal waves was given in chapter 3. It is believed that the high non-linearity of the internal waves is the main cause of this phenomenon. However, the problem demands further study.

In the present work, Mathematica® was extensively used to perform the long algebraic calculations and simplify the interaction coefficients. However, the expressions for these coefficients even after exhaustive simplifications are still complex and long. As study of this type may have considerable applications in the engineering studies of mixing in the aquatic systems, finding simple closed-form expressions to predict the onset of the interfacial instability is a need. This can be accomplished by simplification of the problem through making further approximations. Mathematically, it can be achieved by incorporating the other possible small parameters of the problem into an appropriate multi-parameter perturbation analysis. For this purpose, the density difference of the two layers is a potential candidate.

BIBLIOGRAPHY

1. Ball, K.F. (1964) "Energy transfer between external and internal gravity waves," *J. Fluid Mech.*, V 19, p 465.

2. Bogoliubov, N. N., Mitropolski, Y. A. (1958) *Asymptotic methods of non-linear Mechanics*, Moscow. (English Translation: Bogoliubov, N. N., Mitropolski, Y. A. (1961) *Asymptotic methods in the theory of non-linear oscillations,* Hindustan Publishing Corp, Delhi)

3. Benny, D. J. (1962) "Non-linear gravity wave interactions," *J. Fluid Mech.,* V 14, p 577.

4. Brekhovskikh, L. M., Goncharov, V. V., Kurtipov, V. M., and Nangol'nykh, K. A. (1972) "Resonant excitation of internal waves by nonlinear interaction of surface waves," *Atmos. Oceanic Phys.*, V 8, p 192.

5. Clough, R. W., and Penzien J. (1993) *Dynamic of structures*, 2nd Ed., McGraw-Hill, New York.

6. Craik, A. D. D. (1985) *Wave interactions and fluid flows,* Cambridge University Press.

7. Davis, R. E., and Acrivos, A. (1967) "The stability of oscillatory internal waves," *J. Fluid Mech.*, V 30, p 723.

8. Drazin, P. G., and Reid W. H. (1981) *Hydrodynamic stability*, Cambridge University Press.

9. Fritts, D. C., Sun, S. J., and Wang, D. Y. (1993) "Wave-wave interactions in a compressible atmosphere, Part 1: a general formulation including rotation and wind shear," *J. Geophys. Res.*, V 97, p 9975.

10. Gargett, A. E., and Hughes, B. A. (1972) "On the interaction of surface and internal waves," *J. Fluid Mech.*, V 52, p 179.

11. Groen, P. (1948) "Contribution to the theory of the internal waves," *Mededelinger en verhandeligen, Serie B,* Deel II, No. II, Koninkijk Nederlands Meterologisch.

12. Hammack, J. L., Henderson, D. M. (1993) "Resonant Interactions among surface water waves," *Ann. Rev. Fluid Mech.*, V 25, p 55.

13. Hasselmann, K. (1966) "Feynman diagrams and interaction rules of wave-wave scattering processes," *Rev. Geophys.*, V 4, p 1.

14. Hasselmann, K. (1967) "A criterion for nonlinear wave stability," *J. Fluid Mech.*, V 30, p 737.

15. Hill, D. F. (1997) *The subharmonic resonance of interfacial waves by progressive surface waves*, Ph.D. Thesis, University of California at Berkeley.

16. Hill, D. F., and Foda, M. A. (1996) "Subharmonic resonance of short internal standing waves by progressive surface waves," *J. Fluid Mech.*, V 321, p 217.

17. Jamali, M. (1997a) "Surface wave motion over a viscous bed, a resonant wave interaction model," *Proc. 4th Int. Conf. Civil Eng,* Teheran, V 2, p112.

18. Jamali, M. (1997b) "Resonant excitation of internal waves by a surface wave". *Proc. XXVIIth Conf. IAHR*, San Francisco, p 1334.

19. Komen G., Cavaleri, L., Donelan, M., Hasselmann, K., Hasselmann, S., and Jansser, P. (1994) *Dynamics and Modeling of Ocean Waves*, Cambridge University Press.

20. Koop, C. G., and Redekopp, L. G. (1981) "The interaction of long and short internal gravity waves: theory and experiment," *J. Fluid Mech.*, V 111, p 367.

21. Lamb, H. (1934) *Hydrodynamics*, Cambridge University Press.

22. Lawrence, G. A., Ward, P. R. B., and MacKinnon, M. D. (1991) "Wind-wave-induced suspension of mine tailings in disposal ponds- a case study," *Can. J. Civil Eng.*, V 18, p 1047.

23. Lewis, J. E., Lake, B. M., and Ko, D. R. S. (1974) "On the interaction of internal waves and surface gravity waves," *J. Fluid Mech.*, V 63, p 773.

24. Longuett-Higgins, M. S. (1962) "Resonant interactions between two trains of gravity waves," *J. Fluid Mech.*, V 12, p321.

25. Luettich, R. A., Harleman, D. R. F., and Somlyody, L. (1990) "Dynamic behavior of suspended sediment concentrations in a shallow lake perturbed by episodic wind events," *Limnol. Oceanogr.*, V 35, p 1050.

26. MacPherson, H. (1980) " The attenuation of water waves over a non-rigid bed," *J. Fluid Mech.*, V 97, p 721.

27. McComas C. H., and Bretherton, F. P., (1977) "Resonant interactions of oceanic internal waves," *J. Geophys. Res.*, V 82, p 1397.

28. McComas, C. H., and Muller P. (1981) "The dynamic balance of internal waves," *J. Phys. Oceanogr.*, V 11, p 970.

29. McGoldrick, L. F. (1965) "Resonant interactions among capillary-gravity waves," *J. Fluid Mech.*, V 21, p 305.

30. McGoldrick, L. F. (1970) "An experiment on second-order capillary gravity resonant wave interactions," *J. Fluid Mech.*, V 40, p 251.

31. McGoldrick, L. F. (1972) "On the rippling of small waves: a harmonic nonlinear nearly resonant interaction," *J. Fluid Mech.*, V 52, p 725.

32. Mehta, A., Lee, S., and Li, Y. (1994) *Fluid mud and water waves: a brief review of interactive processes and simple modeling approaches*, Contract Report DRP-94-4, U.S. Army Corps of Engineers, July 1994.

33. Miche, R. (1944) "Movements ondulatoires des mers en profondeus constante ou decroissante," *Annales des points et chausses*, pp. 25-78, 131-164, 270-292, 369-406.

34. Muller, P., Holloway, G., Henyey, F., and Pomphrey, N. (1986) "Nonlinear interactions among internal gravity waves," *Rev. Geophys.*, V 24, p 493.

35. Philips, O. M. (1960) "On the dynamics of unsteady gravity waves of finite amplitude. Part I," *J. Fluid Mech.*, V 9, p 193.

36. Philips, O. M. (1977) *The dynamics of the upper ocean,* 2nd Ed., Cambridge University Press.

37. Philips, O. M. (1981) "Wave interactions- evolution of an idea", *J. Fluid Mech.*, V 106, p 215.

38. Rott, N. (1970) "A multiple pendulum for the demonstration of non-linear coupling", *Z. Angew. Math. Phys.,* V 21, p 570.

39. Simmons, W. F. (1969) "A variational method for weak resonant wave interactions", *Proc. Royal Soc. London, Series A*, V 309, p 551.

40. Turner, J. S. (1973) *Buoyancy effects in fluids*, Cambridge University Press.

41. U.S. Army Coastal Engineering Research Center (1984) *Shore Protection Manual*, Vicksburg, MS.

42. Wen, F. (1995) "Resonant generation of internal waves on the soft sea bed by a surface water wave", *Phys. Fluids*, V 7, p 1915.

43. Whitham, G. B. (1965) "A general approach to linear and nonlinear dispersive waves using a Lagrangian," *J. Fluid Mech.*, V 22, p 273.

44. Whitham, G. B. (1967) "Nonlinear dispersion of water waves," *J. Fluid Mech.*, V 27, p 399.

45. Yeh, K. C., and Liu, C. H. (1981) "The instability of atmospheric gravity waves through wave-wave interactions," *J. Geophys. Res.,* V 86, p 9722.

46. Yi, F. and Xiao Z. (1996) "Evolution of gravity waves through resonant and nonresonant interactions in a dissipative atmosphere," *J. Atmospheric and Solar-Terrestrial Physics*, V 59, N 3, p305.

APPENDIX A

LINEAR SOLUTION

Here the solution to the linear equations of motion of a wave in a two-layer inviscid medium is presented. The equations of motion are given by (2.3) to (2.10). The wave is assumed to move in the $x-y$ plane with wave number $\vec{k}=(k_x,k_y)$ and frequency ω. The solution to the linearized equations of motion for a surface wave can be obtained as (e.g., see Lamb 1934)

$$\phi'(x,y,z)=\{C_1Sinh(kz)+C_2Cosh(kz)\}e^{i(k_xx+k_yy-\omega t)} \tag{A.1}$$

$$\phi(x,y,z)=\{D_1Sinh(k(z+d))+D_2Cosh\{k(z+d))\}e^{i(k_xx+k_yy-\omega t)} \tag{A.2}$$

$$\xi(x,y,t)=ae^{i(k_xx+k_yy-\omega t)} \tag{A.3}$$

$$\eta(x,y)=be^{i(k_xx+k_yy-\omega t)} \tag{A.4}$$

where

$$C_1=\frac{ia(gkSinh(kh)-\omega^2Cosh(kh))}{k\omega} \tag{A.5}$$

$$C_2=\frac{-ia(gkCosh(kh)-\omega^2Sinh(kh))}{k\omega} \tag{A.6}$$

$$D_1 = 0 \tag{A.7}$$

$$D_2 = \frac{ia(gkSinh(kh) - \omega^2 Cosh(kh))}{k\omega Sinh(kd)} \tag{A.8}$$

$$b = a\left(Cosh(kh) - \frac{gkSinh(kh)}{\omega^2}\right) \tag{A.9}$$

In the above equations, a is the amplitude of the surface wave, and the system parameters are defined in figure 2.1. The dispersion relation can be written as

$$\frac{\frac{\rho'}{\rho}(\omega^4 - g^2k^2)tanh(kh)}{(gk\,tanh(kh) - \omega^2)} + gk - \omega^2\,coth(kd) = 0 \tag{A.10}$$

For the motion of an internal wave, the above equations are still valid. However, It is convenient to write the coefficients in equations (A.1) to (A.4) in terms of the internal wave amplitude b:

$$C_1 = \frac{-ib\omega}{k} \tag{A.11}$$

$$C_2 = \frac{ib\omega\left(gkCosh(kh) - \omega^2 Sinh(kh)\right)}{-k\left(\omega^2 Cosh(kh) - gkSinh(kh)\right)} \tag{A.12}$$

$$D_1 = 0 \tag{A.13}$$

$$D_2 = \frac{-ib\omega Csch(kd)}{k} \tag{A.14}$$

$$a = \frac{b\omega^2}{\left(\omega^2 Cosh(kh) - gkSinh(kh)\right)} \tag{A.15}$$

The dispersion relation remains the same.

APPENDIX B

RESONANCE SOLUTION

Here the solution to the governing equations at second order in the three-dimensional interaction (chapter 2) is sought. The equations of motion are given by equations 2.3 to 2.10. As the free surface and interface boundary conditions are applied on the unknown free surface and interface, it is convenient to transfer these equations to the undisturbed fluid surfaces using Taylor's series expansion. After truncating the expansions at second order, equations 2.5 to 2.9 reduce to

$$\xi_t + \phi'_x \xi_x + \phi'_y \xi_y - \phi'_z - \phi'_{zz} \xi = 0, \qquad z = h \qquad \text{(B.1)}$$

$$\rho' \phi'_t + \tfrac{1}{2} \rho' (\phi'^2_x + \phi'^2_y + \phi'^2_z) + \rho' g h - C'(t) + \rho' (\phi'_{tz} + g) \xi = 0, \quad z = h \qquad \text{(B.2)}$$

$$\eta_t + \phi'_x \eta_x + \phi'_y \eta_y - \phi'_z - \phi'_{zz} \eta = 0, \qquad z = 0 \qquad \text{(B.3)}$$

$$\eta_t + \phi_x \eta_x + \phi_y \eta_y - \phi_z - \phi_{zz} \eta = 0, \qquad z = 0 \qquad \text{(B.4)}$$

$$\rho'\phi'_t + \tfrac{1}{2}\rho'(\phi'^2_x + \phi'^2_y + \phi'^2_z) - C'(t) + \rho'(\phi'_{tz} + g)\eta =$$
$$\rho\phi_t + \tfrac{1}{2}\rho(\phi_x^2 + \phi_y{}^2 + \phi_z^2) - C(t) + \rho(\phi_{tz} + g)\eta$$
$$, \qquad z = 0 \qquad \text{(B.5)}$$

To simplify the resonance calculations further, equations (B.1) and (B.2) as well as equations (B.3), (B.4), and (B.5) are combined together to eliminate linear terms involving ξ and η (e.g., see Benny, 1962, for the simplification of the free surface boundary conditions). The resulting equations are

$$\phi'_{tt} + g\phi'_z = \{-\frac{1}{2}(\phi'^2_x + \phi'^2_y + \phi'^2_z) + \frac{1}{g}\phi'_t\phi'_{zt}\}_t - \{\phi'_x\phi'_t\}_x - \{\phi'_y\phi'_t\}_y, \quad z = h \qquad \text{(B.6)}$$

$$\phi_z - \phi'_z = \{(\phi_x - \phi'_x)\eta\}_x + \{(\phi_y - \phi'_y)\eta\}_y, \qquad z = 0 \qquad \text{(B.7)}$$

$$(\phi_{tt} + g\phi_z) - r(\phi'_{tt} + g\phi'_z) = \{(\phi_x - r\phi'_x)g\eta\}_x + \{(\phi_y - r\phi'_y)g\eta\}_y$$
$$+ \frac{1}{2}\{r(\phi'^2_x + \phi'^2_y + \phi'^2_z) - (\phi_x^2 + \phi_y^2 + \phi_z^2)\}_t - \{(\phi_{zt} - r\phi'_{zt})\eta\}_t$$
$$, \qquad z = 0 \qquad \text{(B.8)}$$

where $r = \rho'/\rho$. The above equations are correct to second order.

The systems of equations at second order are linear and have forcing functions that are products of first-order terms. When the resonance conditions (2.1) hold among the waves, resonance appears at $O(a_0\bar{b}_1)$, $O(a_0\bar{b}_2)$, $O(b_1b_2)$, and at the corresponding conjugate orders. As the calculations at each order are quite similar, here only the equations at $O(a_0\bar{b}_1)$ are considered.

First, the following form for the linear solution to the motion of wave 2 is assumed.

$$\eta_2(x,t) = b_2 e^{i\vartheta_i}$$
$$\xi_2(x,t) = b_2 \hat{\xi}_2 e^{i\vartheta_2}$$
$$\phi_2'(x,z,t) = b_2 \hat{f}_2(z) e^{i\vartheta_2}$$
$$\phi_2(x,z,t) = b_2 \hat{g}_2(z) e^{i\vartheta_2}$$

where $\vartheta_2 = \vec{k}_2 \cdot \vec{x} - \omega_2 t$. The quantities $\hat{\xi}_2$, $\hat{f}_2(z)$, and $\hat{g}_2(z)$ can be easily determined from Appendix A. Substituting the expansions (2.11) in the Laplace's equations gives the following equations at $O(a_0\bar{b}_1)$.

$$\nabla^2 \phi_{01}' = 0 , \qquad 0 < z < h \qquad \text{(B.9)}$$

$$\nabla^2 \phi_{01} = 0 \qquad -d < z < 0 \qquad \text{(B.10)}$$

The free surface and interface boundary conditions at this order have forcing functions that are proportional to $e^{i\vartheta_2}$. For instance, consider equation B.6. At $O(a_0\bar{b}_1)$ this equation becomes

$$(\phi_{01}')_{tt} + g(\phi_{01}')_z = \left\{ -(\phi_0')_x(\overline{\phi_1'})_x - (\phi_0')_y(\overline{\phi_1'})_y - (\phi_0')_z(\overline{\phi_1'})_z + \frac{1}{g}(\phi_0')_t(\overline{\phi_1'})_{zt} + \frac{1}{g}(\phi_1')_t(\overline{\phi_0'})_{zt} \right\}_t$$
$$- \left\{ (\phi_0')_x(\overline{\phi_1'})_t + (\phi_0')_t(\overline{\phi_1'})_x \right\}_x - \left\{ (\phi_0')_y(\overline{\phi_1'})_t + (\phi_0')_t(\overline{\phi_1'})_y \right\}_y$$
$$+ 2i\omega_2 \hat{f}_2(z) \frac{db_2}{dt} e^{i\vartheta_2}$$

$$z = h \qquad \text{(B.11)}$$

Note that the third equation in (2.13) leads to the appearance of the time derivative of b_2 in the above equation. It is seen that products of the first-order terms of waves 0 and 1 form part of the forcing function. Implementation of the resonance conditions (2.1) in these products leads to the appearance of $e^{i\vartheta_2}$. Consider the product $(\phi_0')_x(\overline{\phi_1'})_x$, for instance. The

terms $(\phi_0')_x$ and $(\overline{\phi_1'})_x$ are proportional to $e^{i\vartheta_0}$ and $e^{-i\vartheta_1}$ respectively. Hence the term $e^{i(\vec{k}_0.\vec{x}-\omega_0 t)-i(\vec{k}_1.\vec{x}-\omega_1 t)}$ appears in the product. Using the resonance conditions (2.1), $e^{i(\vec{k}_0.\vec{x}-\omega_0 t)-i(\vec{k}_1.\vec{x}-\omega_1 t)}$ can be simplified to $e^{i\vartheta_2}$, and hence $(\phi_0')_x(\overline{\phi_1'})_x$ becomes proportional to $e^{i\vartheta_2}$. Similarly, all the other products on the right hand side of (B.11) are proportional to $e^{i\vartheta_2}$, and hence (B.11) can be simplified to

$$(\phi_{01}')_{tt} + g(\phi_{01}')_z = m_1 e^{i\vartheta_2} + 2i\omega_2 \hat{f}_2(z)\frac{db_2}{dt}e^{i\vartheta_2}, \qquad z = h \qquad \text{(B.12)}$$

where m_1 is a constant given by

$$m_1 e^{i\vartheta_2} = \left\{-(\phi_0')_x(\overline{\phi_1'})_x - (\phi_0')_y(\overline{\phi_1'})_y - (\phi_0')_z(\overline{\phi_1'})_z + \frac{1}{g}(\phi_0')_t(\overline{\phi_1'})_{zt} + \frac{1}{g}(\phi_1')_t(\overline{\phi_0'})_{zt}\right\}_t - \left\{(\phi_0')_x(\overline{\phi_1'})_t + (\phi_0')_t(\overline{\phi_1'})_x\right\}_x - \left\{(\phi_0')_y(\overline{\phi_1'})_t + (\phi_0')_t(\overline{\phi_1'})_y\right\}_y \qquad \text{(B.13)}$$

Having the linear solutions of waves 0 and 1, m_1 is obtained as follows.

$$m_1 = ia_0\overline{b_1}\frac{\omega_1}{\omega_0}\left(\omega_0\omega_1\left(-\omega_0^3 + 2\omega_0^2\omega_1 - 2\omega_0\omega_1^2 + \omega_1^3\right) + g^2\left(-k_1^2\omega_0 + k_0\left(2k_{1,x}\omega_2 + k_0\omega_1\right)\right)\right)/ \left(\omega_1^2 Cosh(k_1 h) - gk_1 Sinh(k_1 h)\right) \qquad \text{(B.14)}$$

By a similar argument it can be shown that the term $e^{i\vartheta_2}$ appear as a factor in the forcing functions of equations B.7 and B.8 as well. Similar to (B.6), equations B.8 and B.7 at $O(a_0\overline{b_1})$ reduce to

$$\left\{(\phi_{01})_{tt} + g(\phi_{01})_z\right\} - r\left\{(\phi_{01}')_{tt} + g(\phi_{01}')_z\right\} = m_2 e^{i\vartheta_2} + 2i\omega_2\left(\hat{g}_2(z) - r\hat{f}_2(z)\right)\frac{db_2}{dt}e^{i\vartheta_2}$$

$$, \qquad z = 0 \qquad \text{(B.15)}$$

$$(\phi_{01})_z - (\phi_{01}')_z = m_3 e^{i\vartheta_2}, \qquad z = 0 \qquad \text{(B.16)}$$

where m_2 and m_3 are constants. The expressions for these constants are quite long. The outputs of Mathematica® for m_2 and m_3 after simplification are given in figures B.1 and B.2 respectively. In the figures, $I = \sqrt{-1}$ and $\mathrm{a0} = a_0$.

Equations B.9, B.10, B.12, B.15, B.16, and the bed boundary condition

$$(\phi_{01})_z = 0, \qquad z = -d \qquad \text{(B.17)}$$

form a complete set of equations at $O(a_0\overline{b}_1)$. It is interesting to note that the associated homogeneous equations are the same as those from the linear theory, and hence each of the linear waves 0, 1, and 2 is an eigen-solution to the associated homogeneous system. Since the term $e^{i(\vec{k}_2.\vec{x}-\omega_2 t)}$ appears in the forcing functions with $\vec{k}_2$ and ω_2 being the eigenvalues of the homogeneous equations, the forcing functions may cause resonance in the system. At resonance, the solution takes the form $te^{i\vartheta_2}$, which has a secular form. A secular solution grows with time and destroys the uniformity of the perturbation expansion.

To solve the preceding system of equations, the following form for the solution is assumed.

$$\phi'_{01}(x,y,z,t) = f_{01}(z)e^{i\vartheta_2}$$

$$\phi_{01}(x,y,z,t) = g_{01}(z)e^{i\vartheta_2} \qquad \text{(B.18)}$$

By substituting (B.18) in the governing equations, the following set of ordinary differential equations is obtained.

$$\frac{d^2 f_{01}(z)}{dz^2} - {k_2}^2 f_{01}(z) = 0, \qquad 0 < z < h \qquad \text{(B.19)}$$

$$\frac{d^2 g_{01}(z)}{dz^2} - {k_2}^2 g_{01}(z) = 0, \qquad -d < z < 0 \qquad \text{(B.20)}$$

$$g\frac{df_{01}(z)}{dz}-\omega_2{}^2 f_{01}(z)=m_1+2i\omega_2\hat{f}_2(z)\frac{db_2}{dt}, \qquad z=h \tag{B.21}$$

$$\left(g\frac{dg_{01}(z)}{dz}-\omega_2{}^2 g_{01}(z)\right)-r\left(g\frac{df_{01}(z)}{dz}-\omega_2{}^2 f_{01}(z)\right)=m_2+2i\omega_2\left(\hat{g}_2(z)-r\hat{f}_2(z)\right)\frac{db_2}{dt}$$

$$z=0 \tag{B.22}$$

$$\frac{dg_{01}(z)}{dz}-\frac{df_{01}(z)}{dz}=m_3, \qquad z=0 \tag{B.23}$$

$$\frac{dg_{01}(z)}{dz}=0, \qquad z=-d \tag{B.24}$$

where $k_2=\left|\vec{k}_2\right|$. Since (ω_2,k_2) is an eigenvalue of the associated homogeneous system, a non-secular solution exists only if the forcing functions are orthogonal to the homogenous solution of the adjoint system. To obtain the desired solvability condition, (B.19) and (B.20) are multiplied by $F(z)$ and $G(z)$ respectively, and integrated over the corresponding depths. Adding the integrals and applying the Green's theorem result in the following equation with the subscripts dropped.

$$\int_0^h F\left(\frac{d^2f}{dz^2}-k^2f\right)dz+\int_{-d}^0 G\left(\frac{d^2g}{dz^2}-k^2g\right)dz=\int_0^h f\left(\frac{d^2F}{dz^2}-k^2F\right)dz+\int_{-d}^0 g\left(\frac{d^2G}{dz^2}-k^2G\right)dz+$$
$$+\left(F\frac{df}{dz}-\frac{dF}{dz}f\right)\Bigg|_0^h+\left(G\frac{dg}{dz}-\frac{dG}{dz}g\right)\Bigg|_{-d}^0 \tag{B.25}$$

Following Drazin and Reid (1981), for instance, the adjoint system is obtained as follows (see also Appendix D).

$$\frac{d^2F(z)}{dz^2}-k_2{}^2F(z)=0, \qquad 0<z<h \tag{B.26}$$

$$\frac{d^2G(z)}{dz^2}-k_2{}^2G(z)=0, \qquad -d<z<0 \tag{B.27}$$

$$g\frac{dF(z)}{dz}-\omega_2{}^2F(z)=0, \qquad z=h \tag{B.28}$$

$$g\frac{r-1}{\omega_2{}^2}\frac{dG(z)}{dz}+G(z)-F(z)=0 \qquad z=0 \tag{B.29}$$

$$\frac{dF(z)}{dz}-r\frac{dF(z)}{dz}=0, \qquad z=0 \tag{B.30}$$

$$\frac{dG(z)}{dz}=0, \qquad z=-d \tag{B.31}$$

where $F(z)$ and $G(z)$ are now the solution to the adjoint system.

It is interesting to note that the adjoint system and the homogeneous form of equations B.19 to B.24 are not the same. This implies that the systems of equations at second order are not self-adjoint. The difference between the two systems of equations stems from the interface boundary conditions.

Replacing f and g in (B.25) with $f_{01}(z)$ and $g_{01}(z)$ respectively, (B.25) reduces to the following orthogonality condition, which is the desired solvability condition.

$$\left\{\frac{F(z)}{g}(m_1+2i\omega_2\hat{f}_2(z)\frac{db_2}{dt}\right\}\Bigg|_{z=h}+\left\{\left(G(z)-\frac{g}{\omega_2{}^2}\frac{dG(z)}{dz}\right)m_3\right\}\Bigg|_{z=0}+$$
$$\left\{\frac{1}{\omega_2{}^2}\frac{dG(z)}{dz}\left(m_2+2i\omega_2\left(\hat{g}_2(z)-r\hat{f}_2(z)\right)\frac{db_2}{dt}\right)\right\}\Bigg|_{z=0}=0 \tag{B.32}$$

For a similar calculation, see Appendix D. Knowing $F(z)$ and $G(z)$, the above equation simplifies to

$$\frac{db_2}{dt}=\alpha_2 a_0\overline{b_1} \tag{B.33}$$

which is the evolution equation for internal wave 2. The expression for α_2 as calculated by Mathematica® is given in figure B.3.

Taking a similar procedure as above for the equations at $O(a_0\bar{b}_2)$ and $O(b_1b_2)$ leads to

$$\frac{db_1}{dt} = \alpha_1 a_0 \bar{b}_2 \tag{B.34}$$

and

$$\frac{da_0}{dt} = \alpha_0 b_1 b_2 \tag{B.35}$$

respectively, which are the other desired evolution equations. In chapter 2 it is shown that by approximation equation B.35 can be neglected in the analysis, so there is no need to compute α_0. Mathematica® output for α_1 is given in figure B.4.

The equations at the corresponding conjugate orders, i.e., $O(\bar{a}_0 b_1)$, $O(\bar{a}_0 b_2)$, and $O(\bar{b}_1\bar{b}_2)$, are the complex conjugates of the equations at $O(a_0\bar{b}_1)$, $O(a_0\bar{b}_2)$, and $O(b_1b_2)$ respectively and hence lead to the same evolution equations.

$$\frac{1}{4}\,\mathrm{I\,a0\,Conjugate}[b_1]\,\omega_1\Bigg(\Big(4\,(\omega_0-\omega_1)\,\omega_1$$
$$\Big(\mathrm{Sinh}[h\,k_0]\,\Big(g\,\mathrm{Sinh}[h\,k_1]\,\Big(g\,\mathrm{Coth}[d\,k_1]\,k_0^2\,k_1-g\,\mathrm{Coth}[d\,k_0]\,k_0\,k_1^2+r\,k_1^2\,\omega_0^2-r\,k_0^2\,\omega_1^2\Big)+$$
$$\mathrm{Cosh}[h\,k_1]\,\Big(g^2\,r\,k_0^2\,k_1-g\,\mathrm{Coth}[d\,k_1]\,k_0^2\,\omega_1^2+g\,\mathrm{Coth}[d\,k_0]\,k_0\,k_1\,\omega_1^2-r\,k_1\,\omega_0^2\,\omega_1^2\Big)\Big)+$$
$$\mathrm{Cosh}[h\,k_0]\,\Big(\mathrm{Sinh}[h\,k_1]$$
$$\Big(-g^2\,r\,k_0\,k_1^2-g\,\mathrm{Coth}[d\,k_1]\,k_0\,k_1\,\omega_0^2+g\,\mathrm{Coth}[d\,k_0]\,k_1^2\,\omega_0^2+r\,k_0\,\omega_0^2\,\omega_1^2\Big)+\mathrm{Cosh}[h\,k_1]$$
$$\Big(-g\,r\,k_0\,k_1\,\omega_0^2+g\,r\,k_0\,k_1\,\omega_1^2+\mathrm{Coth}[d\,k_1]\,k_0\,\omega_0^2\,\omega_1^2-\mathrm{Coth}[d\,k_0]\,k_1\,\omega_0^2\,\omega_1^2\Big)\Big)\Big)\Big)\Big/$$
$$\Big(g\,k_0\,k_1\,\Big(g\,\mathrm{Sinh}[h\,k_1]\,k_1-\mathrm{Cosh}[h\,k_1]\,\omega_1^2\Big)\Big)+\Big(\mathrm{Csch}[d\,k_0]\,\mathrm{Csch}[d\,k_1]$$
$$\Big(g\,(-\mathrm{Sinh}[(d-h)\,k_0]+r\,\mathrm{Sinh}[(d-h)\,k_0]+\mathrm{Sinh}[(d+h)\,k_0]+r\,\mathrm{Sinh}[(d+h)\,k_0])\,k_0+$$
$$(-1+r)\,\mathrm{Cosh}[(d-h)\,k_0]\,\omega_0^2-(1+r)\,\mathrm{Cosh}[(d+h)\,k_0]\,\omega_0^2\Big)$$
$$\Big(g\,(-\mathrm{Sinh}[(d-h)\,k_1]+r\,\mathrm{Sinh}[(d-h)\,k_1]+\mathrm{Sinh}[(d+h)\,k_1]+r\,\mathrm{Sinh}[(d+h)\,k_1])\,k_1+$$
$$(-1+r)\,\mathrm{Cosh}[(d-h)\,k_1]\,\omega_1^2-(1+r)\,\mathrm{Cosh}[(d+h)\,k_1]\,\omega_1^2\Big)$$
$$(k_0-k_{1,x})\,(k_0\,\omega_1+\omega_0\,k_{1,x})\Big)\Big/$$
$$\Big((-1+r)\,k_0\,k_1\,\omega_0\,\Big(g\,\mathrm{Sinh}[h\,k_1]\,k_1-\mathrm{Cosh}[h\,k_1]\,\omega_1^2\Big)\Big)+\frac{1}{\omega_0}\Bigg(4\,(\omega_0-\omega_1)\Bigg(-g\,\mathrm{Sinh}[h\,k_0]\,k_0+$$
$$\mathrm{Cosh}[h\,k_0]\,\omega_0^2+\frac{\mathrm{Coth}[d\,k_0]\,\mathrm{Coth}[d\,k_1]\,\Big(-g\,\mathrm{Sinh}[h\,k_0]\,k_0+\mathrm{Cosh}[h\,k_0]\,\omega_0^2\Big)\,k_{1,x}}{k_1}-$$
$$r\Bigg(-g\,\mathrm{Sinh}[h\,k_0]\,k_0+\mathrm{Cosh}[h\,k_0]\,\omega_0^2-$$
$$\frac{\Big(g\,\mathrm{Cosh}[h\,k_0]\,k_0-\mathrm{Sinh}[h\,k_0]\,\omega_0^2\Big)\,\Big(g\,\mathrm{Cosh}[h\,k_1]\,k_1-\mathrm{Sinh}[h\,k_1]\,\omega_1^2\Big)\,k_{1,x}}{g\,\mathrm{Sinh}[h\,k_1]\,k_1^2-\mathrm{Cosh}[h\,k_1]\,k_1\,\omega_1^2}\Bigg)\Bigg)\Bigg)+$$
$$\Big(4\,\Big(\mathrm{Sinh}[h\,k_0]\,\Big(g\,\mathrm{Coth}[d\,k_0]\,k_0-r\,\omega_0^2\Big)+\mathrm{Cosh}[h\,k_0]\,\Big(g\,r\,k_0-\mathrm{Coth}[d\,k_0]\,\omega_0^2\Big)\Big)$$
$$\Big(\mathrm{Sinh}[h\,k_1]\,\Big(-g\,\mathrm{Coth}[d\,k_1]\,k_1+r\,\omega_1^2\Big)+\mathrm{Cosh}[h\,k_1]\,\Big(-g\,r\,k_1+\mathrm{Coth}[d\,k_1]\,\omega_1^2\Big)\Big)\,k_{1,y}^2\Big)\Big/$$
$$\Big((-1+r)\,k_0\,k_1\,\Big(g\,\mathrm{Sinh}[h\,k_1]\,k_1-\mathrm{Cosh}[h\,k_1]\,\omega_1^2\Big)\Big)\Bigg)$$

Figure B.1 Mathematica® output for m_2.

$$\Bigg(\text{I a0 Conjugate}[b_1]\,\omega_1\Bigg(\frac{1}{\omega_0}\Big(\text{Csch}[d\,k_0]\,k_0\Big(g\,\text{Sinh}[(d+h)\,k_0]\,k_0-\text{Cosh}[(d+h)\,k_0]\,\omega_0^2\Big)\omega_1$$
$$\Big(\text{Sinh}[h\,k_1]\Big(g\,\text{Coth}[d\,k_1]\,k_1-r\,\omega_1^2\Big)+\text{Cosh}[h\,k_1]\Big(g\,r\,k_1-\text{Coth}[d\,k_1]\,\omega_1^2\Big)\Big)+$$
$$\text{Csch}[d\,k_1]\Big(\text{Sinh}[h\,k_0]\Big(g\,\text{Coth}[d\,k_0]\,k_0-r\,\omega_0^2\Big)+\text{Cosh}[h\,k_0]\Big(g\,r\,k_0-\text{Coth}[d\,k_0]\,\omega_0^2\Big)\Big)$$
$$\Big(g\,\text{Sinh}[(d+h)\,k_1]\,k_1-\text{Cosh}[(d+h)\,k_1]\,\omega_1^2\Big)\,k_{1,x}+$$
$$\frac{1}{\omega_0}\Big(\text{Csch}[d\,k_0]\Big(-g\,\text{Sinh}[(d+h)\,k_0]\,k_0+\text{Cosh}[(d+h)\,k_0]\,\omega_0^2\Big)\omega_1$$
$$\Big(\text{Sinh}[h\,k_1]\Big(g\,\text{Coth}[d\,k_1]\,k_1-r\,\omega_1^2\Big)+\text{Cosh}[h\,k_1]\Big(g\,r\,k_1-\text{Coth}[d\,k_1]\,\omega_1^2\Big)\Big)\,k_{1,x}\Big)+$$
$$\frac{1}{k_0}\Big(\text{Csch}[d\,k_1]\Big(\text{Sinh}[h\,k_0]\Big(g\,\text{Coth}[d\,k_0]\,k_0-r\,\omega_0^2\Big)+\text{Cosh}[h\,k_0]\Big(g\,r\,k_0-\text{Coth}[d\,k_0]\,\omega_0^2\Big)\Big)$$
$$\Big(-g\,\text{Sinh}[(d+h)\,k_1]\,k_1+\text{Cosh}[(d+h)\,k_1]\,\omega_1^2\Big)\,k_{1,x}^2\Big)+$$
$$\frac{1}{k_0}\Big(\text{Csch}[d\,k_1]\Big(\text{Sinh}[h\,k_0]\Big(g\,\text{Coth}[d\,k_0]\,k_0-r\,\omega_0^2\Big)+\text{Cosh}[h\,k_0]\Big(g\,r\,k_0-\text{Coth}[d\,k_0]\,\omega_0^2\Big)\Big)$$
$$\Big(-g\,\text{Sinh}[(d+h)\,k_1]\,k_1+\text{Cosh}[(d+h)\,k_1]\,\omega_1^2\Big)\,k_{1,y}^2\Big)\Bigg)\Bigg/$$
$$\Big(g\,(-1+r)\,k_1\Big(g\,\text{Sinh}[h\,k_1]\,k_1-\text{Cosh}[h\,k_1]\,\omega_1^2\Big)\Big)$$

Figure B.2 Mathematica® output for m_3.

$$
-\Bigg(\Bigg(I\omega_1\left(\mathrm{Sinh}[h\,k_2]+\frac{\mathrm{Cosh}[h\,k_2](-g\,\mathrm{Cosh}[h\,k_2]\,k_2+\mathrm{Sinh}[h\,k_2]\,\omega_2^2)}{g\,\mathrm{Sinh}[h\,k_2]\,k_2-\mathrm{Cosh}[h\,k_2]\,\omega_2^2}\right)
$$

$$
(\omega_0\,\omega_1\,(-\omega_0^3+2\,\omega_0^2\,\omega_1-2\,\omega_0\,\omega_1^2+\omega_1^3)+g^2\,(-k_1^2\,\omega_0+k_0\,(k_0\,\omega_1+2\,\omega_0\,k_{1,x}-2\,\omega_1\,k_{1,x})))\Bigg)\Big/
$$

$$
(g\,\omega_0\,(-g\,\mathrm{Sinh}[h\,k_1]\,k_1+\mathrm{Cosh}[h\,k_1]\,\omega_1^2))+
$$

$$
\Bigg(I\omega_1\left(\frac{\mathrm{Coth}[d\,k_2]}{r}-\frac{g\,k_2}{r\,\omega_2^2}\right)\Bigg(\frac{1}{\omega_0}(\mathrm{Csch}[d\,k_0]\,k_0\,(g\,\mathrm{Sinh}[(d+h)\,k_0]\,k_0-\mathrm{Cosh}[(d+h)\,k_0]\,\omega_0^2)\,\omega_1
$$

$$
(\mathrm{Sinh}[h\,k_1]\,(g\,\mathrm{Coth}[d\,k_1]\,k_1-r\,\omega_1^2)+\mathrm{Cosh}[h\,k_1]\,(g\,r\,k_1-\mathrm{Coth}[d\,k_1]\,\omega_1^2)))+
$$

$$
\mathrm{Csch}[d\,k_1]\,(\mathrm{Sinh}[h\,k_0]\,(g\,\mathrm{Coth}[d\,k_0]\,k_0-r\,\omega_0^2)+\mathrm{Cosh}[h\,k_0]\,(g\,r\,k_0-\mathrm{Coth}[d\,k_0]\,\omega_0^2))
$$

$$
(g\,\mathrm{Sinh}[(d+h)\,k_1]\,k_1-\mathrm{Cosh}[(d+h)\,k_1]\,\omega_1^2)\,k_{1,x}+
$$

$$
\frac{1}{\omega_0}(\mathrm{Csch}[d\,k_0]\,(-g\,\mathrm{Sinh}[(d+h)\,k_0]\,k_0+\mathrm{Cosh}[(d+h)\,k_0]\,\omega_0^2)\,\omega_1
$$

$$
(\mathrm{Sinh}[h\,k_1]\,(g\,\mathrm{Coth}[d\,k_1]\,k_1-r\,\omega_1^2)+\mathrm{Cosh}[h\,k_1]\,(g\,r\,k_1-\mathrm{Coth}[d\,k_1]\,\omega_1^2))\,k_{1,x})+
$$

$$
\frac{1}{k_0}(\mathrm{Csch}[d\,k_1]\,(\mathrm{Sinh}[h\,k_0]\,(g\,\mathrm{Coth}[d\,k_0]\,k_0-r\,\omega_0^2)+\mathrm{Cosh}[h\,k_0]\,(g\,r\,k_0-\mathrm{Coth}[d\,k_0]\,\omega_0^2))
$$

$$
(-g\,\mathrm{Sinh}[(d+h)\,k_1]\,k_1+\mathrm{Cosh}[(d+h)\,k_1]\,\omega_1^2)\,k_{1,x}^2)+
$$

$$
\frac{1}{k_0}(\mathrm{Csch}[d\,k_1]\,(\mathrm{Sinh}[h\,k_0]\,(g\,\mathrm{Coth}[d\,k_0]\,k_0-r\,\omega_0^2)+\mathrm{Cosh}[h\,k_0]\,(g\,r\,k_0-\mathrm{Coth}[d\,k_0]\,\omega_0^2))
$$

$$
(-g\,\mathrm{Sinh}[(d+h)\,k_1]\,k_1+\mathrm{Cosh}[(d+h)\,k_1]\,\omega_1^2)\,k_{1,y}^2)\Bigg)\Bigg)\Big/
$$

$$
(g\,(-1+r)\,k_1\,(g\,\mathrm{Sinh}[h\,k_1]\,k_1-\mathrm{Cosh}[h\,k_1]\,\omega_1^2))+\frac{1}{4\,r\,\omega_2^2}\Bigg(I\,k_2\,\omega_1\Bigg((4\,(\omega_0-\omega_1)\,\omega_1
$$

$$
(\mathrm{Sinh}[h\,k_0]\,(g\,\mathrm{Sinh}[h\,k_1]\,(g\,\mathrm{Coth}[d\,k_1]\,k_0^2\,k_1-g\,\mathrm{Coth}[d\,k_0]\,k_0\,k_1^2+r\,k_1^2\,\omega_0^2-r\,k_0^2\,\omega_1^2)+
$$

$$
\mathrm{Cosh}[h\,k_1]\,(g^2\,r\,k_0^2\,k_1-g\,\mathrm{Coth}[d\,k_1]\,k_0^2\,\omega_1^2+g\,\mathrm{Coth}[d
$$

$$
k_0]\,k_0\,k_1\,\omega_1^2-r\,k_1\,\omega_0^2\,\omega_1^2))+\mathrm{Cosh}[h\,k_0]\,(\mathrm{Sinh}[h\,k_1]\,
$$

$$
(-g^2\,r\,k_0\,k_1^2-g\,\mathrm{Coth}[d\,k_1]\,k_0\,k_1\,\omega_0^2+g\,\mathrm{Coth}[d\,k_0]\,k_1^2\,\omega_0^2+r\,k_0\,\omega_0^2\,\omega_1^2)+
$$

$$
\mathrm{Cosh}[h\,k_1]\,(-g\,r\,k_0\,k_1\,\omega_0^2+g\,r\,k_0\,k_1\,\omega_1^2+\mathrm{Coth}[d
$$

$$
k_1]\,k_0\,\omega_0^2\,\omega_1^2-\mathrm{Coth}[d\,k_0]\,k_1\,\omega_0^2\,\omega_1^2)))))/
$$

$$
(g\,k_0\,k_1\,(g\,\mathrm{Sinh}[h\,k_1]\,k_1-\mathrm{Cosh}[h\,k_1]\,\omega_1^2))+(\mathrm{Csch}[d\,k_0]\,\mathrm{Csch}[d\,k_1]\,
$$

$$
(g\,(-\mathrm{Sinh}[(d-h)\,k_0]+r\,\mathrm{Sinh}[(d-h)\,k_0]+\mathrm{Sinh}[(d+h)\,k_0]+r\,\mathrm{Sinh}[(d+h)\,k_0])\,k_0+
$$

$$
(-1+r)\,\mathrm{Cosh}[(d-h)\,k_0]\,\omega_0^2-(1+r)\,\mathrm{Cosh}[(d+h)\,k_0]\,\omega_0^2)
$$

$$
(g\,(-\mathrm{Sinh}[(d-h)\,k_1]+r\,\mathrm{Sinh}[(d-h)\,k_1]+\mathrm{Sinh}[(d+h)\,k_1]+r\,\mathrm{Sinh}[(d+h)\,k_1])\,k_1+
$$

$$
(-1+r)\,\mathrm{Cosh}[(d-h)\,k_1]\,\omega_1^2-(1+r)\,\mathrm{Cosh}[(d+h)\,k_1]\,\omega_1^2)
$$

$$
(k_0-k_{1,x})\,(k_0\,\omega_1+\omega_0\,k_{1,x}))/
$$

$$
((-1+r)\,k_0\,k_1\,\omega_0\,(g\,\mathrm{Sinh}[h\,k_1]\,k_1-\mathrm{Cosh}[h\,k_1]\,\omega_1^2))+
$$

$$
\frac{1}{\omega_0}\Bigg(4\,(\omega_0-\omega_1)\Bigg(-g\,\mathrm{Sinh}[h\,k_0]\,k_0+\mathrm{Cosh}[h\,k_0]\,\omega_0^2+
$$

$$
\frac{\mathrm{Coth}[d\,k_0]\,\mathrm{Coth}[d\,k_1]\,(-g\,\mathrm{Sinh}[h\,k_0]\,k_0+\mathrm{Cosh}[h\,k_0]\,\omega_0^2)\,k_{1,x}}{k_1}-
$$

$$
r\,(-g\,\mathrm{Sinh}[h\,k_0]\,k_0+\mathrm{Cosh}[h\,k_0]\,\omega_0^2-((g\,\mathrm{Cosh}[h
$$

$$
k_0]\,k_0-\mathrm{Sinh}[h\,k_0]\,\omega_0^2)\,(g\,\mathrm{Cosh}[h\,k_1]\,k_1-\mathrm{Sinh}[h
$$

$$
k_1]\,\omega_1^2)\,k_{1,x})/(g\,\mathrm{Sinh}[h\,k_1]\,k_1^2-\mathrm{Cosh}[h\,k_1]\,k_1\,\omega_1^2))\Bigg)+
$$

$$
(4\,(\mathrm{Sinh}[h\,k_0]\,(g\,\mathrm{Coth}[d\,k_0]\,k_0-r\,\omega_0^2)+\mathrm{Cosh}[h\,k_0]\,(g\,r\,k_0-\mathrm{Coth}[d\,k_0]\,\omega_0^2))
$$

$$
(\mathrm{Sinh}[h\,k_1]\,(-g\,\mathrm{Coth}[d\,k_1]\,k_1+r\,\omega_1^2)+\mathrm{Cosh}[h\,k_1]\,(-g\,r\,k_1+\mathrm{Coth}[d\,k_1]\,\omega_1^2))\,k_{1,y}^2)/
$$

$$
((-1+r)\,k_0\,k_1\,(g\,\mathrm{Sinh}[h\,k_1]\,k_1-\mathrm{Cosh}[h\,k_1]\,\omega_1^2))\Bigg)\Bigg)\Bigg)\Big/
$$

$$
\Bigg(\frac{2\,I\,k_2\left(-\frac{I\,\mathrm{Coth}[d\,k_2]\,\omega_2}{k_2}-\frac{I\,r\,\omega_2\,(g\,\mathrm{Cosh}[h\,k_2]\,k_2-\mathrm{Sinh}[h\,k_2]\,\omega_2^2)}{g\,\mathrm{Sinh}[h\,k_2]\,k_2^2-\mathrm{Cosh}[h\,k_2]\,k_2\,\omega_2^2}\right)}{r\,\omega_2}+
$$

$$
\frac{1}{g}\Bigg(2\,I\,\omega_2\Bigg(\mathrm{Sinh}[h\,k_2]+\frac{\mathrm{Cosh}[h\,k_2]\,(-g\,\mathrm{Cosh}[h\,k_2]\,k_2+\mathrm{Sinh}[h\,k_2]\,\omega_2^2)}{g\,\mathrm{Sinh}[h\,k_2]\,k_2-\mathrm{Cosh}[h\,k_2]\,\omega_2^2}\Bigg)
$$

$$
\left(-\frac{I\,\mathrm{Sinh}[h\,k_2]\,\omega_2}{k_2}+\frac{I\,\mathrm{Cosh}[h\,k_2]\,\omega_2\,(g\,\mathrm{Cosh}[h\,k_2]\,k_2-\mathrm{Sinh}[h\,k_2]\,\omega_2^2)}{g\,\mathrm{Sinh}[h\,k_2]\,k_2^2-\mathrm{Cosh}[h\,k_2]\,k_2\,\omega_2^2}\right)\Bigg)\Bigg)
$$

Figure B.3 Mathematica output for α_2.

$$
-\left(\left\{I\left\{\sinh[h\,k_1]+\frac{\cosh[h\,k_1]\,\left(-g\cosh[h\,k_1]\,k_1+\sinh[h\,k_1]\,\omega_1^2\right)}{g\sinh[h\,k_1]\,k_1-\cosh[h\,k_1]\,\omega_1^2}\right\}\right.\right.
$$

$$
\omega_2\left(\omega_0\,\omega_2\left(-\omega_0^2+2\,\omega_0^2\,\omega_2-2\,\omega_0\,\omega_2^2+\omega_2^3\right)+\right.
$$

$$
\left.\left.g^2\left(-k_2^2\,\omega_0+k_0\,\left(k_0\,\omega_2+2\,\omega_0\,k_{2,x}-2\,\omega_2\,k_{2,x}\right)\right)\right)\right\}\Big/
$$

$$
\left(g\,\omega_0\left(-g\sinh[h\,k_2]\,k_2+\cosh[h\,k_2]\,\omega_2^2\right)\right)+
$$

$$
\left\{I\left\{\frac{\coth[d\,k_1]}{r}-\frac{g\,k_1}{r\,\omega_1^2}\right\}\omega_2\right.
$$

$$
\left\{\frac{1}{\omega_0}\left(\operatorname{csch}[d\,k_0]\,k_0\left(g\sinh[(d+h)\,k_0]\,k_0-\cosh[(d+h)\,k_0]\,\omega_0^2\right)\omega_2\right.\right.
$$

$$
\left(\sinh[h\,k_2]\,\left(g\coth[d\,k_2]\,k_2-r\,\omega_2^2\right)+\cosh[h\,k_2]\,\left(g\,r\,k_2-\coth[d\,k_2]\,\omega_2^2\right)\right)\Big)+
$$

$$
\operatorname{csch}[d\,k_2]
$$

$$
\left(\sinh[h\,k_0]\,\left(g\coth[d\,k_0]\,k_0-r\,\omega_0^2\right)+\cosh[h\,k_0]\,\left(g\,r\,k_0-\coth[d\,k_0]\,\omega_0^2\right)\right)
$$

$$
\left(g\sinh[(d+h)\,k_2]\,k_2-\cosh[(d+h)\,k_2]\,\omega_2^2\right)\,k_{2,x}+
$$

$$
\frac{1}{\omega_0}\left(\operatorname{csch}[d\,k_0]\,\left(-g\sinh[(d+h)\,k_0]\,k_0+\cosh[(d+h)\,k_0]\,\omega_0^2\right)\omega_2\,\left(\sinh[h\,k_2]\right.\right.
$$

$$
\left.\left.\left(g\coth[d\,k_2]\,k_2-r\,\omega_2^2\right)+\cosh[h\,k_2]\,\left(g\,r\,k_2-\coth[d\,k_2]\,\omega_2^2\right)\right)\,k_{2,x}\right\}+
$$

$$
\frac{1}{k_0}\left(\operatorname{csch}[d\,k_2]\right.
$$

$$
\left(\sinh[h\,k_0]\,\left(g\coth[d\,k_0]\,k_0-r\,\omega_0^2\right)+\cosh[h\,k_0]\,\left(g\,r\,k_0-\coth[d\,k_0]\,\omega_0^2\right)\right)
$$

$$
\left(-g\sinh[(d+h)\,k_2]\,k_2+\cosh[(d+h)\,k_2]\,\omega_2^2\right)\,k_{2,x}^2\Big)+\frac{1}{k_0}\left(\operatorname{csch}[d\,k_2]\right.
$$

$$
\left(\sinh[h\,k_0]\,\left(g\coth[d\,k_0]\,k_0-r\,\omega_0^2\right)+\cosh[h\,k_0]\,\left(g\,r\,k_0-\coth[d\,k_0]\,\omega_0^2\right)\right)
$$

$$
\left.\left.\left(-g\sinh[(d+h)\,k_2]\,k_2+\cosh[(d+h)\,k_2]\,\omega_2^2\right)\,k_{2,y}^2\right)\right\}\Big/
$$

$$
\left(g\,(-1+r)\,k_2\left(g\sinh[h\,k_2]\,k_2-\cosh[h\,k_2]\,\omega_2^2\right)\right)+
$$

$$
\frac{1}{4\,r\,\omega_1^2}\left\{I\,k_1\,\omega_2\left\{\left(4\,(\omega_0-\omega_2)\,\omega_2\left(\sinh[h\,k_0]\,\left(g\sinh[h\,k_2]\,\left(g\coth[d\,k_2]\,k_0^2\,k_2-g\coth[d\right.\right.\right.\right.\right.
$$

$$
\left.\left.\left.\left.\left.k_0]\,k_0\,k_2^2+r\,k_2^2\,\omega_0^2-r\,k_0^2\,\omega_2^2\right)+\cosh[h\,k_2]\,\left(g^2\,r\,k_0^2\,k_2-g\coth[d\right.\right.\right.\right.\right.
$$

$$
\left.\left.\left.\left.\left.k_2]\,k_0^2\,\omega_2^2+g\coth[d\,k_0]\,k_0\,k_2\,\omega_2^2-r\,k_2\,\omega_0^2\,\omega_2^2\right)\right)+\right.\right.\right.\right.
$$

$$
\left.\left.\left.\left.\cosh[h\,k_0]\,\left(\sinh[h\,k_2]\,\left(-g^2\,r\,k_0\,k_2^2-g\coth[d\,k_2]\,k_0\,k_2\,\omega_0^2+g\coth[d\right.\right.\right.\right.\right.
$$

$$
\left.\left.\left.\left.\left.k_0]\,k_2^2\,\omega_0^2+r\,k_0\,\omega_0^2\,\omega_2^2\right)+\cosh[h\,k_2]\,\left(-g\,r\,k_0\,k_2\,\omega_0^2+g\,r\,k_0\right.\right.\right.\right.\right.
$$

$$
\left.\left.\left.\left.\left.k_2\,\omega_2^2+\coth[d\,k_2]\,k_0\,\omega_0^2\,\omega_2^2-\coth[d\,k_0]\,k_2\,\omega_0^2\,\omega_2^2\right)\right)\right)\right)\right\}\Big/
$$

$$
\left(g\,k_0\,k_2\left(g\sinh[h\,k_2]\,k_2-\cosh[h\,k_2]\,\omega_2^2\right)\right)+
$$

$$
\left(\operatorname{csch}[d\,k_0]\,\operatorname{csch}[d\,k_2]\,\left\{g\,(-\sinh[(d-h)\,k_0]+r\sinh[(d-h)\,k_0]+\right.\right.
$$

$$
\left.\left.\sinh[(d+h)\,k_0]+r\sinh[(d+h)\,k_0]\right)\,k_0+(-1+r)\cosh[(d-h)\,k_0]\,\omega_0^2-\right.
$$

$$
\left.(1+r)\cosh[(d+h)\,k_0]\,\omega_0^2\right)\,\left(g\,(-\sinh[(d-h)\,k_2]+\right.
$$

$$
\left.r\sinh[(d-h)\,k_2]+\sinh[(d+h)\,k_2]+r\sinh[(d+h)\,k_2]\right)\,k_2+
$$

$$
\left.(-1+r)\cosh[(d-h)\,k_2]\,\omega_2^2-(1+r)\cosh[(d+h)\,k_2]\,\omega_2^2\right)
$$

$$
\left.(k_0-k_{2,x})\,(k_0\,\omega_2+\omega_0\,k_{2,x})\right\}\Big/
$$

$$
\left((-1+r)\,k_0\,k_2\,\omega_0\left(g\sinh[h\,k_2]\,k_2-\cosh[h\,k_2]\,\omega_2^2\right)\right)+
$$

$$
\frac{1}{\omega_0}\left\{4\,(\omega_0-\omega_2)\left\{-g\sinh[h\,k_0]\,k_0+\cosh[h\,k_0]\,\omega_0^2+\right.\right.
$$

$$
\frac{\coth[d\,k_0]\,\coth[d\,k_2]\,\left(-g\sinh[h\,k_0]\,k_0+\cosh[h\,k_0]\,\omega_0^2\right)\,k_{2,x}}{k_2}-
$$

$$
r\left\{-g\sinh[h\,k_0]\,k_0+\cosh[h\,k_0]\,\omega_0^2-\right.
$$

$$
\left.\left.\left.\frac{\left(g\cosh[h\,k_0]\,k_0-\sinh[h\,k_0]\,\omega_0^2\right)\,\left(g\cosh[h\,k_2]\,k_2-\sinh[h\,k_2]\,\omega_2^2\right)\,k_{2,x}}{g\sinh[h\,k_2]\,k_2^2-\cosh[h\,k_2]\,k_2\,\omega_2^2}\right\}\right\}\right\}+
$$

$$
\left(4\left(\sinh[h\,k_0]\,\left(g\coth[d\,k_0]\,k_0-r\,\omega_0^2\right)+\cosh[h\,k_0]\,\left(g\,r\,k_0-\coth[d\,k_0]\,\omega_0^2\right)\right)\right.
$$

$$
\left(\sinh[h\,k_2]\,\left(-g\coth[d\,k_2]\,k_2+r\,\omega_2^2\right)+\right.
$$

$$
\left.\left.\cosh[h\,k_2]\,\left(-g\,r\,k_2+\coth[d\,k_2]\,\omega_2^2\right)\right)\,k_{2,y}^2\right)\Big/
$$

$$
\left.\left.\left.\left(\left(-1+r\right)\,k_0\,k_2\,\left(g\sinh[h\,k_2]\,k_2-\cosh[h\,k_2]\,\omega_2^2\right)\right)\right\}\right\}\right\}\Big/
$$

$$
\left\{\frac{2\,I\,k_1\left(-\frac{I\coth[d\,k_1]\,\omega_1}{k_1}-\frac{I\,r\,\omega_1\left(g\cosh[h\,k_1]\,k_1-\sinh[h\,k_1]\,\omega_1^2\right)}{g\sinh[h\,k_1]\,k_1^2-\cosh[h\,k_1]\,k_1\,\omega_1^2}\right)}{r\,\omega_1}+\right.
$$

$$
\frac{1}{g}\left\{2\,I\,\omega_1\left(\sinh[h\,k_1]+\frac{\cosh[h\,k_1]\,\left(-g\cosh[h\,k_1]\,k_1+\sinh[h\,k_1]\,\omega_1^2\right)}{g\sinh[h\,k_1]\,k_1-\cosh[h\,k_1]\,\omega_1^2}\right)\right.
$$

$$
\left.\left.\left(-\frac{I\sinh[h\,k_1]\,\omega_1}{k_1}+\frac{I\cosh[h\,k_1]\,\omega_1\left(g\cosh[h\,k_1]\,k_1-\sinh[h\,k_1]\,\omega_1^2\right)}{g\sinh[h\,k_1]\,k_1^2-\cosh[h\,k_1]\,k_1\,\omega_1^2}\right)\right\}\right\}
$$

Figure B.4 Mathematica output for α_1.

APPENDIX C

WAVE MOTION IN A VISCOUS, TWO-LAYER FLUID

To find a wave-like solution to the linear equations 4.43 to 4.53, it is assumed that the solution has the following form.

$$\begin{aligned} \xi(x,t) &= \hat{a}e^{i(kx-\omega t)} \\ \eta(x,t) &= \hat{b}e^{i(kx-\omega t)} \\ \phi(x,z,t) &= \hat{\phi}(z)e^{i(kx-\omega t)} \\ \psi(x,z,t) &= \hat{\psi}(z)e^{i(kx-\omega t)} \\ p(x,z,t) &= \hat{p}(z)e^{i(kx-\omega t)} \end{aligned} \tag{C.1}$$

The resulting equations after substituting the above in the governing equations are

$$\hat{\phi}_{zz} - k^2\hat{\phi} = 0, \qquad 0 < z < h \tag{C.2}$$

$$\hat{\psi}_{zzzz} - (k^2 + \lambda^2)\hat{\psi}_{zz} + k^2\lambda^2\hat{\psi} = 0, \qquad -d < z < 0 \tag{C.3}$$

$$(i\omega)^2\hat{\phi} + (ik)\hat{\phi}_z = 0, \qquad z = h \tag{C.4}$$

$$-i\omega\hat{a} = \hat{\phi}_z, \qquad z = h \tag{C.5}$$

$$-i\omega\,\hat{b} = \hat{\phi}_z, \qquad z = 0 \qquad \text{(C.6)}$$

$$-i\omega\,\hat{b} = -i\,k\,\hat{\psi}, \qquad z = 0 \qquad \text{(C.7)}$$

$$\hat{p}(z) + 2\rho\nu(ik)\hat{\psi}_z - \rho g\,\hat{b} + \rho'(-i\omega\hat{\phi} + g\,\hat{b}) = 0, \qquad z = 0 \qquad \text{(C.8)}$$

$$\hat{\psi}_{zz} - (ik)^2\hat{\psi} = 0, \qquad z = 0 \qquad \text{(C.9)}$$

$$\hat{\psi}_z = 0, \qquad z = -d \qquad \text{(C.10)}$$

$$ik\hat{\psi} = 0, \qquad z = -d \qquad \text{(C.11)}$$

where in equation C.3

$$\lambda^2 = k^2 - \frac{i\omega}{\nu} \qquad \text{(C.12)}$$

Equations C.2 and C.3 have the general solution

$$\hat{\phi}(z) = C_1\,Sinh(kz) + C_2\,Cosh(kz) \qquad \text{(C.13)}$$

$$\hat{\psi}(z) = D_1\,Sinh(kz) + D_2\,Cosh(kz) + D_3\,Sinh(\lambda z) + D_4\,Cosh(\lambda z) \qquad \text{(C.14)}$$

The first two terms in C.14 represent the irrotational part of the velocity field, whereas the next two terms are the rotational part due to viscosity. The irrotational part dominates in regions far from the boundaries while the rotational part persists near the boundaries.

By substituting C.13 and C.14 in the boundary conditions, except (C.9), $\hat{b}$ and coefficients C_1, C_2, D_1, D_2, D_3, and D_4 are obtained in terms of $\hat{a}$. The result is

$$C_1 = \frac{i\hat{a}(gkS_h - \omega^2 C_h)}{k\omega} \qquad \text{(C.15)}$$

$$C_2 = \frac{-i\hat{a}(gkC_h - \omega^2 S_h)}{k\omega} \qquad \text{(C.16)}$$

$$D_1 = \{ \frac{2i\hat{a}\lambda\nu C_k^{-1} S_\lambda}{\omega^2} + \frac{-k^2 - \lambda^2 + 2k^2 C_k C_\lambda - 2k\lambda S_k S_\lambda}{k\omega^2 (\lambda S_k C_\lambda - k C_k S_\lambda)} \left(i\hat{a}\lambda\nu C_\lambda C_k^{-1} \right)$$
$$- \frac{i\hat{a}\nu S_k (k^2 + \lambda^2)}{k\omega^2 C_k} \} \left(gkS_h - \omega^2 C_h \right) \qquad \text{(C.17)}$$

$$D_2 = \frac{-i\hat{a}\nu (k^2 + \lambda^2)(g\, kS_h - \omega^2 C_h)}{k\omega^2} \qquad \text{(C.18)}$$

$$D_3 = \frac{-i\hat{a}\nu(k^2 + \lambda^2 - 2k^2 C_k C_\lambda + 2k\lambda S_k S_\lambda)(g\, kS_h - \omega^2 C_h)}{\omega^2 (-C_\lambda \lambda S_k + C_k k S_\lambda)} \qquad \text{(C.19)}$$

$$D_4 = \frac{2i\hat{a}k\nu(gkS_h - \omega^2 C_h)}{\omega^2} \qquad \text{(C.20)}$$

and
$$\hat{b} = \hat{a} \left(C_h - \frac{gkS_h}{\omega^2} \right) \qquad \text{(C.21)}$$

where

$$S_h = Sinh(kh), \qquad C_k = Cosh(kd), \qquad S_\lambda = Sinh(\lambda d),$$
$$C_h = Cosh(kh), \qquad S_k = Sinh(kd), \qquad C_\lambda = Cosh(\lambda d) \qquad \text{(C.22)}$$

Equation C.9 serves to develop the dispersion relation:

$$\frac{\rho'(\omega^4 - g^2 k^2) S_h}{C_h (gk \frac{S_h}{C_h} - \omega^2)} + \rho g\, k + \rho(2k^2\nu - i\omega)^2 \left\{ \frac{(2k^2 - i\omega/\nu)[\lambda C_k C_\lambda - k S_k S_\lambda] - 2k^2\lambda}{(2k^2 - i\omega/\nu)[\lambda S_k C_\lambda - k\, C_k S_\lambda]} \right\}$$
$$- 4\rho k^3 \nu^2 \lambda \left\{ \frac{(2k^2 - i\omega/\nu) - 2k[k\, C_k C_\lambda - \lambda S_k S_\lambda]}{2k[\lambda S_k C_\lambda - k\, C_k S_\lambda]} \right\} = 0$$

(C.23)

APPENDIX D

SOLVABILITY CONDITION

The general form of the sets of differential equations and the corresponding boundary conditions in chapter 4 is

$$L_1[p(z)] = S_1(z), \qquad 0 < z < h \qquad \text{(D.1)}$$

$$L_2[q(z)] = S_2(z), \qquad -d < z < 0 \qquad \text{(D.2)}$$

$$-\omega^2 p(z) + g\, p'(z) = S_3, \qquad z = h \qquad \text{(D.3)}$$

$$q(z) + \frac{p'(z)}{ik} = S_4, \qquad z = 0 \qquad \text{(D.4)}$$

$$q''(z) + k^2 q(z) = S_5, \qquad z = 0 \qquad \text{(D.5)}$$

$$q'''(z) + \left(\frac{i\omega - 3\nu k^2}{\nu}\right) q'(z) + \frac{r\omega k}{\nu} p(z) - \frac{(r-1)gk}{\nu\,\omega} p'(z) = S_6,$$

$$z = 0 \qquad \text{(D.6)}$$

$$q(z) = S_7, \qquad z = -d \qquad \text{(D.7)}$$

$$q'(z) = 0, \qquad z = -d \qquad \text{(D.8)}$$

where operators L_1 and L_2 are

$$L_1 = \frac{d^2}{dz^2} - k^2$$

$$L_2 = \frac{d^4}{dz^4} - (k^2 + \lambda^2)\frac{d^2}{dz^2} + k^2\lambda^2,$$

S_1 and S_2 are known functions of z, and S_3 to S_6 are constants. The primes refer to the derivatives with respect to z. For the above system of equations not to yield a secular solution, the solution of the associated adjoint system should be orthogonal to the forcing functions. In the following the adjoint system as well as the desired solvability condition are obtained

Assume that $P(z)$ and $Q(z)$ are the solution to the adjoint system in the upper and lower layer respectively. Equation D.1 and D.2 are multiplied by $P(z)$ and $Q(z)$ respectively. The products are integrated over the respective domains, and the results are added up. Finally, after applying the Green's theorem to the integrals, the following is obtained.

$$\int_0^h P(z)\,\mathrm{L}_1[p(z)]\,\mathrm{dz} - \int_0^h p(z)\,\mathrm{L}_1[P(z)]\,\mathrm{dz} + \int_{-d}^0 Q(z)\,\mathrm{L}_2[q(z)]\,\mathrm{dz} - \int_{-d}^0 q(z)\,\mathrm{L}_2[Q(z)]\,\mathrm{dz} =$$
$$[Pp' - P'p]\Big|_{z=0}^{z=h} + [Qq''' - Q'q'' + Q''q' - Q'''q - (k^2+\lambda^2)(q'Q - qQ')]\Big|_{z=-d}^{z=0} \qquad \text{(D.9)}$$

The field equations of the adjoint system are obtained by requiring $L_1[P(z)]$ and $L_2[Q(z)]$ be zero:

$$L_1[P(z)] = 0\,, \qquad 0 < z < h \qquad \text{(D.10)}$$

$$L_2[Q(z)] = 0\,, \qquad -d < z < 0 \qquad \text{(D.11)}$$

The boundary conditions for the adjoint system are obtained by requiring that the right side of (D.9) be zero when S_3 to S_6 are zero. For this to be true, the following equations are to hold at the boundaries.

$$-\omega^2 P(z) + g\, P'(z) = 0, \qquad z = h \tag{D.12}$$

$$Q(z) = 0, \qquad z = -d \tag{D.13}$$

$$Q'(z) = 0, \qquad z = -d \tag{D.14}$$

$$P'(z) - \frac{r\,\omega\,k}{\nu} Q(z) = 0, \qquad z = 0 \tag{D.15}$$

$$\frac{Q'''(z)}{i\,k} - \frac{(2\,k^2 + \lambda^2)}{i\,k} Q'(z) + \frac{(r-1)\,g\,k}{\nu\,\omega} Q(z) - P(z) = 0, \qquad z = 0 \tag{D.16}$$

$$Q''(z) + k^2\, Q(z) = 0, \qquad z = 0 \tag{D.17}$$

It is interesting to note that the adjoint system and the homogeneous form of equations D.1 to D.8 are not the same. This implies that the systems of equations at second order are not self-adjoint. The difference between the two systems stems from the interface boundary conditions.

Differential equations (D.10) and (D.11), and boundary conditions D.12 to D.17 form a complete set of equations from which $P(z)$ and $Q(z)$ can be computed. Marthematica® was used to find the expressions for $P(z)$ and $Q(z)$:

$$P(z) = C_1\, Sinh(kz) + C_2\, Cosh(kz) \tag{D.18}$$

$$Q(z) = D_1\, Sinh(kz) + D_2\, Cosh(kz) + D_3\, Sinh(\lambda z) + D_4\, Cosh(\lambda z) \tag{D.19}$$

where $$C_1 = 1 \tag{D.20}$$

$$C_2 = \frac{-(g\,kC_h - \omega^2 S_h)}{(g\,kS_h - \omega^2 C_h)} \tag{D.21}$$

$$D_1 = \frac{-2ik\lambda\nu^2 C_k^{-1} S_\lambda}{r\omega^2} + \frac{\lambda C_\lambda C_k^{-1} k\nu^2 (2ik^2 + \frac{\omega}{\nu})}{r\omega^2 k(\lambda S_k C_\lambda - kC_k S_\lambda)}$$
$$- \frac{2\lambda C_\lambda C_k^{-1} ik^2\nu^2(-\lambda S_k S_\lambda + kC_k C_\lambda)}{r\omega^2 k(\lambda S_k C_\lambda - kC_k S_\lambda)} + \frac{\nu^2 S_k (2ik^2 + \frac{\omega}{\nu})}{r\omega^2 C_k} \tag{D.22}$$

$$D_2 = \frac{\nu^2 (2ik^2 + \frac{\omega}{\nu})}{r\omega^2} \tag{D.23}$$

$$D_3 = \frac{-k\nu^2 (2ik^2 + \frac{\omega}{\nu})}{r\omega^2(\lambda S_k C_\lambda - kC_k S_\lambda)} + \frac{2ik^2\nu^2(-\lambda S_k S_\lambda + kC_k C_\lambda)}{r\omega^2(\lambda S_k C_\lambda - kC_k S_\lambda)} \tag{D.24}$$

$$D_4 = \frac{-2ik^2\nu^2}{r\omega^2} \tag{D.25}$$

where
$$S_h = Sinh(kh), \quad C_k = Cosh(kd), \quad S_\lambda = Sinh(\lambda d),$$
$$C_h = Cosh(kh), \quad S_k = Sinh(kd), \quad C_\lambda = Cosh(\lambda d) \tag{D.26}$$

The adjoint system gives the same dispersion relation as by the linear wave theory. Hence, its inclusion here is avoided.

After $P(z)$ and $Q(z)$ are determined, (D.9) changes to

$$\int_0^h P(z)\,S_1(z)\,dz + \int_{-d}^0 Q(z)\,S_2(z)\,dz =$$
$$[P(z)S_3/g]\Big|_{z=h} + \{-Q'(z)S_5 + Q(z)S_6 + [-Q'''(z) + (2k^2 + \lambda^2)\,Q'(z)]S_4\}\Big|_{z=0}$$
$$+ \{[Q'''(z) - (k^2 + \lambda^2)Q'(z)]S_7\}\Big|_{z=-d} \tag{D.27}$$

The above equation is the desired solvability condition.